

SYNTHESIS OF TITANIUM DIOXIDE NANOTUBES
FROM THIN FILM ON SILICON WAFER
FOR PHOTOELECTROCHEMICAL
CELL

by

Karumbayah Chappanda Nanaiah

A dissertation submitted to the faculty of
The University of Utah
in partial fulfillment of the requirements for the degree of

Doctor of Philosophy

Department of Electrical and Computer Engineering
The University of Utah

December 2013

Copyright © Karumbaiyah Chappanda Nanaiah 2013

All Rights Reserved

ABSTRACT

TiO₂ is an extensively studied material due to its nontoxic, environmental friendly, corrosion-resistant nature and wide band gap (~3 eV). TiO₂ nanotubes (T-NTs) synthesized via electrochemical anodization have been studied extensively, with particular focus on their electrical and optical properties. The advantage of T-NT is the large surface area to volume ratio. T-NT has been used to demonstrate many applications such as sensors and energy harvesting. These applications have traditionally been demonstrated via T-NT synthesized on Ti foil. However, there is currently no commercially available T-NT-based device, which may be due to a lack of fabrication techniques, to make such devices on a large scale. One of the requirements for fabricating compact T-NT-based devices is the need for a stable and planar substrate. The titanium foils commonly used for T-NT synthesis are mechanically flexible, making them more prone to bending, limiting the integration of T-NT with microfabrication techniques.

Here, we present the synthesis of T-NT on Si wafer at room temperature from direct current (D.C.) sputtered as well as e-beam evaporated thin Ti film. Hundred nm SiO₂ was used to electrically isolate the T-NT from the substrate. We demonstrate integration of the synthesis of T-NT with photolithography, which is one of the most important requirements for scaling up a T-NT-based device. The T-NT was stable up to 500°C, which is required for improved charge transport. The T-NT was 1.4 times longer

than the thickness of the Ti film, showing selective electric field-assisted etching of Ti by the electrolyte. We also report site-specific and patterned growth of the T-NT. The effect of properties of thin films such as grain size, residual stress and density on the morphology of T-NT was studied to improve the stability and quality of the T-NT. We demonstrate the synthesis of $\text{TiO}_2\text{-WO}_3$ composite nanotubes for photoelectrochemical cells with up to a 40% increase in photocurrent in comparison to plain T-NT. The T-NT was extensively studied and characterized using SEM, AFM, UV-Vis spectroscopy, XRD, and XPS.

This dissertation is dedicated to all the beer lovers in the world.

TABLE OF CONTENTS

ABSTRACT.....	iii
LIST OF TABLES.....	ix
ACKNOWLEDGEMENTS.....	x
Chapter	
1. INTRODUCTION.....	1
1.1. Need for miniaturization.....	3
1.2. TiO ₂ an interesting material.....	5
1.3. Why nanotubes and nanostructures?.....	6
1.4. Research objectives.....	7
1.5. Organization and structure of dissertation.....	9
1.6. References.....	11
2. TECHNICAL BACKGROUND.....	18
2.1. Need for alternative fuel.....	19
2.2. Methods used in water splitting.....	20
2.3. Materials used in photoelectrochemical water splitting.....	22
2.4. Polymorphs of TiO ₂	24
2.5. Reported methods for synthesis of TiO ₂ nanotubes.....	28
2.5.1. Sol-Gel.....	28
2.5.2. Hydrothermal method.....	31
2.5.3. Electrochemical anodization.....	34
2.5.4. Template-based synthesis.....	41
2.6. Applications of TiO ₂ nanotubes.....	43
2.6.1. Photocatalysis.....	43
2.6.2. Solar cells.....	46
2.6.3. Drug delivery.....	48
2.6.4. Sensors.....	49
2.7. Modification TiO ₂ nanotubes properties.....	50
2.7.1. Annealing.....	50
2.7.2. Doping.....	52
2.7.3. Surface deposition and filling.....	53

2.8.	Thin Film TiO ₂ nanotubes	54
2.9.	Incorporating WO ₃ in TiO ₂ nanotubes	55
2.10.	References	57
3.	GROWTH AND CHARACTERIZATION OF TiO₂ NANOTUBES FROM SPUTTERED Ti FILM ON Si SUBSTRATE.....	74
3.1.	Abstract.....	75
3.2.	Background.....	75
3.3.	Methods	76
3.3.1.	Thin film deposition.....	76
3.3.2.	T-NT synthesis	76
3.3.3.	Characterization.....	77
3.4.	Results and discussions	77
3.5.	Conclusions.....	81
3.6.	References.....	82
4.	SITE-SPECIFIC AND PATTERNED GROWTH OF TiO₂ NANOTUBE ARRAYS FROM E-BEAM EVAPORATED THIN TITANIUM FILM ON Si WAFER.....	83
4.1.	Abstract.....	84
4.2.	Introduction.....	84
4.3.	Experimental methods	85
4.3.1.	Deposition of Ti on Si wafer.....	85
4.3.2.	Anodization e-beam deposited Ti film	85
4.3.3.	Site-specific growth of TiO ₂ nanotubes	85
4.3.4.	Characterization.....	85
4.4.	Results and discussions	86
4.5.	Conclusions.....	90
4.6.	References.....	90
4.7.	Supplementary information.....	92
5.	EFFECT OF SPUTTERING PARAMETERS ON THE MORPHOLOGY OF TiO₂ NANOTUBES SYNTHESIZED FROM THIN Ti FILM ON Si SUBSTRATE	94
5.1.	Abstract.....	95
5.2.	Introduction.....	95
5.3.	Experimental procedure	97
5.3.1.	Thin film deposition.....	97
5.3.2.	T-NT synthesis	98
5.3.3.	Characterization.....	99
5.4.	Results and discussions	100
5.4.1.	Summary of sputtering process mechanism.....	100
5.4.2.	Effect of gas pressure	101
5.4.3.	Effect of sputtering power	106
5.4.4.	Effect of substrate temperature	110

5.4.5.	Comparison of the three sputtering runs	113
5.5.	Conclusions.....	114
5.6.	References.....	116
6.	TiO ₂ -WO ₃ COMPOSITE NANOTUBES FROM COSPUTTERED THIN FILMS ON Si SUBSTRATE FOR ENHANCED PHOTOELECTROCHEMICAL WATER SPLITTING	120
6.1.	Abstract.....	121
6.2.	Introduction.....	122
6.3.	Experimental procedure	123
6.3.1.	Thin film deposition.....	123
6.3.2.	Nanotube synthesis	124
6.3.4.	Characterization and testing.....	125
6.4.	Results and discussions	126
6.4.1.	Synthesis of TiO ₂ -WO ₃ composite nanotubes	126
6.4.2.	Water splitting using TiO ₂ -WO ₃ composite nanotube	136
6.5.	Conclusions.....	144
6.6.	References.....	145
7.	CONCLUSIONS.....	150
7.1.	Summary.....	151
7.1.1.	Thin film deposition.....	152
7.1.2.	Electrochemical anodization.....	153
7.1.3.	Characterization.....	156
7.2.	Conclusions.....	157
7.3.	Future work.....	162

LIST OF TABLES

Table

2.1: Comparison of different techniques used in water splitting	23
2.2: Commonly used semiconductor material in PEC water splitting.....	25
2.3: Comparison of the rutile, anatase and brookite polymorphs of TiO ₂	25
2.4: Comparison of the TiO ₂ nanotube synthesis techniques	29
2.5: List of reports on TiO ₂ nanotube based PEC water splitting	47
2.6: List of reports on thin film based TiO ₂ nanotubes	56
2.7: List of reports on WO ₃ incorporated in TiO ₂ nanotubes.....	56
5.1: Summary of the sputtering parameters and properties of the thin Ti film	103
6.1: Sputtering parameters used for depositing the Ti–W composite film and the Ti–W, and the atomic ratio before and after anodization	129
7.1: Summary of the tools used and the paramters analysed using the tools	158
7.2: Summary of the experimental parameters varied/studied and the results achieved.	163

ACKNOWLEDGEMENTS

I would sincerely like to thank my advisors, Dr. Mano Misra and Dr. Florian Solzbacher, for providing me this opportunity to work on this project which has sharpened my skills and nurtured me professionally. I would like to thank them for the continual support and mentoring that I have received for the entire duration of my PhD. I would also like to thank Dr Swomitra Mohanty, Dr. Bruce Gale, Dr. Loren Rieth, and Dr. Prashant Tathireddy for providing support and mentoring with the project.

I would like to thank the staff members of Utah Nanofab at the University of Utah for their support and training on various microfabrication processes. I would like to thank Dr. Brian van Devener for help with the tools used in Micron Microscopy Core at the University of Utah. I would like to thank York Smith for his valuable inputs and ideas on the project.

I would like to thank my parents, Mr. and Mrs. C. K. Nanaiah, my brother, C.N. Cariappa and my sister, C.N. Manasa for their love and support to pursue my dream of higher studies. I would like to thank the University of Utah and all the staff members for making me a part of the university.

I would like to once again thank everyone above for the support with the project, as it would have been impossible to finish this project without their help.

CHAPTER 1

INTRODUCTION

A nanotube is a one-dimensional (1-D) tubular structure with a high diameter to length ratio. One of the biggest advantages of nanotubes is the high surface to volume ratio. Synthesis of nanotubes made of carbon has been reported by various research groups since 1953 [1]–[5], and it has been shown that carbon nanotubes have better electrical conductivity properties [6], [7], stronger mechanical properties [8], [9] and better thermal properties [10], [11] compared to bulk allotropes of carbon. Along with the interest in carbon nanotubes for their unique properties compared to the bulk form, carbon nanotubes also triggered research into synthesizing other 1-D materials in order to have the advantages of a high surface to volume ratio and better thermal, optical, electrical, and mechanical properties. Since then various nanosized materials such as nanorods (silver [12], [13], gold [14], [15], ZnO [16], [17]), nanowires (SiO₂ [18], [19], Pt [20], [21], GaN [22], [23]), and nanotubes (TiO₂ [24], Ta₂O₅ [25]) have been reported, opening new 1-D material based research and applications.

TiO₂ is a widely studied material due to being chemically inert, nontoxic, environmentally friendly, and having wide band gap. The ability to synthesize high aspect nanotubular [24] and nanoporous [26] TiO₂ further increased the interest in the material, resulting in over 40 000 publications in the last 15 years. In this chapter, we provide a description of the need for miniaturizing semiconductor devices, a brief description on advantages of TiO₂ as a material, the advantages of nanosized materials, methods used to achieve the goal of this project and an outline of the dissertation.

1.1 Need for miniaturization

Gordon E. Moore, the co-founder of Intel, predicted in the year 1965 that the number of components in integrated circuits will double every two years [27]. He predicted that the trend would continue for the next 10 years, and it is called Moore's law. However, the need for faster computing power, long battery life, larger memory capacity, and compact devices kept the trend of shrinking gate length going for longer than 10 years. Fig. 1.1 shows the trend in the shrinking transistor with time [28]. The advantages of shrinking components are that the cost of the device is reduced, power consumption of the device is reduced, the sensitivity of the device is increased, and the size of the device is reduced. Based on Moore's law there are other laws such as "transistors per integrated circuit," "hard disk storage cost per unit of information," "pixels per dollar," etc. These laws, similar to Moore's law, have the common motive of improving device performance and capabilities. Effort to reduce the size of devices such as accelerometers [29], gyroscopes [30], and sensors [31], [32] can be observed. The technique used to miniaturize these devices is microfabrication. These devices are fabricated on stable and planar substrates such as Si. A lot of research is also focused on reducing the feature size that can be fabricated using microfabrication techniques [31]–[34]. A lot of companies such as Intel and Micron are successful since they are keeping up Moore's law, which has proven to be advantageous. Therefore, the key in production of devices on a large commercial scale is to reduce the size of devices to make these devices compact and cost effective.

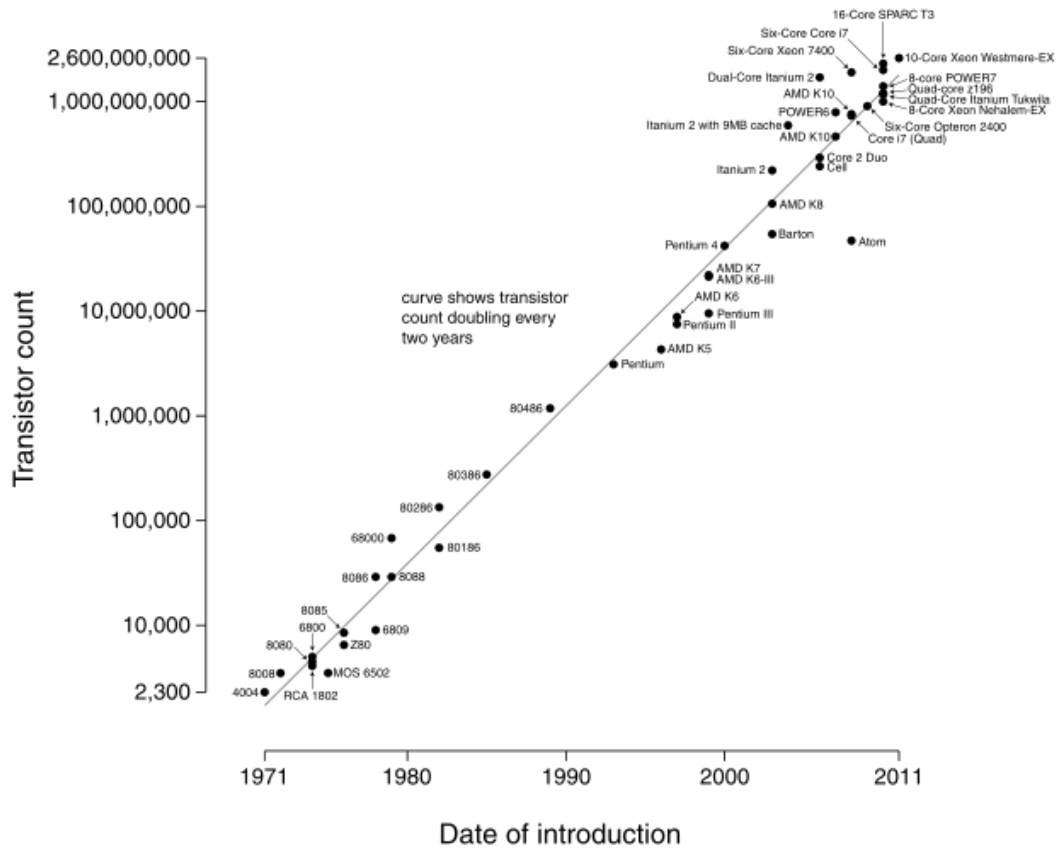


Figure 1.1: Microprocessor transistor counts from 1971 to 2011 and Moore's law [28]

1.2 TiO₂ an interesting material

TiO₂ is a wide band gap material (~ 3 eV [35]) making it suitable for harvesting solar energy. Wide band gap materials have the advantages of being able to operate at higher temperatures and having a longer carrier lifetime, reducing recombination losses. The harvested solar energy is used for various applications such as splitting water for hydrogen generation [36], [37] (where hydrogen could be used as an alternative to fossil fuel), for treating waste water (where the process has the advantage of mineralization of organic pollutants [38]), for electricity generation [24], [39], and for degradation of pesticides [40]. Due to its wide band gap, it also has an interesting property of self-cleaning where it prevents growth of bacteria and fungi when exposed to sunlight and hence, buildings (which are constantly exposed to sunlight) can be protected when coated with a thin layer [41]. This is because the absorption range of TiO₂ is in the UV range of the solar spectrum that prevents any damage caused by UV light. It is also used for self-cleaning of cotton textiles [42] and as a corrosion resistant coating [43]. Another interesting property of TiO₂ is its biocompatibility. It is shown to be used in dental implants [44], as blends with lifesaving drugs [45] and bone grafting [46]. Most of the implants or biomedical devices that use Ti metal are due to the presence of a thick layer of TiO₂ which is formed when exposed to bodily fluids [44], [46]. Other applications of TiO₂ in daily life are in toothpaste [47], pigments [48], and sunscreen [49] due to its safe, nontoxic nature. Since TiO₂ is already in an oxidized state, the material is relatively more chemically inert compared to its metallic state.

TiO₂ is a semiconducting material like silicon whose electrical property and optical properties can similarly be changed by doping and alloying. The band gap of TiO₂ is

changed by doping with nitrogen [50], sulphur [51], chromium [52], and zinc [53]. TiO_2 can be made semimetallic by doping with carbon [54]. By alloying with other materials such as WO_3 [55] and Cu_2O [56], TiO_2 is also shown to modify its electrical and optical properties. Titanium is relatively cheap compared to other metals such as gold and platinum, making TiO_2 (which can be obtained by oxidizing Ti) an interesting and attractive material.

1.3 Why nanotubes and nanostructures?

Materials in their nanosized form have certain advantages over their bulk form. There are a higher number of atoms of the materials on the surface compared to when the material is in the bulk form (an increase in surface area to volume ratio). The surface energy associated with the materials is increased. This leads to an increase in the chemical and catalytic activity of the material [57]. Also, its mechanical and electrical properties change, which can be advantageous based on the requirement. Nanosized materials have a better self-assembling capability where the molecules rearrange themselves easily compared to their bulk form [58]. Nanosized materials have better solubility and higher absorption [57]. They provide better and more uniform surface coverage when used as dispersion and coating materials [58]. By synthesizing nanosized materials, the devices fabricated are more economical, have lower power consumption, higher sensitivity, and lower response time along with an increase in performance.

TiO_2 similarly in its nanosized structure has different properties compared to its bulk properties. The Young's modulus of bulk anatase TiO_2 (282 GPa [59]) is lower when compared with the Young's modulus of thin anatase TiO_2 film (varies from 65 GPa to

147 GPa [60]). The Young's modulus of TiO₂ nanotubes is tested to be as low as 23 GPa [61]. The density of bulk rutile TiO₂ is 4.26 g/cm³ [62], while the thin films have a density as low as 3.8 g/cm³ [60]. The band gap of TiO₂ nanoparticles (anatase) is shown to be 3.4 eV, whereas that of bulk is 3.2 eV [63].

1.4 Research objectives

As stated in the previous sections, TiO₂ is an interesting material with a wide range of applications, and TiO₂-based nanoparticles and nanotubes are shown to have advantages compared to bulk TiO₂. A lot of work has been done to understand and study the advantages of TiO₂ as a material. With the current trend of nanotechnology, a lot of research is focused on miniaturizing current TiO₂-based devices [64], [65]. Interest in the research of TiO₂ increased two-fold with the ability of synthesizing TiO₂ nanotubes, which are shown to have better advantages compared to bulk as well as nanoparticles [66], [67]. However, most of the applications demonstrated by TiO₂ nanotubes were synthesized on Ti foil. With the current trend of transistors being reduced in size by half every two years, there is a need to reduce the size of TiO₂-based devices. Nanotubes synthesized on foil inhibit the ability to utilize the advantages of microfabrication for miniaturizing. Ti foil is flexible and a nonplanar substrate that cannot be integrated into the current semiconductor fabrication techniques for miniaturizing. One of the methods is to synthesize TiO₂ nanotubes on stable, planar substrates that can be integrated with current microfabrication techniques.

Our goal is to synthesize TiO₂ nanotubes on Si substrate, which is a stable and planar substrate and can be integrated with current microfabrication techniques. We study,

characterize, and compare TiO_2 nanotubes synthesized on foil with the ones synthesized on Si substrate. To limit the path of the electrical current in TiO_2 nanotube based devices, the nanotubes must be electrically isolated from the Si substrate, which is a semiconducting material (conductive enough to disturb the path of the electrical current). We synthesize TiO_2 nanotubes on Si substrate with an insulating layer consisting of silicon dioxide to electrically isolate the nanotubes from the substrate. The nanotubes are synthesized from two kinds of thin Ti film, one being deposited via D.C. magnetron sputtering and the other via e-beam evaporation, demonstrating the flexibility of the process. Simply synthesizing the nanotubes on Si substrate from different kinds of thin films will not be sufficient proof for use of planar and stable substrate. We demonstrate the ability of site-specific and patterned growth of TiO_2 nanotubes via the use of photolithography, which is one of the most commonly used microfabrication steps in the current semiconductor industry. We also study the property of thin film that is required for synthesizing stable TiO_2 nanotubes. The properties of the thin film are varied by changing the parameters used for depositing thin films via the D.C. magnetron sputtering technique. Since a lot of work is done to improve the performance of TiO_2 nanotube based devices, one of them being synthesis of composite nanotubes, we demonstrate the capability of synthesizing $\text{TiO}_2\text{-WO}_3$ composite nanotubes on Si substrate from composite thin film (by using the advantages of microfabrication). We use the synthesized composite nanotube to demonstrate an application. We fabricate a photoelectrochemical cell used for splitting water into hydrogen and oxygen in which hydrogen can be used as a clean alternative to fossil fuels as well as for other uses. We compare the performance of the composite nanotube with plain nanotubes for the ability

to split water.

1.5 Organization and structure of dissertation

Chapter 2 gives the background on polymorphs of TiO_2 , a literature review on reported methods for synthesis of TiO_2 nanotubes (sol-gel, hydrothermal, electrochemical anodization, and template-based) with emphasis on electrochemical anodization and applications demonstrated by TiO_2 nanotubes (photocatalysis, degradation of pollutants, water splitting, solar cells, drug delivery, sensors) with the emphasis on water splitting. It then talks about reported techniques used for modifying the electrical and optical properties of TiO_2 nanotubes such as annealing, doping, and surface modifications. It also gives a review on reported thin film based TiO_2 nanotubes.

Chapter 3 provides a detailed analysis and characterization of the self-assembled TiO_2 nanotube arrays synthesized from thin titanium film deposited via D.C. magnetron sputtering on Si substrate. The nanotubes were synthesized using a fluorinated organic electrolyte via electrochemical anodization. The change in the morphology with anodization potential, band gap of the material, crystalline phase, and growth mechanism were studied. The selectivity of the electrolyte in etching oxidized titanium to form nanotubes was studied. The nanotubes were analyzed using scanning electron microscope (SEM) micrographs, atomic force microscope (AFM) micrographs, x-ray diffraction (XRD) and diffuse-reflectance UV-Vis spectroscopy. The chapter also talks about the parameters used for depositing the thin film on the Si substrate.

Chapter 4 is about synthesis and characterization of TiO_2 nanotubes on Si substrate from thin film deposited via e-beam evaporation. The change in the morphology with

anodization potential, band gap of the material, crystalline phase, and growth mechanism was studied. The nanotubes are synthesized using ethylene glycol, water, and ammonium fluoride based electrolyte. Using two simple photolithography steps, site-specific and patterned growth of TiO₂ nanotubes is demonstrated. TiO₂ nanotubes arrays are grown in the pattern of a 'U' symbol resembling the logo of the University of Utah to demonstrate the flexibility of the synthesis technique. Site-specific growth of nanotubes is demonstrated in regions consisting of 0.01 mm² in area with self-aligned Ti electrodes.

Chapter 5 talks about the properties of the thin film that affect the morphology of the TiO₂ nanotubes. The thin film was deposited via the D.C. magnetron sputtering technique. Parameters such as process gas, sputtering power, and substrate temperature were varied to change the properties of a thin film. Influence of thin film properties such as grain size, biaxial residual stress, and relative density on the morphology of the anodized film are studied. The film before and after anodization were characterized using SEM micrographs and laser interferometry.

Chapter 6 shows the synthesis and characterization of TiO₂-WO₃ composite nanotubes on Si substrate from thin film. The nanotubes were synthesized using an electrolyte similarly as before. The W-Ti nanocomposite thin film was deposited by multi-target cosputtering. The change in the morphology of the anodized film with W-Ti ratio is studied. The nanotubes are characterized for band gap and crystalline phase. The composite nanotube is used to fabricate a photoelectrochemical cell (PEC) for splitting water. The photocurrent of the TiO₂-WO₃ composite nanotube based photoelectrochemical cell is compared with that of plain a TiO₂ nanotube based photoelectrochemical cell. The performance of the PEC is compared with the change in

tungsten percentage, nanotube length, and calcination temperature to improve the photocurrent of the PEC.

Chapter 7 provides an overview of the project. The accomplishments made and the methods used for achieving the same are presented. Future work, which includes further techniques to understand the synthesis of the nanotubes and to improve the performance of the photoelectrochemical, is discussed. Synthesis of other possible transition metaloxide/TiO₂ composite based nanotube synthesis is discussed. The scope of the synthesized plain as well as composite nanotubes for other applications are discussed and reviewed.

1.6 References

- [1] W. R. Davis, R. J. Slawson, and G. R. Rigby, "An unusual form of carbon," *Nature*, vol. 171, pp. 756, 1953.
- [2] L. J. E. Hofer, E. Sterling, and J. T. McCartney, "Structure of carbon deposited from carbon monoxide on iron, cobalt and nickel," *J. Phys. Chem.*, vol. 59, pp. 1153–1155, 1955.
- [3] P. L. Walker, J. F. Rakszawski, and G. R. Imperial, "Carbon formation from carbon monoxide-hydrogen mixtures over iron catalysts. Properties of carbon formed," *J. Phys. Chem.*, vol. 63, pp. 133–140, 1959.
- [4] T. Baird, J. R. Fryer, and B. Grant, "Structure of fibrous carbon," *Nature*, vol. 233, pp. 329–330, 1971.
- [5] R. T. K. Baker, M. A. Barber, P. S. Harris, F. S. Feates, and R. J. Waite, "Nucleation and growth of carbon deposits from the nickel catalyzed decomposition of acetylene," *J. Catalysis*, vol. 26, pp. 51–62, 1972.
- [6] P. R. Bandaru, "Electrical properties and applications of carbon nanotube structures," *J. Nanosci. Nanotechnol.*, vol. 7, pp. 1–29, 2007.
- [7] M. Miao, "Electrical conductivity of pure carbon nanotube yarns," *Carbon*, vol. 49, pp. 3755–3761, 2011.

- [8] J.-P. Salvetat, J.-M. Bonard, N.H. Thomson, A.J. Kulik, L. Forró, W. Benoit, and L. Zuppiroli, "Mechanical properties of carbon nanotubes," *Appl. Phys. A*, vol. 69, pp. 255–260, 1999.
- [9] M. S. Dresselhaus, G. Dresselhaus, J. C. Charlier, and E. Hernandez, "Electronic, thermal and mechanical properties of carbon nanotubes," *Phil. Trans. R. Soc. Lond. A*, vol. 362, pp. 2065–2098, 2004.
- [10] J. Hone, M. Whitney, C. Piskoti, and A. Zettl, "Thermal conductivity of single-walled carbon nanotubes," *Phys. Rev. B*, vol. 59, pp. 2514–2516, 1999.
- [11] D. J. Yang, Q. Zhang, G. Chen, S. F. Yoon, J. Ahn, S. G. Wang, Q. Zhou, Q. Wang, and J. Q. Li, "Thermal conductivity of multiwalled carbon nanotubes," *Phys. Rev. B*, vol. 66, pp. 165440–165445, 2002.
- [12] N. R. Jana, L. Gearheart and C. J. Murphy, "Wet chemical synthesis of silver nanorods and nanowires of controllable aspect ratio," *Chem. Commun.*, pp. 617–618, 2001.
- [13] G.-J. Lee, S.-I. Shin, Y.-C. Kim, and S.-G. Oh, "Preparation of silver nanorods through the control of temperature and pH of reaction medium," *Mater. Chem. Phys.*, vol. 84, pp. 197–204, 2004.
- [14] Yu-Ying, S.-S. Chang, C.-L. Lee, and C. R. C. Wang, "Gold nanorods: Electrochemical synthesis and optical properties," *J. Phys. Chem. B*, vol. 101, pp. 6661–6664, 1997.
- [15] N. R. Jana, L. Gearheart, and C. J. Murphy, "Wet chemical synthesis of high aspect ratio cylindrical gold nanorods," *J. Phys. Chem. B*, vol. 105, pp. 4065–4067, 2001.
- [16] B. Liu and H. C. Zeng, "Hydrothermal synthesis of ZnO nanorods in the diameter regime of 50 nm," *J. Am. Chem. Soc.*, vol. 125, pp. 4430–4431, 2003.
- [17] L. Vayssieres, "Growth of arrayed nanorods and nanowires of ZnO from aqueous Solutions," *Adv. Mater.*, vol. 15, pp. 464–466.
- [18] Z. Xiao, L. Zhang, G. Meng, X. Tian, H. Zeng, and M. Fang, "High-density, aligned SiO₂ nanowire arrays: Microscopic imaging of the unique growth style and their ultraviolet light emission properties," *J. Phys. Chem. B*, vol. 110, pp. 15724–15728, 2006.
- [19] J. Hu, Y. Bando, J. Zhan, X. Yuan, T. Sekiguchi, and D. Golberg, "Self-assembly of SiO₂ nanowires and Si microwires into hierarchical heterostructures on a large scale," *Adv. Mater.*, vol. 17, pp. 971–975, 2005.

- [20] H.-W. Liang, X. Cao, F. Zhou, C.-H. Cui, W.-J. Zhang, and S.-H. Yu, "A free-standing Pt-nanowire membrane as a highly stable electrocatalyst for the oxygen reduction reaction," *Adv. Mater.*, vol. 23, pp. 1467–1471, 2011.
- [21] Y. Song, R. M. Garcia, R. M. Dorin, H. Wang, Y. Qiu, E. N. Coker, W. A. Steen, J. E. Miller, and J. A. Shelnett, "Synthesis of platinum nanowire networks using a soft template," *Nano Lett.*, vol. 7, pp. 3650–3655, 2007.
- [22] T. Kuykendall, P. Pauzauskie, S. Lee, Y. Zhang, J. Goldberger, and P. Yang, "Metalorganic chemical vapor deposition route to GaN nanowires with triangular cross sections," *Nano Lett.*, vol. 3, pp. 1063–1066, 2003.
- [23] X. Duan and C. M. Lieber, "Laser-assisted catalytic growth of single crystal GaN nanowires," *J. Am. Chem. Soc.*, vol. 122, pp. 188–189, 2000.
- [24] G. K. Mor, K. Shankar, M. Paulose, O. K. Varghese, and C. A. Grimes, "Use of highly-ordered TiO₂ nanotube arrays in dye-sensitized solar cells," *Nano Lett.*, vol. 6, pp. 215–218, 2006.
- [25] N. K. Allam, X. J. Feng and C. A. Grimes, "Self-assembled fabrication of vertically oriented Ta₂O₅ nanotube arrays, and membranes there of, by one-step tantalum anodization," *Chem. Mater.*, vol. 20, pp. 6477–6481, 2008.
- [26] Z.-S. Wang, C.-H. Huang, Y.-Y. Huang, Y.-J. Hou, P.-H. Xie, B.-W. Zhang, and H.-M. Cheng, "A highly efficient solar cell made from a dye-modified ZnO-covered TiO₂ nanoporous electrode," *Chem. Mater.*, vol. 13, pp. 678–682, 2001.
- [27] G. E. Moore, "Cramming more components onto integrated circuits," *Electronics*, vol. 38, pp. 114–117, 1965
- [28] Wikipedia. *Moore's law*. [Online] Available: http://en.wikipedia.org/wiki/Moore's_law
- [29] G.A. MacDonald, "A review of low cost accelerometers for vehicle dynamics," *Sensor. Actuat. A-Phys.*, vol. 21, pp. 303–307, 1990.
- [30] J. S. Burdess, A. J. Harris, J. Cruickshank, D. Wood and G. Cooper, "A review of vibratory gyroscopes," *Eng. Sci. Educa. J.*, vol. 3, pp. 249–254, 1994.
- [31] P. Muralt, "Ferroelectric thin films for micro-sensors and actuators: A review," *J. Micromech. Microeng.*, vol. 10, pp. 136–146, 2000.
- [32] W. P. Eatony and J. H. Smith, "Micromachined pressure sensors: Review and recent developments," *Smart Mater. Struct.*, vol. 6, pp. 530–539, 1997.

- [33] A. A. Tseng, A. Notargiacomo, and T. P. Chen, "Nanofabrication by scanning probe microscope lithography: A review," *J. Vac. Sci. Technol. B*, vol. 23, pp. 877–894, 2005.
- [34] F. Watt, A. A. Bettiol, J. A. V. Kan, E. J. Teo, and M. B. H. Breese, "Ion beam lithography and nanofabrication: A review," *Int. J. Nanosci.*, vol. 04, pp. 269–287, 2005.
- [35] J. Pascual, J. Camassel, and H. Mathieu, "Resolved quadrupolar transition in TiO_2 ," *Phys. Rev. Lett.*, vol. 39, pp. 1490–1493, 1977.
- [36] S. U. M. Khan, M. Al-Shahry, and W. B. Ingler Jr., "Efficient photochemical water splitting by a chemically modified n- TiO_2 ," *Science*, vol. 297, pp. 2243–2245, 2002.
- [37] M. Ni, M. K. H. Leung, D. Y. C. Leung, and K. Sumathy, "A review and recent developments in photocatalytic water-splitting using TiO_2 for hydrogen production," *Renew. Sust. Energ. Rev.*, vol. 11, pp. 401–425, 2007.
- [38] M. R. Hoffmann, S. T. Martin, W. Choi, and D. W. Bahnemann, "Environmental applications of semiconductor photocatalysis," *Chem. Rev.*, vol. 95, pp. 69–96, 1995.
- [39] U. Bach, D. Lupo, P. Comte, J. E. Moser, F. Weissörtel, J. Salbeck, H. Spreitzer, and M. Grätzel, "Solid-state dye-sensitized mesoporous TiO_2 solar cells with high photon-to-electron conversion efficiencies," *Nature*, vol. 395, pp. 583–585, 1998.
- [40] R. Ali and S. H. Hassan, "Degradation studies on paraquat and malathion using TiO_2/ZnO based photocatalyst," *Malaysian J. Anal. Sci.*, vol. 12, pp. 77–87, 2008.
- [41] R. Benedix, F. Dehn, J. Quaas, and M. Orgass, "Application of titanium dioxide photocatalysis to create self-cleaning building materials," *Lacer*, vol. 5, pp. 157–167, 2000.
- [42] M. Yu, Z. Wang, H. Liu, S. Xie, J. Wu, H. Jiang, J. Zhang, L. Li, and J. Li, "Laundering durability of photocatalyzed self-cleaning cotton fabric with TiO_2 nanoparticles covalently immobilized," *ACS Appl. Mater. Interfaces*, vol. 5, pp. 3697–3703, 2013.
- [43] W. Shao, D. Nabb, N. Renevier, I. Sherrington, and J. K. Luo, "Mechanical and corrosion resistance properties of TiO_2 nanoparticles reinforced Ni coating by electrodeposition," *IOP Conf. Series: Mat. Sci. Eng.*, vol. 40, pp. 012043, 2012.
- [44] N. Suketa, T. Sawase, H. Kitaura, M. Naito, K. Baba, K. Nakayama, A.

- Wennerberg, and M. Atsuta, "An antibacterial surface on dental implants, based on the photocatalytic bactericidal effect," *Clinical Implant Dentistry and Related Research*, vol. 7, pp. 105–111, 2005.
- [45] M. Song, C. Pan, J. Li, X. Wang, and Z. Gu, "Electrochemical study on synergistic effect of the blending of nano TiO₂ and PLA polymer on the interaction of antitumor drug with DNA," *Electroanalysis*, vol. 18, pp. 1995–2000, 2006.
- [46] R. Sabetrsekh, H. Tiainen, S. P Lyngstadaas, J. Reseland, and H. Haugen, "A novel ultra-porous titanium dioxide ceramic with excellent biocompatibility," *J. Biomat. App.*, vol. 25, pp. 559–580, 2010.
- [47] Q. Li, G. Luo, and J. Feng, "Direct electron transfer for heme proteins assembled on nanocrystalline TiO₂ film," *Electroanalysis*, vol. 13, pp. 359–363, 2001.
- [48] E. Reck and S. Seymour, "The effect of TiO₂ pigment on the performance of paratoluene sulphonic acid catalysed paint systems," *Macromolecular Symposia*, vol. 187, pp. 707–718, 2002.
- [49] J. Lademann, H.-J. Weigmann, C. Rickmeyer, H. Barthelmes, H. Schaefer, G. Mueller, and W. Sterry, "Penetration of titanium dioxide microparticles in a sunscreen formulation into the horny layer and the follicular orifice," *Skin Pharmacol Appl Skin Physiol*, vol. 12, pp. 247–256, 1999.
- [50] O. Diwald, T. L. Thompson, T. Zubkov, E. G. Goralski, S. D. Walck, and J. T. Yates Jr., "Photochemical activity of nitrogen-doped rutile TiO₂(110) in visible light," *J. Phys. Chem. B*, vol. 108, pp. 6004–6008, 2004.
- [51] T. Umebayashi, T. Yamaki, H. Itoh, and K. Asai, "Band gap narrowing of titanium dioxide by sulfur doping," *Appl. Phys. Lett.*, vol. 81, pp. 454–456, 2002.
- [52] N. Serpone and D. Lawless, "Spectroscopic, photoconductivity, and photocatalytic studies of TiO₂ colloids: Naked and with the lattice doped with Cr³⁺, Fe³⁺, and V⁵⁺ cations," *Langmuir*, vol. 10, pp. 643–652, 1994.
- [53] A. Monnier and J. Augustynski, "Photoelectrolysis of water: Photoresponses of nickel, chromium and zinc-doped polycrystalline TiO₂ electrodes," *J. Electrochem. Soc.*, vol. 127, pp. 1576–1579, 1980.
- [54] R. Hahn, F. Schmidt-Stein, J. Salonen, S. Thiemann, Y. Song, J. Kunze, V.-P. Lehto, and P. Schmuki, "Semimetallic TiO₂ nanotube," *Angew. Chem.*, vol. 121, pp. 7372–7375, 2009.

- [55] Y.-C. Nah, A. Ghicov, D. Kim, S. Berger, and P. Schmuki, "TiO₂-WO₃ composite nanotubes by alloy anodization: Growth and enhanced electrochromic properties," *J. Am. Chem. Soc.*, vol. 130, pp. 16154–16155, 2008.
- [56] Y. Hou, X. Li, X. Zou, X. Quan, and G. Chen, "Photoelectrocatalytic activity of a Cu₂O-loaded self-organized highly oriented TiO₂ nanotube array electrode for 4-chlorophenol degradation," *Environ. Sci. Technol.*, vol. 43, pp. 858–863, 2009.
- [57] D. P. Macwan and P. N. Dave, "A review on nano-TiO₂ sol-gel type syntheses and its applications," *J. Mater. Sci.*, vol. 46, pp. 3669–3686, 2011.
- [58] J. A. Riaz, *Advantages of nanotechnology-Features of nanotechnology-Uses of nanotechnology*. [Online]. Available: <http://www.wifinotes.com/nanotechnology/advantages-of-nanotechnology.html>
- [59] MEMSnet. *Material: Titanium Oxide (TiO₂), bulk*. [Online]. Available: <http://www.memsnet.org/material/titaniumoxidetio2bulk/>
- [60] C.R. Ottermann, R. Kuschnerreit, O. Anderson, P. Hess, and K. Bange, "Young's modulus and density of thin TiO₂ films produced by different methods," *MRS Proceedings*, vol. 436, pp. 251–256, 1996.
- [61] T. Shokuhfar, G. K. Arumugam, P. A. Heiden, R. S. Yassar, and C. Friedrich, "Direct compressive measurements of individual titanium dioxide nanotubes," *ACS Nano*, vol. 3, pp. 3098–3102, 2009.
- [62] Azom. *Titanium dioxide - Titania (TiO₂)*. [Online]. Available: <http://www.azom.com/article.aspx?ArticleID=1179>
- [63] K. M. Reddy, S. V. Manoramaa, A. R. Reddy, "Bandgap studies on anatase titanium dioxide nanoparticles," *Mat. Chem. Phys.*, vol. 78, pp. 239–245, 2002.
- [64] K. Shankar, J. I. Basham, N. K. Allam, O. K. Varghese, G. K. Mor, X. Feng, M. Paulose, J. A. Seabold, K.-S. Choi and C. A. Grimes, "Recent advances in the use of TiO₂ nanotube and nanowire arrays for oxidative photoelectrochemistry," *J. Phys. Chem. C*, vol. 113, pp. 6327–6359, 2009.
- [65] L. Yang, S. Luo, Q. Cai, and S. Yao, "A review on TiO₂ nanotube arrays: Fabrication, properties, and sensing applications," *Chinese Science Bulletin*, vol. 55, pp. 331–338, 2010.
- [66] V. Zwillling, E. Darque-Ceretti, A. Boutry-Forveille, D. David, M. Y. Perrin, and M. Aucouturie, "Structure and physicochemistry of anodic oxide films on titanium and TA6V alloy," *Surf. Interface Anal.*, vol. 27, pp. 629–637, 1999.

- [67] V. Zwillig, M. Aucouturier, and E. Darque-Ceretti. "Anodic oxidation of titanium and TA6V alloy in chromic media. An electrochemical approach," *Electrochim. Acta*, vol. 45, pp. 921–929, 1999.

CHAPTER 2

TECHNICAL BACKGROUND

This chapter provides a brief description on the need for alternative fuel (which is the motive for researching applications of TiO₂ nanotubes (T-NT)), a literature review on materials used for water splitting, a literature review of polymorphs of TiO₂, reported methods for synthesis of T-NT, and applications of TiO₂ nanotubes/nanoparticles. The polymorphs reviewed of TiO₂ are anatase, rutile, and brookite. The nanotube synthesis methods reviewed are the sol-gel technique, hydrothermal method, electrochemical anodization technique, and template-assisted synthesis. It provides an overview on various applications demonstrated by TiO₂ nanotubes such as with a photocatalysis, solar cells, drug delivery, and sensors, with a particular emphasis on photoelectrochemical water splitting.

2.1 Need for alternative fuel

Fossil fuel such as crude oil, coal, and gas, which are nonrenewable sources of fuel, is rapidly diminishing along with an increase in the world population. According to an article published in Energy Policy, “When will fossil fuel reserves be diminished?” [1], the world’s fossil fuel reserve may diminish in 35, 37, and 107 years for oil, gas, and coal, respectively. Along with the issue of diminishing fossil fuels, the use of fossil fuel adds to the problem of global warming. The Earth’s surface temperature has increased by 0.8 °C, of which 0.6 °C has happened in the last 30 years [2]. Due to global warming the polar ice caps are melting, resulting in a rise of the sea level [3]. This is alarming, and there is a need for alternative fuel which reduces greenhouse effects and is renewable. There are several alternative fuel sources: biofuel [4], biomass [5], ammonia [6], hydrogen [7], compressed air [8], solar cell [9], and windmills [10]. Among all these fuel

types, which have little or no greenhouse gas effect, a lot of research has also been focused on fuels that have clean combustion. Hydrogen is one of the promising alternate sources of clean energy. The biggest advantage of hydrogen is, upon combustion, it is converted to water vapour which is not a greenhouse gas and has no effect on global warming. Another challenge is in the production of hydrogen without having the greenhouse effect.

Hydrogen is abundant in the universe making up 75% of the universe's baryonic mass [11]. The Earth's atmosphere consists of 0.000055%, making it a trace material in the air [12]. Different methods are used for generating hydrogen since the use of hydrogen is not just limited to an alternative to fossil fuel. In a laboratory, hydrogen can be produced in a Kipp's apparatus by a reaction between a nonoxidizing acid and reactive metals such as zinc [13]. In industries and large scale production, hydrogen is generated from hydrocarbons such as methane and coal [14]. Use of hydrocarbon will also not reduce greenhouse gases and hence, will not form a source of clean energy. However, water is made of hydrogen and oxygen and can be used for generating hydrogen as well as oxygen by splitting water. In addition, hydrogen has applications such as in upgrading fossil fuels [15], in production of ammonia [16], as a coolant in turbo generators [17], etc., making it an important source of energy.

2.2 Methods used in water splitting

Production of hydrogen using clean zero emission methods to result in hydrogen economy is still in a prototype phase [18], [19]. A lot of research is being done in production of hydrogen using zero emission methods [20] and water splitting is one of

the approaches [21]. Water splitting is a chemical reaction in which water is converted into hydrogen and oxygen. Electrolysis is one of the methods in which water is split into hydrogen and oxygen by passing an electric current through the water [22]. In this method, when sufficient potential is applied between the anode and cathode, hydrogen will be produced in the cathode and oxygen in the anode. Pure water requires a large potential for water splitting (~ 1.3 V is the minimum theoretical value [23]), which makes it a less feasible method even when a conductive electrolyte such as KOH solution is used. To overcome the need for a high electric potential, electrolysis can be carried out in a high temperature environment where the efficiency can be increased by 50% [24]. The method is similar to low temperature electrolysis, but some of the energy required for water splitting is provided by thermal energy where nuclear thermal power or solar thermal energy can be used as the thermal source (solar is a renewable source of energy making it a preferred method). In another approach, a membrane is used in the electrolyzer where the hydrogen output is at pressure, which is called high-pressure electrolysis [25]. In this approach the added advantage is the need for an external compressor for storing hydrogen is removed. However, these are not zero emission hydrogen generation methods. The approach to zero emission methods is to integrate solar energy with the water splitting such as photoelectrochemical cell (PEC) water splitting or photocatalytic water splitting. In this technique, the solar energy is converted to hydrogen (by splitting water into hydrogen and oxygen) which is used as the energy source. The advantage of this technique is that most of the materials used such as the electrolyte can be recycled [21]. In this technique, the anode is illuminated with solar light (electromagnetic radiation), and the absorbed solar energy is used for water

splitting. Usually, semiconductor materials, such as TiO_2 [21], with a wide band gap are used as the photoanode. Three kinds of setup are used in which (1) the photoanode is an n-type semiconductor and the cathode is a corrosion resistant metal [21], [26], (2) the photoanode is an n-type semiconductor and the cathode is a p-type semiconductor [26], or (3) the photoanode is a p-type semiconductor and the cathode is metal [26]. Another zero emission approach is photobiological water splitting [27]. In this technique, algae are used in converting solar energy to hydrogen fuel in a controlled environment. Under certain conditions (deprived of sulfur) algae would emit hydrogen. However, this method has certain draw backs such as accumulation of proton gradient and efficiency, limiting its practical applications. Table 2.1 provides an overview of different techniques used in water splitting.

2.3 Materials used in photoelectrochemical water splitting

The ideal material for water splitting is the one which is stable and chemically inert in an aqueous medium and does not undergo light assisted corrosion. Also, wide band gap materials (semiconductors) are required which upon absorption of light will produce electron and hole pairs. With wide band gap materials the lifetime of the charge carriers will be longer, reducing the recombination of charges. However, with wide band gap materials, there is a reduction in the absorption range of the solar spectrum. Materials with a band gap of > 3 eV, have no absorption of the visible range of the solar spectrum, and would only absorb the ultra violet range which is $\sim 6\%$ of the total solar spectrum on the surface of the Earth. Therefore, a lot of research is being done in modifying and optimizing the material to have high efficiency, a wide absorption range in the solar

Table 2.1: Comparison of different techniques used in water splitting

	Electrolysis	High temperature electrolysis	High pressure electrolysis	Photoelectrochemical	Photobiological
Technique	High electric field is used to split water	Electric field + thermal energy is used	Electric field + high pressure is used	Solar energy + photocatalyst	Solar energy + algae
Advantages	Simple technique	Solar energy is used for thermal energy	External hydrogen compressor is eliminated	Clean method since solar energy is used	Clean method since solar energy is used
Disadvantages	Low yield and high electric field required	Not a very clean method and high electric field required	Pumping of electrolyte to high pressure	Low yield and requires catalyst to be inert in aqueous medium	Low yield and controlled environment for algae is required

spectrum, stability and corrosion resistance in an aqueous medium, and a high charge carrier life time (to reduce losses due to recombination). Zou *et al.* reported visible light water splitting using $\text{In}_{1-x}\text{Ni}_x\text{TaO}_4$ ($x=0-0.2$), which was one of first reports on a photo corrosion resistant material [28]. The absorption edge was at >420 nm with quantum efficiency of 0.66%. The photoactive anode was tested for 400 hours and there was no change in the performance of the cell. In another report, Khaselev *et al.* reported 12% efficiency in water splitting using a $\text{GaInP}_2/\text{GaAs}$ p/n, p/n tandem cell device [29]. Similarly, various materials such as NaTaO_3 [30], Cu_2O [31], Fe_2O_3 [32], $\text{K}_2\text{La}_2\text{Ti}_3\text{O}_{10}$ [33], $\text{Ni}_{0.5}\text{Mn}_{0.5}\text{Fe}_2\text{O}_4$ [34], WO_3 [35], In_2O_3 [36], GaAsP [37], GaP [37] and ZnO [38], have been used for water spitting. Table 2.2 lists some of the commonly used semiconductor material (other than TiO_2) in PEC water splitting. A review of TiO_2 nanotubes based on PEC water spitting is presented in the subsequent section.

2.4 Polymorphs of TiO_2

Commonly, TiO_2 occurs naturally; mainly in three polymorphs called rutile, anatase, and brookite. A comparison of the properties of the three polymorphs is provided in Table 2.3. Rutile and anatase both consists of a tetrahedral crystal system, but the anatase has octahedrons that share four edges forming the four-fold axis form making it different from rutile [39]. Brookite consists of an orthorhombic crystal system [40]. The crystal structure of rutile, anatase, and brookite is shown in Fig. 2.1. Rutile is the most common form of TiO_2 . When viewed in transmitted light, rutile is deep red hence the name rutile, which is derived from the Latin word *rutilus* meaning red. Rutile is odorless in nature and the most stable polymorph of TiO_2 . Other polymorphs of TiO_2 can be changed to rutile

Table 2.2: Commonly used semiconductor material in PEC water splitting

Photocatalyst	Co-catalyst / dopant	Morphology	Electrolyte	Band gap (eV)	ref
NaTaO ₃	Lanthanum	nanoparticle	Silver nitrate + water + methanol + NaOH	4	[30]
Cu ₂ O	None	nanoparticle	Water	2.2	[31]
Fe ₂ O ₃	Si	Thin film	NaOH soln	2.1	[32]
K ₂ La ₂ Ti ₃ O ₁₀	Ni	nanoparticle	KOH soln	3.5	[33]
Ni _{0.5} Mn _{0.5} Fe ₂ O ₄	None	microparticles	Water	N/A	[34]
WO ₃	Mg	Powder	NaOH	2.25	[35]
In ₂ O ₃	Nitrogen	Thin film	KOH soln	2	[36]
GaAsP	Nitrogen	Thin film	KOH soln	1.8	[37]
GaP	Nitrogen	Thin film	KOH soln	2	[37]
ZnO	Nitrogen	Nanorod	NaClO ₄	3.3	[38]

Table 2.3: Comparison of the rutile, anatase, and brookite polymorphs of TiO₂

	Rutile	Anatase	Brookite
Crystal structure	Tetragonal	Tetragonal	Orthorhombic
Unit cell (Å)	$a = b = 4.584,$ $c = 2.953$	$a = b = 3.7845,$ $c = 9.5143$	$a = 5.4558, b =$ $9.1819, c = 5.1429$
Color under transmitted light	deep red	yellow to blue	yellowish brown to dark brown
Density	4.25	3.899	4.1
Unit cell volume (Å³)	62.43	136.27	257.63
Refractive index	2.6	2.49	2.58

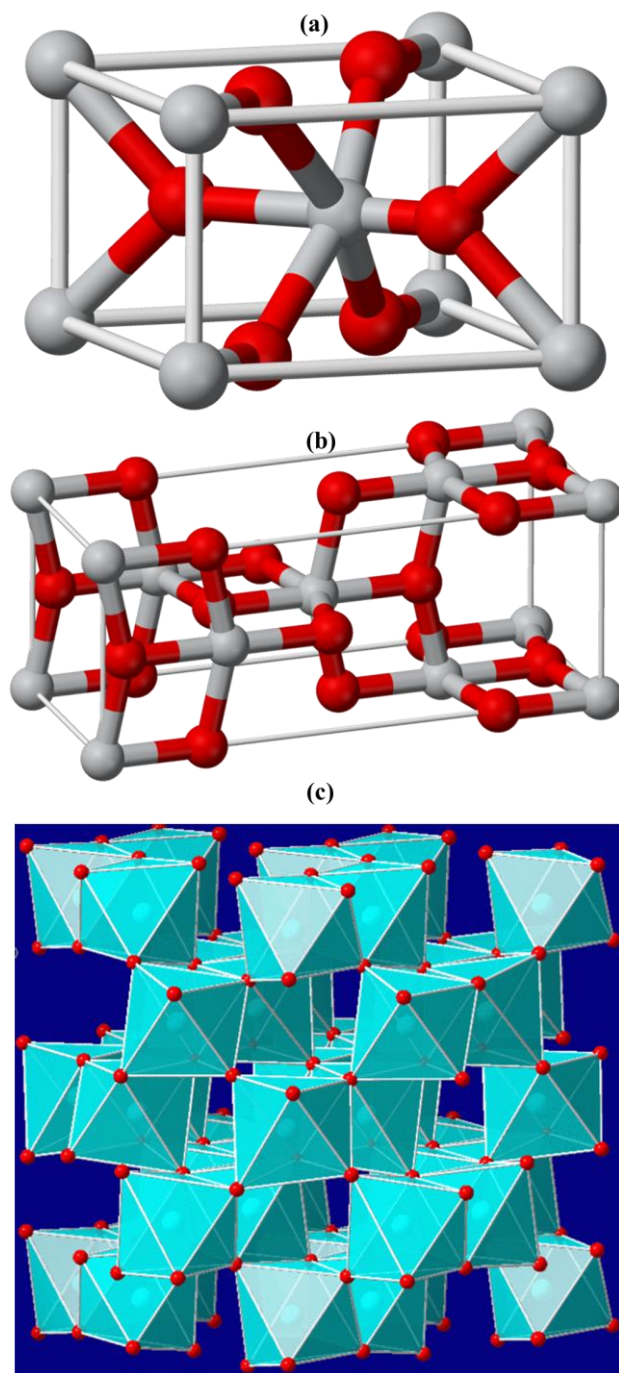


Figure 2.1: The crystal structure of rutile, anatase, and brookite TiO₂. (a) Rutile TiO₂ where the Ti atoms are gray and O atoms are red.[41] (b) Anatase TiO₂ where Ti atoms are gray and O atoms are red. [42] (c) Brookite TiO₂ where Ti atoms are blue and O atoms are red [40].

polymorph by high temperature annealing, and the process is irreversible [43]. The unit cell of rutile which is tetragonal in shape has the following dimensions of $a = b = 4.584$ Å, and $c = 2.953$ Å [42]. The calculated volume cell is 62.43 Å³. Rutile is the densest polymorph of TiO₂. Its calculated density value is 4.250 g/cm³ [45]. The refractive index of rutile TiO₂ is 2.6 [46]. It is transparent in visible light and is effective in absorbing of ultra violet (UV) light. Hence, they are used in sunlight lotions since they absorb UV light and help in protecting the skin.

Anatase is derived from the Greek *ανάτασις* (*anataxis*) for extension since its pyramidal faces are longer compared to the relation of their base length when compared with other tetragonal minerals [39]. Anatase is yellow to blue in color when viewed in transmitted light [47]. Anatase is not stable at high temperatures and when annealed at temperatures above 550 °C will transform to rutile TiO₂ [48]. Anatase is less dense compared to the rutile polymorph with its calculated density value of 3.899 g/cm³ [47]. The free energy of anatase at all temperatures is higher than that of rutile, making rutile a relatively more stable polymorph of TiO₂. The unit cell of anatase which is orthorhombic in shape has the following dimensions of $a = b = 3.7845$ Å, $c = 9.5143$ Å [47]. The calculated volume of the unit cell is 136.27 Å³. The refractive index of anatase TiO₂ is 2.488 [49]. Rutile has a higher absorption property compared to anatase. However, both rutile and anatase forms of TiO₂ are used in daily applications demonstrated by TiO₂.

Brookite is named after Henry James Brooke (1771-1857) who was an English crystallographer and mineralogist. Brookite transforms into rutile when annealed at temperatures above 750 °C [50]. The free energy of brookite at all temperatures is higher than that of rutile but it has a lower free energy than that of anatase, making it the second

most stable polymorph of TiO₂. The unit cell of brookite which is tetragonal in shape has the following dimensions $a = 5.4558 \text{ \AA}$, $b = 9.1819 \text{ \AA}$ and $c = 5.1429 \text{ \AA}$ [51]. The refractive index of brookite is 2.58 to 2.7 [40]. Brookite has the largest unit cell volume. The density of brookite is 4.1 g/cm^3 , which is lower than that of rutile but higher than that of anatase, making brookite the second densest polymorph of TiO₂. It is yellowish brown to dark brown when viewed in transmitted light [52]. Both brookite and rutile polymorphs of TiO₂ have a refractive index higher than that of a diamond, making them materials of high luster. Their mechanical properties are similar to that of rutile, but it is the least naturally found polymorph of TiO₂ and hence has had very little commercial use.

2.5 Reported methods for synthesis of TiO₂ nanotubes

This section provides a technical review on the reported techniques used for synthesis of TiO₂ nanotubes. The methods reviewed are the sol-gel technique, hydrothermal method, electrochemical anodization, and template-assisted. Table 2.4 provides a comparison of the mentioned nanotube synthesis techniques.

2.5.1 Sol-Gel

Sol-gel is a wet chemical technique used for producing nanosized solid materials from small molecules [53]. The chemical process consists of converting a solution (sol) into a gel like form. The gel consists of both a solid and liquid phase. Another approach in the sol-gel technique is to use the colloid form of the material in the liquid where the liquid percentage is reduced to obtain the gel like phase. When in gel phase, the

Table 2-4: Comparison of the TiO₂ nanotube synthesis techniques

	Sol-gel	Hydrotherm- al	Electrochemi- cal anodization	Template assisted
Technique	Wet chemical technique of converting solution into a gel	Crystallizing substance at high temperature and high vapor pressure	Anodic potential is applied to metal in the presence of an electrotype	Nanoporous mold's wall is coated and then the mold is etched
Temperat- ure (°C)	Room temperature	100 to 200	Room temperature	Room temperature
Type	Anatase, rutile, brookite	Anatase, rutile, brookite	Anatase, rutile	Anatase, rutile
Tube length (nm)	Few 100	Few 100	Up to 220 000	Few 100
Features	Powder form	Random powder form	Amorphous	Powder form
Advantages	Low cost and low temperature	Simple technique and properties of nanotube can be changed	Desirable for most application, high aspect ratio and can be synthesized from thin films	Low contamination and the tube diameter can be controlled
Disadvan- tages	Reduced charge transport	Long reaction time, NaOH contamination and non-uniformity	Fluoride ion contamination, limited mass production and expensive	Complicated fabrication process and tube morphology can be destroyed

remaining liquid/solvent is removed by a process called drying. The rate at which the drying is carried out will define the morphology of the resulting nanosized material. Thermal treatment is followed after the drying process. This is done to improve the stability and mechanical properties of the nanosized material. The substance which takes part in the chemical reaction can be deposited on a substrate to form a thin film or cast into a mold based on the requirement of the desired shape of the nanosized materials. The advantage of the sol-gel technique is that it is a low cost and low temperature process. The sol-gel technique can be used to fabricate membranes [54], nano/microspheres [55], nanofibers [56], and nanotubes [57].

In one of the reports, TiO₂ nanotube arrays were synthesized via the sol-gel technique using alumina membrane [58]. A solution consisting of titanium isopropoxide and 2-propanol was used for obtaining the nanotubes arrays. The solution was poured onto an alumina membrane with a pore size of 200 nm and treated. The alumina template was dissolved to get the TiO₂ nanotube arrays. This method has the advantage of changing the diameter of the nanotube by changing the diameter of the nanotemplate. Also, the smoothness of the outer wall of nanotubes can be very uniform by having the pores of the template uniform. In another approach, TiO₂ nanotubes were synthesized using two solutions [59]. The first solution consisted of titanium isopropoxide and ethanol. The second solution consisted of ethanol, water, and acetylacetone. The second solution was slowly added to the first solution to form TiO₂ sol. Porous alumina was used as the template to synthesize the nanotubes. Using the same technique, the molar ratio of solution 1 and 2 was changed to synthesis nanorods, which demonstrates the flexibility of the method. Using the sol-gel process, other nanotubes such as ZnO [60] and silicon

dioxide [59] can also be synthesized.

2.5.2 Hydrothermal method

The first report of the hydrothermal growth of crystals was by German geologist Karl Emil in 1845 [62]. The hydrothermal method is a process of crystallizing a substance at a high temperature and high vapor pressure using an aqueous solution of the material [62]. The hydrothermal method can be used to synthesize a single crystal of the material depending on the solubility of the material in the solvent. Single crystal growth is done in a high pressure vessel called an autoclave. These are hermitically sealed steel vessels that can withstand high temperatures and pressure for long durations. Also, the vessel must be chemically inert and must not take part in the hydrothermal process. A number of substances such as oxides [63], tungstates [64], molybdates [65], carbonates [66], and silicates [67] can be synthesized. The different approaches in the hydrothermal technique can be broadly classified as temperature-difference technique, temperature-reduction technique and metastable-phase technique [68]. Temperature-difference technique is a method in which the autoclave is heated to two temperature zones. The solute dissolves in the hotter zone (lower part) and the saturated solution moves from the lower part to the upper part (at a relatively lower temperature) due to the difference in temperature. The cooler solution in the upper portion descends to the lower part resulting in a counter flow. Eventually, the solution in the upper part becomes supersaturated due to the reduction in temperature and the material starts to crystallize. Temperature-reduction technique is a method in which instead of having the two temperature zones, the autoclave is slowly cooled down with the saturated solution inside it. However, this technique has the

disadvantage of difficulty in controlling the growth process. Metastable-phase technique is a method based on the difference in solubility between the crystal growth phase and that serving as the starting material. The solution consists of compounds that are thermodynamically unstable under the growth conditions. The solubility of the compounds that are in the metastable phase is more than that of its stable phase. The compounds crystallize due to the decomposition of the metastable phase.

Various groups have demonstrated synthesis of TiO_2 nanotubes using the hydrothermal technique. Myahkostupov demonstrated a dye-sensitized solar cell using TiO_2 nanotubes synthesized using hydrothermal technique [69]. Anatase TiO_2 nanoparticles were dispersed in water under ultrasonication. TiO_2 mixture with NaOH solution was placed in a nonreactive autoclave and heated to 150 °C for 24 hours. On cooling to room temperature, white gel-like crude TiO_2 nanotubes were obtained. The TiO_2 nanotubes were separated by centrifugation followed by washing with 0.1 M HCL and water. The nanotubes were dried and then used for dye-sensitized solar cell. The yield of TiO_2 nanotubes was greater than 90%. Using a similar experimental procedure and chemistry, Kolen'ko *et al.* demonstrated the synthesis of TiO_2 nanorods [70]. In another approach, thin film TiO_2 nanotubes were synthesized via the hydrothermal process [71]. A TiO_2 suspension using TiO_2 powder and deionized water was prepared. The suspension was centrifuged to remove coarse particles. TiO_2 suspension was deposited on a titanium substrate through dip coating at room temperature. The coated substrates were then hydrothermally reacted in an alkaline aqueous solution containing 10 M NaOH in an autoclave reactor with temperature ranging from 110 to 150 °C. The substrate was then cleaned in deionized (DI) water and dried. In another report, TiO_2

nanotubes were synthesized by obtaining titanium hydroxide precipitates by adding ammonia hydroxide solution drop wise to the aqueous TiCl_4 solution [72]. The precipitate was washed in DI water five times and filtered to form a wet gel. The gel was dried and heat treated to form TiO_2 nano powder. The TiO_2 nano powder was mixed with TiO_2 sodium hydroxide to be heat treated in an autoclave followed by treatment with (hydrochloric acid) HCl and water to form nanotubes. By varying the starting material composition and by varying the annealing temperature, the group demonstrated that the morphology of the nanotubes can be varied. Cui *et al.* demonstrated microwave-assisted hydrothermal synthesis of TiO_2 nanotubes [73]. The TiO_2 nanotubes were synthesized on porous nickel foam. The substrate was immersed in a solution containing TiO_2 powders, de-ionized water and polyvinyl alcohol to form a TiO_2 coat on the substrate. The substrate was then placed in a sodium hydroxide solution and irradiated using microwaves. It was shown that by changing the irradiation time, NaOH solution concentration, and immersion time, the morphology of the TiO_2 can be varied from nanoparticles to nanotubes. Similarly, sonic assisted hydrothermal synthesis of TiO_2 nanotubes has also been demonstrated [74]. Also, with the presence of Na_2S during the hydrothermal reaction, composite nanotubes can be synthesized [75]. With the use of urea and thiourea during the hydrothermal reaction, doped TiO_2 nanotubes can be synthesized [76]. With the presence of H_2O_2 during the hydrothermal reaction, relatively more ordered nanotubes can be synthesized [77].

In conclusions, the advantages of the hydrothermal method are that it is an easy method to obtain nanotube morphology, variation in the synthesis method can be implemented to enhance the properties of TiO_2 nanotubes, and it is feasible for a lot of

applications. However, the disadvantages are a long synthesis duration, the need for a highly concentrated NaOH solution (contaminating the TiO₂ nanotubes with NaOH) and precisely controlling the diameter of the nanotubes [78].

2.5.3 Electrochemical anodization

Anodization is the process of increasing the metal oxide on the surface of metals [79]. Anodization is possible for metals such as aluminum [80], niobium [81], tantalum [82], titanium [83], [84], tungsten [85], and zirconium [86], which belong to the category called valve metals or transition metals. When sufficient anodic potential is applied to metal in the presence of an electrolyte (usually water which is the source of oxygen), the metal is converted to metal oxide. The oxide growth rate will slow down and self-passivate as the thickness increases. The thickness reached depends on the electrolyte, metal, and the applied potential. By modifying the electrolyte, the metal-oxide can be also be etched as it is grown. By having the etch direction be selective, we can synthesis nanopores and nanotubes. The electric field is used to define the etch direction in forming nanopores and nanotubes. When a sufficient anodic potential is applied to the metal in the electrolyte, the metal loses electrons (to become positively charged). Based on the electrolyte, the metal ion can be dissolved in the electrolyte (which can be used for polishing the metal surface) [87], react with the electrolyte to form a metal oxide (oxygen source from the electrolyte) where the metal oxide layer is stable (does not dissolve in the electrolyte) [88], or simultaneous oxidation as well as selective dissolution can occur [83], [84]. When anodized in alkaline or a neutral electrolyte a passive metal oxide layer is formed. However, when an acidic solution is used, then simultaneous oxidation as well

as selective dissolution would occur (not always true in the case of acidic solution). By controlling the anodization parameters, self-assembling arrays of nanotubes and nanopores can be synthesized. The advantages of the electrochemical anodization method are that it is the most desired method for practical applications, has ordered arrays, and is feasible for a wide range of applications. The disadvantages of this method are that the mass production capability is limited, fluoride ions are required, and it is relatively more expensive.

2.5.3.1 Initial reports on synthesis of TiO₂ nanotubes

Zwilling *et al.* in the year 1999 first reported the synthesis of TiO₂ nanotubes using electrochemical anodization [83], [84]. However, the authors stated the synthesized structure was porous rather than tubular in structure. The self-organized TiO₂ nanotubes arrays were synthesized on Ti substrate using a chromic acid and hydrofluoric acid solution. It was shown that the presence of fluoride ions, in the electrolyte, was necessary for synthesis of the nanotubes. Without the presence of fluoride ions the film would self-passivate with a thick (thick enough to prevent the diffusion of oxygen for further anodization) TiO₂ layer. Fluoride ions play an antidote role (relative to the role of chromic acid) where it etches the TiO₂. There is competitive etching and oxidation by the electrolyte to form nanotubes. It was shown that with the increase in the anodization potential the diameter of the nanotubes would increase. The walls of the nanotubes were contaminated with fluoride ions. The amount of fluoride ions present is important since excess ions would overtake the oxidation process and just polish the Ti substrate. Since then a lot of work has been done to understand and improve the synthesis of TiO₂

nanotubes using fluoride based electrolytes [89]. Later reports showed that the length of the tube is limited due to the equilibrium that is established in the etching and oxidation [89]. The nanotubes elongate along the bottom of the tubes. However, there is etching of TiO_2 by the electrolyte in all directions (more selectively in the direction of the electric field). Therefore, the walls of the nanotubes would become thinner and eventually a portion of the nanotube would be etched, limiting the length of the nanotube. Since the upper portion of the nanotubes is exposed to the electrolyte for a longer duration compared to the lower portion, the nanotubes have walls with a tapered structure with the thickness increasing from the lower to the upper portion [90]. Nanotubes as long as 250 μm have been reported [91]. The pH of the electrolytes plays an important role in defining the length of the nanotubes. It is shown the more neutral the electrolyte is, the longer the nanotubes are that can be synthesized. Also, the walls of nanotubes are relatively thicker when compared to a low pH (acidic) electrolyte. This is because when the pH is near neutral the etching of the TiO_2 is defined by the direction of the electric field, and there is very little undesired etching by the electrolyte. Therefore, it is demonstrated that the use of organic electrolytes is better in order to have longer nanotubes and thicker walls since the pH of the electrolyte would be near neutral.

2.5.3.2 Growth mechanism

There are three stages during the growth of TiO_2 nanotubes via electrochemical anodization, and they are explained in detail in this section. In the absence of fluoride ions, the reactions that occur can be described using the following equations [89].





Equation 1 shows the formation of Ti ions when a sufficient potential is applied to the metal. Equations 2, 3, and 4 show the reaction of Ti with water to form TiO_2 which is in the presence of an electric field. The equation also represents the electric field assisted ion migration of Ti^{4+} and O^{2-} that occurs through the oxide formed at the interface of the Ti metal and electrolyte. Equation 5 shows the reaction occurring at the counter electrode (cathode) which results in the generation of hydrogen. Once a thin layer of TiO_2 is formed, the reaction should stop since it self-protects the Ti metal from the oxygen atoms. However, due to the electric field the negatively charged O^{2-} ions will move against the direction of the electric field and diffuse through the thin layer of TiO_2 and reach the surface Ti metal and oxidize the metal. Therefore, the new layer oxide is grown in the TiO_2 and Ti metal interface. As the oxide grows, the strength of the electric field reduces, in turn, reducing the force that drives the ion migration at the interface. Eventually a finite thickness is reached until the applied electric field cannot drive the ion migration anymore. The finite thickness depends on the applied electric field (the higher the electric field, the thicker the finite layer). Similarly, the Ti^{4+} ions migrate from the Ti metal surface (in the direction of the electric field) through the already present oxide layer to the oxide-electrolyte interface to form TiO_2 and $\text{Ti}(\text{OH})_4$. Therefore, the TiO_2 grows at both interfaces. It should be noted that all the metal-hydroxide will not decompose to form TiO_2 , and hence the oxide formed at the metal-oxide interface is

denser and more stable when compared to the oxide formed at the oxide-electrolyte interface [92]. With the above setup, only an oxide layer of finite thickness is formed and not nanotubes. Therefore, the electrolyte chemistry is modified by the addition of fluoride ions to synthesis nanotubes. The reactions that occur with the presence of fluoride ions can be summarized as follows [89].



Fluoride ions react with Ti to form water soluble $[\text{TiF}_6]^{2-}$ ions. Equation 6 shows that the fluoride ions, also like O^{2-} , migrate through the oxide layer in the direction of the electric field and react with the TiO_2 being formed at the metal-oxide interface and dissolve the TiO_2 . However, the etching will not occur uniformly everywhere and is limited by the electric field. Equation 7 shows that the fluoride ions will also react with the Ti^{4+} which migrates out of the oxide layer at the oxide-electrolyte interface. Based on the amount of fluoride present one of three scenarios will occur. When the fluoride ions' concentration is very low, then the anodization is such that a compact finite layer of TiO_2 will form which would self-passivate without any nanotubes (similar to the case where there are no fluoride ions). If the concentration is too high, then there would be no oxide formed, and the electrolyte would polish the Ti substrate. All the Ti^{4+} will react with the excess fluoride ions that migrate outside the oxide layer. Any TiO_2 that is formed will also be etched by the fluoride ions, and hence there will be no oxide or nanotube formation. When the optimum amount of fluoride ions are present then nanotubes are formed. A competition exists between formation of TiO_2 and dissolution of Ti. During the formation of nanotubes, it consists of three stages [89]. The first stage is similar to the

fluoride free case in which an oxide layer is formed. In this stage, no diffusion of fluoride ions occurs. The second stage consists of the formation of initial pores in the substrate. The pore formation sites would depend on the surface topology of the substrate and would initially begin where the electric field is the highest. Here the electric field assisted migration of fluoride ions is taking place and penetrates the initial oxide layer. The pores formed are irregular in shape. The third stage consists of the phase where a steady state is established and formation of regular nanotubes takes place. In this stage, the electric field is directed from the bottom of the nanotubes. The nanotubes would ideally continue to grow at a constant rate once the third stage is reached. However, due to undesired etching of the wall in the upper portion of nanotubes, it gets thinner and would be completely etched over time. Also, the fluoride ions will diminish in amount, and the nanotubes' formation rate will reduce and may eventually stop. Another factor is that when the nanotubes are very long, diffusion of fluoride ions reduces since the supply of fresh electrolyte to the bottom of the nanotubes reduces thereby slowing down the rate of nanotube formation.

2.5.3.3 Factors impacting the geometry and composition of nanotubes

From the previous section, it is evident that the length of the nanotube is defined by the anodization time for a particular applied voltage and electrolyte. With an increase in voltage, the diameter of the nanotubes would increase [93]. Also, to demonstrate the flexibility, various groups have synthesized nanotubes with varying diameters by varying the potential during the course of anodization instead of constant potential anodization [94]. The diameter also depends on the type of electrolyte. This is because as the

anodization occurs the byproducts formed would change the resistivity of the electrolyte and hence change the effective electric field [95]. Thus, with longer anodization time, the diameter of the tubes may change (for the same voltage) due to the change in the resistivity of the electrolyte. Nonaqueous (organic) electrolyte grown nanotubes have significant differences in terms of morphology and composition when compared to nanotubes grown using aqueous electrolytes. Nanotubes with larger diameters and longer nanotubes can be synthesized using organic electrolytes [96]. This is because the organic electrolytes have lower water content compared to aqueous electrolytes. Water content in the electrolyte plays an important role on the morphology of the nanotubes. When the water content is low, the walls of the nanotubes are smoother, and hence with organic electrolyte, the nanotubes walls are smoother compared to aqueous electrolytes [97]. Also, for some organic electrolytes, the inner walls of nanotubes contaminated with a layer of carbon can be found [98]. This is because some of the organic electrolytes (such as ethylene glycol based electrolyte) break down when anodized above a certain voltage and act as the source for carbon contamination. In the case of aqueous electrolytes, there is hydroxide contamination on the inner walls of the nanotubes [99]. Organic electrolytes require aging where the anodization is carried on the dummy Ti substrates before carrying out the anodization on the actual substrate [95]. This is because with aging, the $[\text{TiF}_6]^{2-}$ ions increase and reduce undesired etching of TiO_2 . Also, most of the organic electrolytes are hygroscopic and absorb water from the atmosphere and reach a steady water content state. When anodized for very long durations, it may lead to the formation of a grass-like structure in the upper portion of the nanotubes where the walls are too thin and collapse on themselves (the tubes may close on the top portion) [100]. Also, the

nanotubes may become perforated due to uneven and undesired etching of the walls. Another important role that water content plays is that on the dissolution rate. With an increase in the water content, dissolution of Ti is faster since the $[\text{TiF}_6]^{2-}$ ions are water soluble. If the water content is too low (<1%), then the nanotubes have a smooth outer wall with no interconnecting membrane (the anodized substrate will have pores rather than tubes) [101]. At optimum water content, the tubes formed will have interconnecting membranes. This is because some of the fluoride ions that are present on the outer wall (present via ion migration) will etch the outer walls and be dissolved by the water. If the water content is low, then dissolution of the $[\text{TiF}_6]^{2-}$ ion by the water is limited on the outer walls of the nanotubes. Therefore, with optimum water content, the anodized substrate will have a nanotube-like structure instead of a nanoporous structure. Therefore, by varying the water content, anodization potential, type of electrolyte, and fluoride content, the morphology and composition of the nanotubes can be modified.

2.5.4 Template-based synthesis

Template-based synthesis is a technique in which a nanoporous material is used as the mold and the desired nanotube material is coated on the walls of the mold. It should be noted that though the sol-gel technique uses a nanoporous mold, most of the groups report them as sol-gel technique and do not emphasize them as template-based synthesis [69]–[71]. There are two approaches for template-based synthesis. One is negative template and the other is positive template. The template is then dissolved to get the nanotubes. If the material of interest is coated on the inner walls, then it is a negative template-based synthesis. If the material is coated on the outer walls of the template then

it is a positive template-based synthesis. In the negative template synthesis, if the pores of the mold are completely filled, then nanorods can be synthesized. The most commonly used template for negative template synthesis is anodic aluminum oxide. Yuan *et al.* showed the synthesis of TiO₂ nanotubes and nanorods using anodic aluminum oxide as a template [102]. The walls of the template were coated using the hydrolysis method. The anodic aluminum oxide was used as the membrane between DI water and the Ti(OC₄H₉)₄ solution in C₄H₉OH during hydrolysis. The thickness of the nanotubes walls were controlled by varying the concentration of Ti(OC₄H₉)₄. Jiang *et al.* reported the synthesis of TiO₂ nanotubes by immersing anodic aluminum oxide in an aqueous ammonium hexafluorotitanate solution [104]. In another report, Michailowski *et al.* showed the synthesis of TiO₂ nanotubes via a thermal decomposition process of Ti(Oi-Pr)₄ using anodic aluminum oxide as a template [106]. Similarly, Liang *et al.* demonstrated the fabrication of TiO₂ nanotubes via atomic layer deposition [105]. Anodic aluminum oxide was used as the template, and TiCl₄ was used as the precursor for the atomic layer deposition of TiO₂. The atomic layer deposition technique is a highly conformal coating process, and the thickness can be controlled very accurately. Therefore, in this method, the thickness of the walls of the nanotube can be controlled very precisely. The entire undesired TiO₂ deposited layer on the top surface of the template is removed by mechanical polishing. Hoyer showed the synthesis of TiO₂ nanotubes using positive template [106]. In this approach, TiO₂ was deposited on poly(methyl methacrylate) nanorod arrays by the electrochemical deposition technique. The nanorods were selectively etched to form TiO₂ nanotubes. The nanorods were, however, fabricated using an anodic aluminum oxide template. Similarly, TiO₂ nanotubes were synthesized using

electrospun poly(L-lactide) fibers as a positive template [107]. Jung *et al.* demonstrated the synthesis of double wall TiO₂ nanotubes which were fabricated by condensing Ti(Oi-Pr)₄ precursors onto both surfaces of the self-assembled organogel tubes [108]. In comparison to negative template-based synthesis, the positive-based template has a better control on the smoothness of the inner and outer wall. The advantage of this template-based synthesis is that the dimensions of the nanotubes can be controlled by controlling the pore dimensions of the template. The disadvantages of this technique are that the fabrication process is relatively more complicated, and the nanotube morphology can be destroyed during fabrication steps such as mechanical polishing.

2.6 Applications of TiO₂ nanotubes

2.6.1 Photocatalysis

Photocatalysis is an accelerated photoreaction in the presence of a catalyst [109]. The reaction is due to the charge carriers produced at the surface of the semiconductor upon absorption of light. The main interest in photocatalysis research is for applications such as converting sunlight into an energy carrier like hydrogen [21] and degrading environmental pollutants [110]. With its ability to synthesis T-NT, TiO₂ is one of the most highly investigated photocatalytic materials due its high resistance photocorrosion, environmentally friendly nature, and wide band gap. The band gap of TiO₂ is ~ 3eV, making it photocatalytic in ultra violet (UV) light. Upon striking the surface UV light excites electrons from the valence band to the conduction band. The generated electron-hole pair will react with the environment which forms the photocatalytic reaction. Another interesting characteristic of TiO₂ is that it successfully transfers charge carriers

to the water due to the position of the valence and conduction band at the surface of the TiO_2 in comparison to the level of the redox potentials of water [111]. For an electron to transfer from the TiO_2 surface to the electrolyte, the oxidized state in the electrolyte has to be energetically lower than the conduction band of TiO_2 . For a hole to transfer from the TiO_2 surface to the electrolyte, the reduced state in the electrolyte has to be energetically higher than the valence band of TiO_2 . Another advantage of TiO_2 over other semiconductor materials is the long electron lifetime with low electron-hole recombination losses [111]. TiO_2 in an electrochemical curve behaves as an n-type semiconductor, and is conductive in cathodic direction and blocks charge transport in the anodic direction [112]. When the TiO_2 is in contact with an electrolyte a junction is formed at the interface. If the Fermi level of the electrolyte is different from the TiO_2 , then band bending will occur forming a Schottky junction. The band bending and Fermi level can be controlled by applying an external potential. For TiO_2 , if anodic potential is applied, then the band bending is increased, and when cathodic potential is applied, the band bending is decreased. For photocatalysis, the higher the band bending, the faster the electron hole separation is and the lower the recombination probability. When light is absorbed by an n-type material, the minority carrier density increases with the generation of an electron hole pair. The electron hole pair can undergo the following fates. They might be transported to the surrounding electrolyte and react, they might recombine in the surface or the bulk of the material, or they may lead to semiconductor dissolution (TiO_2 , however, does not undergo photocorrosion). Based on the generation of the electron hole, the following photocatalytic applications have been demonstrated by TiO_2 nanotubes.

2.6.1.1 Degradation of pollutants

One of the important purposes of research in the field of photocatalysis is to decompose carcinogenic, nonenvironmentally friendly and toxic materials. TiO_2 is widely used for this application since it is one of the most suited materials for the same purpose. Many pollutant materials such as organochlorine compounds [113], aromatic pesticides [114], polychlorinated biphenyl [115], dioxins [115], azo dyes [116] and dichlorodiphenyltrichloroethane [117] can be decomposed to a less pollutant state via photocatalysis using TiO_2 nanotubes/nanoparticles. In addition, they have been demonstrated to decompose gases pollutants also [118]. Bacteria such as *Escherichia coli*, *Staphylococcus aureus*, and *Pseudomonas aeruginosa* can also be destroyed up to a certain extent [119], [120]. TiO_2 is shown to have an antibacterial effect under UV light. Cancer cells can also be destroyed and treated up to a certain extent using a similar property of TiO_2 [121].

2.6.1.2 Water splitting

In 1972, the first report on splitting water into hydrogen and oxygen using TiO_2 was first made [112]. Since then it has attracted a lot of interest because hydrogen is a clean alternative energy source to fossil fuel. The holes and electron pair that are formed react with water to form hydrogen and oxygen. At the conduction band of TiO_2 , the reduction potentials for $\text{O}_2 \rightarrow \text{O}_2^-$ and $\text{H}^+ \rightarrow \frac{1}{2}\text{H}_2$ are competitive. At the valence band of TiO_2 , oxygen from water can be formed. When an external potential (with a suitable cathode) is applied, the efficiency of water splitting by TiO_2 is increased. This is because the slow cathodic reaction of hydrogen evolution can be enhanced by the use of a suitable

electrode such as platinum along with the external potential. Also with the use of a suitable catalyst, such as IrO_2 , and dopants in TiO_2 , the oxygen evolution at the photoanode can be increased [137]. A very low concentration can cause a significant increase in water splitting capability. The generated majority charge carriers have to travel through the nanotubes to reach the base of the nanotube where they are in contact with the external circuit. Therefore, the conductivity of the TiO_2 is important, and hence doping of TiO_2 helps in improving the conductivity and the efficiency. Also by doping, the band gap of TiO_2 is reduced where the photoanode is active under visible light, increasing the absorption spectrum. Table 2.5 shows a list of reports of TiO_2 nanotube based photoelectrochemical water splitting.

2.6.2 Solar cells

Another interesting application of TiO_2 is dye sensitized solar cells (DSSC). The first report on DSSC was with ruthenium bipyridyl sensitization on TiO_2 in the year 1980 [138]. Gratzel and O'Regan used the same principle and fabricated DSSC using TiO_2 nanoparticles [139]. The principle of DSSC is to use a dye that absorbs visible light and excites electrons from the highest occupied molecular orbital and the lowest unoccupied molecular orbital. These electrons are injected to the conduction band of TiO_2 where they are transported to the bottom of the nanotubes to the metal contact. The oxidized dye is regenerated using an electrolyte and the cycle is repeated. However, the electron generated may undergo recombination and/or react with the electrolyte. Another limiting factor is a recombination in the grain boundaries in the TiO_2 and a longer charge

Table 2.5: List of reports on TiO₂ nanotube based PEC water splitting

Co-catalyst	Surface modification	Dopant	Electrolyte	Photocurrent (mA/cm ² at V)	Band gap (eV)	Nanotube length (μm)	ref
None	None	carbon	KOH	1.8 at 0.3	2.2	3.3	[122]
CdS	None	None	Na ₂ S	5 at 0.2	2.4	2.5	[123]
WO ₃	None	None	HClO ₄	2 at 1.1	2.5	2	[124]
None	Lotus-root-shape	None	KOH	0.9 at 1.23	N/A	6	[125]
Pt	None	None	KOH	N/A	N/A	0.65	[126]
None	None	Boron	Na ₂ SO ₄	0.15 at 0.3	3.1	0.8	[127]
Ethylene glycol	None	None	KOH	3.3 at 0.2	3.1	0.6	[128]
None	Nanolace	None	KOH	24 at 1	N/A	18	[129]
None	None	None	KOH	26 at 0.5	N/A	220	[130]
Bacteriorhodopsin	None	None	citrate buffer	0.65 at 0.5	N/A	7	[131]
None	None	Nb	KOH	0.9 at 0.4	2.8	7	[132]
Pt	None	Iron	Ethanol + water	N/A	3	0.3	[133]
None	nanohole nano cave	None	KOH	1.59 at 1.23	N/A	1.5	[134]
None	Infrared annealing	None	KOH	32 at 0.5	N/A	7	[135]
CdTe	None	None	Na ₂ S	0.23 at 0	1.5	0.3	[136]

diffusion path through the TiO_2 . However, the nanotubes have a lower charge transport path and hence reduce recombination. Studies have shown that nanotubes have a higher electron diffusion length when compared to nanoparticles [140]. Anatase TiO_2 nanotubes are shown to be more efficient than rutile phase [141]. Optimum annealing temperature for the highest efficiency for TiO_2 nanotubes is shown to be at 450°C , which is due to the formation of anatase phase. The limiting factor in DSSC is the dye loading due to which the surface area is lowered. Many approaches have been reported to increase the surface area, such as TiCl_4 treatment [142], double walled nanotubes, and bamboo-type structures [144]. In another approach, the TiO_2 nanotube walls were loaded with silver particles to increase the photoconversion efficiency [145]. Processes such as rapid-breakdown anodization also have been demonstrated to increase the efficiency [146].

2.6.3 Drug delivery

Due to enhanced surface area and biocompatibility, TiO_2 is a promising material for drug delivery. If the nanotubes are separated from each other, then it can be used as a drug delivery capsule, or it can be used as a coating on biomedical implants for drug-eluting. The drug adhering to the surface can be released photocatalytically. If the surface is loaded with magnetic material such as Fe_3O_4 , then the movement of the nanotubes can be guided by a magnetic field [147]. Also, the drug release from the surface of the nanotubes can be triggered electrically [148] or by x-rays [149]. Such magnetic particles plus drug loaded nanotubes can be used to kill cancer cells by guiding the nanotubes to the cell of interest using a magnetic field [147]. Another interesting drug delivery mechanism was demonstrated by Song *et al.* [150] in which drug loaded

nanotubes were hydrophilic and prevented bodily fluids from entering the nanotubes. The nanotubes would, however, interact with the bodily fluids under photocatalytic interaction and harvest the purpose of the loaded drug. One of the main drawbacks of TiO₂ nanotubes is the low mechanical flexibility. However, TiO₂ nanotubes have been shown to be a promising material for drug delivery systems.

2.6.4 Sensors

TiO₂ nanotubes have been demonstrated in sensing hydrogen [151], ethanol [152], chemical oxygen demand (COD) [153], hydrogen peroxide [154], oxygen [155], toluene [156], NO₂ [157], acetone [158], glucose [159], and humidity sensors [160]. In some of the sensing applications demonstrated, TiO₂ itself is not a sensing materials. TiO₂ nanotubes are chosen due to their enhanced surface to volume ratio, high resistivity, and chemical stability. Most of the sensing reaction happens only a few to tens of nanometers deep from the surface, and TiO₂ offers the advantage of an enhanced surface ratio to volume ratio. Chemical stability is required since lots of applications demonstrated will require performing in harsh environments. High resistivity helps in increasing the sensitivity of the device since change in the resistivity will have a wide range in TiO₂ and hence provide a wide sensor range and sensitivity. Therefore, in most applications, the surface of TiO₂ is treated/deposited with the sensing material and is used as the sensor. TiO₂ nanotubes are made sensitive to humidity by doping the nanotubes with LiCl [160]. TiO₂ nanotube/phthalocyanine hybrid structures are used for sensing volatile organic compound [161]. TiO₂ nanotubes loaded with Au are also used for sensing volatile organic compounds [162]. However, for most applications such as hydrogen [151],

oxygen [155], and ethanol [152], TiO₂ nanotubes themselves are used as the sensing materials.

2.7 Modification TiO₂ nanotubes properties

As stated before, TiO₂ is an interesting and useful material, and a lot of effort is being put into improving the performance of nanotube based devices. Most of the effort is in terms of modifying the electrical and optical properties but keeping intact the environmentally friendly and chemically inert nature of TiO₂. The methods/approaches used to modify the properties of TiO₂ can be divided as annealing, doping/forming composites, and depositing materials on the walls of the nanotubes. The goal is to improve the performance of a TiO₂-based device and/or make it suitable for certain applications.

2.7.1 Annealing

The TiO₂ nanotubes synthesized by electrochemical anodization (the most commonly used synthesis method) are amorphous in state. Amorphous TiO₂ has poor charge transport, and hence upon annealing, crystalline TiO₂ can be formed with an improved charge transport. When annealed at a temperature of about 280 °C, amorphous TiO₂ begin to reorient themselves into crystalline anatase form [143]. When annealed at temperatures higher than 280 °C, the quality of anatase increases, but when annealed at about 500 °C, the TiO₂ reorient themselves into crystalline rutile form, and with a further increase in temperature, the quantity of rutile TiO₂ increases. It has been shown that when annealed at 900 °C for 2 hours, the nanotubes form 100 % rutile TiO₂. The annealing time

and temperature ramp up rate also has a significant influence on the morphology of the nanotubes. If the ramp up speed is too fast, then the nanotubes would crack and also may delaminate from the substrate. If the annealing is not long enough, then the tubes would not have enough time to crystallize. Generally 2 hours of annealing time and about 1 °C/min ramp time is used for most TiO₂ nanotube-based applications [143], [144], [146]. Another important factor to consider is that the nanotubes have significant amounts of fluoride ions embedded in them which occur during anodization [163]. If an organic electrolyte is used, then there will also be a significant amount of carbon species due to the breakdown of the organic compound in an electric field [98]. The hydroxide groups formed on the surface of the nanotubes are also considered as contaminants. These contaminants can be removed/reduced via annealing [164]. The drawback of annealing is that cracking the nanotubes can slow down the charge transport a significant amount [140]. When Ti foil is used as the substrate for synthesis of nanotubes and subjected to annealing, a layer of rutile TiO₂ is formed under the nanotubes which can affect the charge transport from the nanotubes to the substrate. By controlling the annealing ramp up time of the nanotubes synthesized in ethylene glycol based electrolyte, double walled or fused membrane structures can be obtained [164]. Annealing time and temperature of nanotubes can also define the depth of the crystalline TiO₂. If annealed in an environment without oxygen then the TiO₂ loses O₂ species to form Ti³⁺ species [165]. This species is shown to have absorption in the visible light and also has better conductivity. By heat treatment, atoms on the surface of the nanotubes can be reduced to Ti³⁺ species to improve the conductivity and absorption.

2.7.2 Doping

Since TiO_2 is a wide band gap material (~ 3 eV) and has an absorption range in the UV range (which is 6–7% of the solar spectrum on the surface of the Earth), various approaches have been made to reduce the band gap and increase the absorption range. Asahi *et al.* has reported the first band change in TiO_2 nanotubes by doping the nanotubes with nitrogen [166]. The p states of nitrogen were introduced with 2p states of oxygen. The methods used to dope TiO_2 nanotubes can be broadly classified as treating/growing the nanotubes in a solution or melt of the dopant of interest, thermal treating or synthesis in the dopant atmosphere, cosputter or sputter in the environment of the dopant, and ion implantation and use of alloy substrates for synthesis. Treating/growing the nanotubes in a solution or melt of the dopant of interest is usually used in the sol-gel technique [167]. The second technique is used for nitrogen and carbon doping where the nanotubes are heat treated in gases such as CO [122] and acetylene [168]. The third technique is similar to the technique used in the semiconductor industry where an ion gun is used to dope the nanotubes [169]. The most commonly used dopant is nitrogen. However, carbon is also gaining significant attention. Usually, the TiO_2 nanotubes are doped with 2% nitrogen which is a significant amount compared to the current semiconductor industry doping percentage. Due to this high nitrogen percentage, the valence band gap is raised by 0.5 eV. Ion implantation is the most successful technique and is used in doping the TiO_2 nanotubes with Cr [170]. As stated before, the fourth technique is the simplest and most straight forward technique in which the alloy is anodized to form TiO_2 nanotubes with a lower band gap and optical absorption in the visible range. Using alloys such as TiN and TiW alloys, nanotubes have been successfully synthesized via electrochemical

anodization [169].

2.7.3 Surface deposition and filling

Another method similar to doping is populating the surface of the nanotubes with the nanoparticles of interest. They can improve the performance by forming heterojunctions leading to band bending or charge injections and have catalytic effects or have surface plasmon effects leading to more charge transfer and an enhanced field. Electrochemical deposition is one of the commonly used techniques to deposit nanoparticles as well as for filling the nanotubes. Since TiO_2 is an n-type material, negative potential, which is required to deposit metals on the surface, would result in a forward bias, resulting in the metal being deposited in the top portion of the nanotubes, and it would not fill the nanotubes completely. To overcome this issue, the trick is to reduce the bottom of the nanotubes to Ti^{3+} and then carry out the electrochemical deposition where the bottom of the nanotubes are filled and then the top part of the nanotubes is filled later [172]. This technique has been successfully demonstrated by filling the nanotubes with Cu. WO_3 [173] and TiO_2 [174] nanoparticles can be deposited on the surface of the nanotubes by slow hydrolysis of precursors such as WCl_5 or TiCl_4 , respectively, where these nanoparticles increase the surface area and in turn increase the efficiency of DSSC. In another approach, nickel oxide nanoparticles can be deposited on the surface of the nanotubes by a slow precipitation reaction of $\text{Ni}(\text{OH})_2$ followed by heat treatment [175]. Similarly, TiO_2 nanotubes can be dipped in a solution consisting of ferromagnetic Fe_3O_4 nanoparticles with a permanent magnet placed under the nanotubes to fill up the nanotubes with Fe_3O_4 [147]. Nobel metals such as Au, Ag, and Pt nanoparticles can also

be deposited on the surface of the nanotubes [176]–[178]. Silver can be deposited by reducing Ag^+ to Ag by illuminating UV light. Similarly, metals can be deposited by a chemical reduction and/or by physical vapor deposition [177], [179]. Nanotubes filled with zeolites have also been demonstrated [180]. Efforts to attach monolayers onto the surface of nanotubes have also been made. Organic monolayers are deposited to change the surface's water affinity, to make it biocompatible, to make it suitable for sensing applications and/or electron injection in the case of DSSC. For certain biomedical implant applications, bifunctional molecules such as (3-Aminopropyl)triethoxysilane [181] that have a terminal NH_2 group are attached on the surface of the nanotubes. This allows attachment of organic compounds onto the nanotube. To modify the wettability of nanotubes (which are hydrophilic in nature) when treated with the appropriate monolayer, the monolayer will make the nanotubes hydrophobic [182]. In another approach, mixed monolayers of N-(3-triethoxysilyl) propylferrocenecarboxamide and perfluorotriethoxysilane are used to change the surface wettability of the nanotubes [183].

2.8 Thin film TiO_2 nanotubes

Moore *et al.* first demonstrated the synthesis of TiO_2 nanotubes from thin Ti film via electrochemical anodization [184]. In this demonstration, the films were deposited using radio frequency (RF) sputtering and the thermal evaporation technique. 400 to 1000 nm thick Ti films were deposited on conductive glass. To improve the adhesion of the film to the substrate, the substrate was heated to 250 or 500 °C during the film deposition. It was found that due to the difference in the electric field in the metal-air interface and the metal-electrolyte interface, the nanotube growth was not uniform. To

solve the issue, a bilayer film was used in which a second layer at least 400 nm thicker was deposited on the already deposited film in regions where the film would not be subjected to anodization (not immersed in the electrolyte). Similarly, various groups have demonstrated synthesis of TiO₂ nanotubes on substrates such as glass [185], Si [187], 188], quartz [161], and Kapton HN tape [189]. One of the interesting uses of using Kapton tape is that the substrate is flexible, further expanding the scope and application of TiO₂ nanotubes. A list of reports on thin film based TiO₂ nanotubes is presented in Table 2.6.

2.9 Incorporating WO₃ in TiO₂ nanotubes

TiO₂ has a band gap of 3–3.4 eV limiting its absorption range to only the UV portion of the solar spectrum which forms about 3–6 % of the total solar spectrum. One of the methods to bring the absorption range to the visible range is to incorporate wide band gap, chemically stable, semiconducting materials such as WO₃ in TiO₂. WO₃, which is in its oxidized state, is chemically stable in harsh environments. It also has a lower band gap of 2.6 eV, increasing the absorption spectrum to a portion of the visible spectrum. W is also a value metal like Ti and can be subjected to electrochemical anodization to form nano WO₃ structures. By incorporating WO₃ in TiO₂, it can also be used for other applications such as gas sensors [190], electrochromic devices [191], conductimetric sensors [192], etc. Also, WO₃ can be used in photocatalytic applications similar to the one demonstrated by TiO₂. Table 2.7 is a list of reports on WO₃ incorporated in TiO₂ nanotubes.

Table 2.6: List of reports on thin film based TiO₂ nanotubes

Deposition technique	Nanotube length (nm)	Substrate	Electrolyte	Anodization potential (v)	Reference
RF sputtering	400-1000	Glass/ITO	Acetic acid + HF	6 to 18	[184]
e-beam evaporation	1000	Glass	HF & NH ₄ F + Ethylene glycol	5 to 60	[185]
e-beam evaporation	1000	Quartz	HF	10	[161]
e-beam evaporation	500	Glass/ITO	Acetic acid + HF & NH ₄ F + glycerol	20	[186]
e-beam evaporation	750	Silicon	NH ₄ F + glycerol	20	[187], [188]
Sputtering	6000	Kapton HN	NH ₄ F + glycerol	25 to 70	[189]

Table 2.7: List of reports on WO₃ incorporated in TiO₂ nanotubes

Method used	at. % of WO ₃	Applications demonstrated	References
Electrochemical anodization of Ti-W alloy	0.2 - 9	Photocatalytic Activity	[193]
Electrochemical anodization of Ti-W alloy	9	None	[194]
Emulsion electrospinning, thermal evaporation, and thermal annealing	n/a	Photocatalysis	[195]
Sol-gel chemical method	20	None	[196]
Anodization in electrolyte containing WO ₄ ⁻ ions	0.05	Photocatalytic, PEC	[197]
electrochemical deposition of WO ₃	n/a	Photocatalytic water splitting into hydrogen and oxygen	[198]
Use phosphotungstic acid in electrolyte during anodization	2.91	Photocatalytic water splitting into hydrogen and oxygen	[199]

2.10 References

- [1] S. Shafiee and E. Topal, "When will fossil fuel reserves be diminished?," *Energy Policy*, vol. 37, pp. 181–189, 2009.
- [2] S. F. B. Tett, P. A. Stott, M. R. Allen, W. J. Ingram, and J. F. B. Mitchell, "Causes of twentieth-century temperature change near the Earth's surface," *Nature*, vol. 399, pp. 569–572, 1999.
- [3] P. U. Clark, A. M. McCabe, A. C. Mix, and A. J. Weaver, "Rapid rise of sea level 19,000 years ago and its global implications," *Science*, vol. 304, pp. 1141–1144, 2004.
- [4] S. C. Barton, J. Gallaway, and P. Atanassov, "Enzymatic biofuel cells for implantable and microscale devices," *Chem. Rev.*, vol. 104, pp. 4867–4886, 2004.
- [5] M. Parikka, "Global biomass fuel resources," *Biomass Bioenergy*, vol. 27, pp. 613–620, 2004.
- [6] R. Metkemeijer and P. Achard, "Ammonia as a feedstock for a hydrogen fuel cell; reformer and fuel cell behavior," *J. Power Sources*, vol. 49, pp. 271–282, 1994.
- [7] T. Kawai and T. Sakata, "Conversion of carbohydrate into hydrogen fuel by a photocatalytic process," *Nature*, vol. 286, pp. 474–476, 1980.
- [8] H. Lund and G. Salgi, "The role of compressed air energy storage (CAES) in future sustainable energy systems," *Energy Convers. Manage.*, vol. 50, pp. 1172–1179, 2009.
- [9] D. E. Carlson and C. R. Wronski, "Amorphous silicon solar cell," *Appl. Phys. Lett.*, vol. 28, pp. 671–673, 1976.
- [10] A. P. Davis, "Tilting at windmills? The second law survives," *Angew. Chem. Int. Ed.*, vol. 37, pp. 909–910, 1998.
- [11] David Palmer, *Ask an astrophysicist*. [Online] Available: http://imagine.gsfc.nasa.gov/docs/ask_astro/answers/971113i.html
- [12] J. M. Eckermann, P. R. Krafft, L. Shoemaker, R. E. Lieberon, S. D. Chang, and A. Colohan, "Potential application of hydrogen in traumatic and surgical brain injury, stroke and neonatal hypoxia-ischemia," *Medical Gas Research*, vol. 2, pp. 11–15, 2012.
- [13] M. Stephenson and L. H. Stickland, "Hydrogenase: A bacterial enzyme activating molecular hydrogen," *Biochem. J.*, vol. 25, pp. 205–214, 1931.

- [14] G. J. Stie gela and M. Ramezan, "Hydrogen from coal gasification: An economical pathway to a sustainable energy future," *Int. J. Coal Geol.*, vol. 65, pp. 173–190, 2006.
- [15] Eni. (2013). *Hydrogen for fuel upgrading*. [Online] Available: http://www.eni.com/en_IT/innovation-technology/technological-answers/hydrogen-fuel-upgrading/hydrogen-fuel-upgrading.shtml.
- [16] J. M. Modak, "Haber process for ammonia synthesis," *Resonance*, pp. 69–77, 2002.
- [17] S. Nagano, T. Kitajima, K. Yoshida, Y. Kazao, Y. Kabata, D. Murata, and K. Nagakura, "Development of world's largest hydrogen-cooled turbine generator," *Power Eng. Soc. Summer Meeting*, vol. 2, pp. 657–663, 2002.
- [18] G. W. Crabtree, M. S. Dresselhaus, and M. V. Buchanan, "The hydrogen economy," *Physics Today*, vol. 57, pp. 39–44, 2004.
- [19] G. Marbán and T. Valdés-Solís, "Towards the hydrogen economy?," *Int. J. Hydrogen Energy*, vol. 32, pp. 1625–1637, 2007.
- [20] A. N. Fatsikostas, D. I. Kondarides, and X. E. Verykios, "Production of hydrogen for fuel cells by reformation of biomass-derived ethanol," *Catal. Today*, vol. 75, pp. 145–155, 2002.
- [21] S. U. M. Khan, M. Al-Shahry, W. B. Ingler Jr., "Efficient photochemical water splitting by a chemically modified n-TiO₂," *Science*, vol. 297, pp. 2243–2245, 2002.
- [22] Wikipedia. *Electrolysis of water*. [Online]. Available: http://en.wikipedia.org/wiki/Electrolysis_of_water
- [23] Wikipedia. *Standard electrode potential (data page)*. [Online]. Available: [http://en.wikipedia.org/wiki/Standard_electrode_potential_\(data_page\)](http://en.wikipedia.org/wiki/Standard_electrode_potential_(data_page))
- [24] J. S. Herring, J. E. O'Brien, C. M. Stoots, G. L. Hawkes, J. J. Hartvigsen, and M. Shahnam, "Progress in high-temperature electrolysis for hydrogen production using planar SOFC technology," *Int. J. Hydrogen Energy*, vol. 32, pp. 440–450, 2007.
- [25] N. A. Kellya, T. L. Gibsona, and D. B. Ouwerkerk, "A solar-powered, high-efficiency hydrogen fueling system using high-pressure electrolysis of water: Design and initial results," *Int. J. Hydrogen Energy*, vol. 33, pp. 2747–2764, 2008.
- [26] D.A. Tryk, A. Fujishima, K. Honda, "Recent topics in photoelectrochemistry:

- Achievements and future prospects,” *Electrochim. Acta*, vol. 45, pp. 2363–2376, 2000.
- [27] T. Melis, (2010). *Maximizing light utilization efficiency and hydrogen production in microalgal cultures*. [Online] Available: http://www.hydrogen.energy.gov/pdfs/progress08/ii_f_2_melis.pdf
- [28] Z. Zou, J. Ye, K. Sayama, and H. Arakawa, “Direct splitting of water under visible light irradiation with an oxide semiconductor photocatalyst,” *Nature*, vol. 414, pp. 625–627, 2001.
- [29] O. Khaselev and J. A. Turner, “A monolithic photovoltaic-photoelectrochemical device for hydrogen production via water splitting,” *Science*, vol. 280, pp. 425–427, 1998.
- [30] H. Kato, K. Asakura, and A. Kudo, “Highly efficient water splitting into H₂ and O₂ over lanthanum-doped NaTaO₃ photocatalysts with high crystallinity and surface nanostructure,” *J. Am. Chem. Soc.*, vol. 125, pp. 3082–3089, 2003.
- [31] M. Hara, T. Kondo, M. Komoda, S. Ikeda, K. Shinohara, A. Tanaka, J. N. Kondo, and K. Domen, “Cu₂O as a photocatalyst for overall water splitting under visible light irradiation,” *Chem. Commun.*, pp. 357–358, 1998.
- [32] I. Cesar, A. Kay, J. A. G. Martinez, and M. Gratzel, “Translucent thin film Fe₂O₃ photoanodes for efficient water splitting by sunlight: Nanostructure-directing effect of Si-doping,” *J. Am. Chem. Soc.*, vol. 128, pp. 4582–4583, 2006.
- [33] T. Takata, K. Shinohara, A. Tanaka, M. Hara, J. N. Kondo, and K. Domen, “A highly active photocatalyst for overall water splitting with a hydrated layered perovskite structure,” *J. Photochem. Photobiol. A: Chemistry*, vol. 106, pp. 45–49, 1997.
- [34] Y. Tamaura, A. Steinfeld, P. Kuhn, and K. Ehrensberger, “Production of solar hydrogen by a novel, 2-step, water-splitting thermochemical cycle,” *Energy*, vol. 20, pp. 325–330, 1995.
- [35] D. W. Hwang, J. Kim, T. J. Park, and J. S. Lee, “Mg-doped WO₃ as a novel photocatalyst for visible light-induced water splitting,” *Catal. Letters*, vol. 80, pp. 53–57, 2002.
- [36] K. R. Reyes-Gil, E. A. Reyes-Garcia, and D. Raftery, “Nitrogen-doped In₂O₃ thin film electrodes for photocatalytic water splitting,” *J. Phys. Chem. C*, vol. 111, pp. 14579–14588, 2007.
- [37] T. G. Deutsch, C. A. Koval, and J. A. Turner, “III-V nitride epilayers for

- photoelectrochemical water splitting: GaPN and GaAsPN,” *J. Phys. Chem. B*, vol. 110, pp. 25297–25307, 2006.
- [38] X. Yang, A. Wolcott, G. Wang, A. Sobo, R. C. Fitzmorris, F. Qian, J. Z. Zhang, and Y. Li, “Nitrogen-doped ZnO nanowire arrays for photoelectrochemical water splitting,” *Nano Lett.*, vol. 9, pp. 2331–2336, 2009.
- [39] Galleries. *The mineral anatase*. [Online]. Available: <http://www.galleries.com/Anatase>
- [40] Wikipedia. *Brookite*. [Online]. Available: <http://en.wikipedia.org/wiki/Brookite>
- [41] Wikipedia. *Anatase*. [Online]. Available: <http://en.wikipedia.org/wiki/Anatase>
- [42] Wikipedia. *Rutile*. [Online]. Available: <http://en.wikipedia.org/wiki/Rutile>
- [43] B. Grzmil, B. Kic, and M. Rabe, “Inhibition of the anatase-rutile phase transformation with addition of K₂O, P₂O₅, and Li₂O,” *Chem. Pap.*, vol. 58, pp. 410–414, 2004.
- [44] U. Diebold, “The surface science of titanium dioxide,” *Surf. Sci. Rep.*, vol. 48, pp. 53–229, 2003.
- [45] Webmineral. *Rutile mineral data*. [Online]. Available: <http://webmineral.com/data/Rutile.shtml>
- [46] Refractiveindex. *Refractive index database*. [Online]. Available: <http://refractiveindex.info/?group=CRYSTALS&material=TiO2>
- [47] Mindat. *Anatase*. [Online]. Available: <http://www.mindat.org/min-213.html>
- [48] A. W. Czanderna, C. N. R. Rao, and J. M. Honi, “The anatase-rutile transition. Part 1.—Kinetics of the transformation of pure anatase,” *Trans. Faraday Soc.*, vol. 54, pp. 1069–1073, 1958.
- [49] Gemdat. *Anatase*. [Online]. Available: <http://www.gemdat.org/gem-213.html>
- [50] Galleries. *The mineral brookite*. [Online]. Available: <http://www.galleries.com/Brookite>
- [51] Mindat. *Brookite*. [Online]. Available: <http://www.mindat.org/min-787.html>
- [52] Webmineral. *Brookite mineral data*. [Online]. Available: <http://www.webmineral.com/data/Brookite.shtml>
- [53] Wikipedia. *Sol-gel*. [Online]. Available: <https://en.wikipedia.org/wiki/Sol-gel>

- [54] L. Xiao, H. Zhang, E. Scanlon, L. S. Ramanathan, E.-W. Choe, D. Rogers, T. Apple, and B. C. Benicewicz, "High-temperature polybenzimidazole fuel cell membranes via a sol-gel process," *Chem. Mater.*, vol. 17, pp. 5328–5333, 2005.
- [55] M. Chatterjee, B. Siladitya, and D. Ganguli, "Chromia microspheres by the sol-gel technique," *Mater. Lett.*, vol. 25, pp. 261–263, 1995.
- [56] S.-S. Choi, S. G. Lee, S. S. Im, S. H. Kim, Y. L. Joo, "Silica nanofibers from electrospinning/sol-gel process," *J. Mater. Sci. Lett.*, vol. 22, pp. 891–893, 2003.
- [57] H. Nakamura and Y. Matsui, "Silica gel nanotubes obtained by the sol-gel method," *J. Am. Chem. Soc.*, vol. 117, pp. 2651–2652, 1995.
- [58] T. Maiyalagan, B. Viswanathan and U. V. Varadaraju, "Fabrication and characterization of uniform TiO₂ nanotube arrays by sol-gel template method," *Bull. Mater. Sci.*, vol. 29, pp. 705–708, 2006.
- [59] M. Zhang, Y. Bando, K. Wada, "Sol-gel template preparation of TiO₂ nanotubes and nanorods," *J. Mater. Sci. Lett.*, vol. 20, pp. 167–170, 2001.
- [60] G. S. Wu, T. Xie, X. Y. Yuan, Y. Lia, L. Yang, Y. H. Xiao, and L. D. Zhang, "Controlled synthesis of ZnO nanowires or nanotubes via sol-gel template process," *Solid State Commun.*, vol. 134, pp. 485–489, 2005.
- [61] M. Zhang, Y. Bando, and K. Wada, "Silicon dioxide nanotubes prepared by anodic alumina as templates," *J. Mater. Res.*, vol. 15, pp. 387–392, 2000.
- [62] K. Byrappa and M. Yoshimura, "Handbook of hydrothermal technology," *Elsevier Science*, 2008
- [63] A. N. Christensen, "Hydrothermal preparation of some oxides and some oxide hydroxides at temperatures up to 900° C and pressures up to 80 kb," *Mater. Res. Bull.*, vol. 6, pp. 691–697, 1971.
- [64] K. P. Reis, A. Ramanan, and M. S. Whittingham, "Hydrothermal synthesis of sodium tungstates," *Chem. Mater.*, vol. 2, pp. 219–221, 1990.
- [65] P. J. Zapf, R. P. Hammond, R. C. Haushalter, and J. Zubietta, "Variations on a one-dimensional theme: The hydrothermal syntheses of inorganic/organic composite solids of the iron molybdate family," *Chem. Mater.*, vol. 10, pp. 1366–1373, 1998.
- [66] W. Zheng, R. Liu, D. Peng, and G. Meng, "Hydrothermal synthesis of LaFeO₃ under carbonate-containing medium," *Mater. Lett.*, vol. 43, pp. 19–22, 2000.

- [67] H. Song, R. M. Rioux, J. D. Hoefelmeyer, R. Komor, K. Niesz, M. Grass, P. Yang, and G. A. Somorjai, "Hydrothermal growth of mesoporous sba-15 silica in the presence of pvp-stabilized pt nanoparticles: Synthesis, characterization, and catalytic properties," *J. Am. Chem. Soc.*, vol. 128, pp. 3027–3037, 2006.
- [68] Wikipedia. *Hydrothermal synthesis*. [Online]. Available: http://en.wikipedia.org/wiki/Hydrothermal_synthesis
- [69] M. Myahkostupov, M. Zamkov, and F. N. Castellano, "Dye-sensitized photovoltaic properties of hydrothermally prepared TiO₂ nanotubes," *Energy Environ. Sci.*, vol. 4, pp. 998–1010, 2011.
- [70] Y. V. Kolen'ko, K. A. Kovnir, A. I. Gavrillov, A. V. Garshev, J. Frantti, O. I. Lebedev, B. R. Churagulov, G. V. Tendeloo, and M. Yoshimura, "Hydrothermal synthesis and characterization of nanorods of various titanates and titanium dioxide," *J. Phys. Chem. B*, vol. 110, pp. 4030–4038, 2006.
- [71] Y. Guo, N.-H. Lee, H.-J. Oh, C.-R. Yoon, K.-S. Park, W.-H. Lee, Y. Li, H.-G. Lee, K.-S. Lee, and S.-J. Kim, "Preparation of titanate nanotube thin film using hydrothermal method," *Thin Solid Films*, vol. 516, pp. 8363–8371, 2008.
- [72] D. D. Vuong, D. T. N. Tram, P. Q. Pho, and N. D. Chien, "Hydrothermal synthesis and photocatalytic properties of TiO₂ nanotubes," *Physics and Engineering of New Materials, Springer Proceedings in Physics*, vol. 127, pp. 95–101, 2009.
- [73] L. Cui, K. N. Hui, K. S. Hui, S. K. Lee, W. Zhou, Z. P. Wan, and C.-N. H. Thuc, "Facile microwave-assisted hydrothermal synthesis of TiO₂ nanotubes," *Mater. Lett.*, vol. 75, pp. 175–178, 2012.
- [74] Y. C. Zhu, H. L. Li, Y. Koltypin, Y. R. Hacohebn, and A. Gedanken, "Sonochemical synthesis of titania whiskers and nanotubes," *Chem. Commun.*, vol. 24, pp. 2616–2617, 2001.
- [75] M. Hodos, E. Horvath, H. Haspel, A. Kukovecz, Z. Konya, and I. Kiricsi, "Photosensitization of ion-exchangeable titanate nanotubes by CdS nanoparticles," *Chem. Phys. Lett.*, vol. 399, pp. 512–515, 2004.
- [76] L. Ren, X. Huang, F. Sun, and X. Je, "Preparation and characterization of doped TiO₂ nanodandelion," *Mater. Lett.*, vol. 61, pp. 427–431, 2007.
- [77] Y. Zhao, J. Jin, X. Yang, "Hydrothermal synthesis of titanate nanowire arrays," *Mater. Lett.*, vol. 61, pp. 384–388, 2007.

- [78] H.-H. Ou and S.-L. Lo, "Review of titania nanotubes synthesized via the hydrothermal treatment: Fabrication, modification, and application," *Sep. Purif. Technol.*, vol. 58, pp. 179–191, 2007.
- [79] Wikipedia. *Anodizing*. [Online]. Available: <http://en.wikipedia.org/wiki/Anodizing>
- [80] T. P. Hoar and N. F. Mott. "A mechanism for the formation of porous anodic oxide films on aluminium," *J. Phys. Chem. Solids*, vol. 9, pp. 97–99, 1959.
- [81] I. Sieber, H. Hildebrand, A. Friedrich, and P. Schmuki, "Formation of self-organized niobium porous oxide on niobium," *Electrochem. Commun.*, vol. 7, pp. 97–100, 2005.
- [82] P. S. Wilcox and W. D. Westwood, "Anodic oxidation of tantalum," *Can. J. Phys.*, vol. 49, pp. 1543-1548, 1971.
- [83] V. Zwillling, E. Darque-Ceretti, A. Boutry-Forveille, D. David, M. Y. Perrin, and M. Aucouturie, "Structure and physicochemistry of anodic oxide films on titanium and TA6V Alloy," *Surf. Interface Anal.*, vol. 27, pp. 629–637, 1999.
- [84] V. Zwillling, M. Aucouturier, and E. Darque-Ceretti. "Anodic oxidation of titanium and TA6V alloy in chromic media. An electrochemical approach," *Electrochim. Acta*, vol. 45, pp. 921–929, 1999.
- [85] K. Ito and T. Ohgami, "Hydrogen detection based on coloration of anodic tungsten oxide film," *Appl. Phys. Lett.*, vol. 60, pp. 938–940, 1992.
- [86] B. Cox, "Factors affecting the growth of porous anodic oxide films on zirconium," *J. Electrochem. Soc.*, vol. 117, pp. 654–663, 1970.
- [87] J. B. Mathieu, H. J. Mathieu, and D. Landolt, "Electropolishing of titanium in perchloric acid-acetic acid solution I . Auger electron spectroscopy study of anodic films," *J. Electrochem. Soc.*, vol. 125, pp. 1039–1043, 1978.
- [88] E. J. Kelly, "Anodic dissolution and passivation of titanium in acidic media III. Chloride solutions," *J. Electrochem. Soc.*, vol. 126, pp. 2064–2075, 1979.
- [89] P. Roy, S. Berger, and P. Schmuki, "TiO₂ nanotubes: Synthesis and applications," *Angew. Chem. Int. Ed.*, vol. 50, pp. 2904–2939, 2011.
- [90] Y.-Y. Song, R. Lynch, D. Kim, P. Roy, and P. Schmuki, "TiO₂ nanotubes: Efficient suppression of top etching during anodic growth," *Electrochem. Solid-State Lett.*, vol. 12, pp. C17–C20, 2009.

- [91] S. P. Albu, A. Ghicov, J. M. Macak, and P. Schmuki, "250 μm long anodic TiO_2 nanotubes with hexagonal self-ordering," *Phys. Status Solidi*, vol. 1, pp. R65–R67, 2007.
- [92] L. V. Taveiraa, J. M. Macákb, H. Tsuchiyab, L. F.P. Dicka, and P. Schmuki, "Initiation and growth of self-organized TiO_2 nanotubes anodically formed in $\text{NH}_4\text{F}/(\text{NH}_4)_2\text{SO}_4$ electrolytes," *J. Electrochem. Soc.*, vol. 152, pp. B405–B410, 2005.
- [93] D. Regonini, A. Satka, A. Jaroenworarluck, D.W.E. Allsopp, C.R. Bowen, R. Stevens, "Factors influencing surface morphology of anodized TiO_2 nanotubes," *Electrochim. Acta*, vol. 74, pp. 244–253, 2012.
- [94] S. P. Albu, D. Kim, and P. Schmuk, "Growth of aligned TiO_2 bamboo-type nanotubes and highly ordered nanolace," *Angew. Chem.*, vol. 120, pp. 1942–1945, 2008.
- [95] K. Lee, J. Kim, H. Kim, Y. Lee, and Y. Tak, "Effect of electrolyte conductivity on the formation of a nanotubular TiO_2 photoanode for a dye-sensitized solar cell," *J. Korean Phys. Soc.*, vol. 54, pp. 1027–1031, 2009.
- [96] S. P. Albu and P. Schmuki, " TiO_2 nanotubes grown in different organic electrolytes: Two-size self-organization, single vs. double-walled tubes, and giant diameters," *Phys. Status Solidi RRL*, vol. 4, pp. 215–217, 2010.
- [97] J. M. Macak, H. Tsuchiya, L. Taveira, S. Aldabergerova, and P. Schmuki, "Glattwandige anodische TiO_2 -nanoröhren," *Angew. Chem.*, vol. 117, pp. 7629–7632, 2005.
- [98] Y.-Y. Song, P. Roy, I. Paramasivam, and P. Schmuki, "Voltage-induced payload release and wettability control on TiO_2 and TiO_2 nanotubes," *Angew. Chem.*, vol. 122, pp. 361–364, 2010.
- [99] J. Kunze, A. Ghicov, H. Hildebrand, J. M. Macak, L. Traveira, and P. Schmuki, "Challenges in the surface analytical characterisation of anodic TiO_2 films – A Review," *Z. Phys. Chem.*, vol. 219, pp. 1561–1582, 2005.
- [100] D. Kim, A. Ghicov, and P. Schmuki, " TiO_2 nanotube arrays: Elimination of disordered top layers ("nanograss") for improved photoconversion efficiency in dye-sensitized solar cells," *Electrochem. Commun.*, vol.10, pp. 1835–1838, 2008.
- [101] Y. Y. Song and P. Schmuki, "Modulated TiO_2 nanotube stacks and their use in interference sensors," *Electrochem. Commun.*, vol. 12, pp. 579–582, 2010.

- [102] L. Yuan, S. Meng, Y. Zhou, and Z. Yue, "Controlled synthesis of anatase TiO₂ nanotube and nanowire arrays via AAO template-based hydrolysis," *J. Mater. Chem. A*, vol. 1, pp. 2552–, 2557, 2013.
- [103] W. F. Jiang, Y. H. Ling, S. J. Hao, H. Y. Li, X. D. Bai, and D. Q. Cang, "In situ template synthesis of TiO₂ nanotube array films," *Key Eng. Mater.*, vol. 336-338, pp. 2200–2202, 2007.
- [104] A. Michailowski, D. AlMawlawi, G. Cheng, and M. Moskovits, "Highly regular anatase nanotubule arrays fabricated in porous anodic templates," *Chem. Phys. Lett.*, vol. 349, pp. 1–5, 2001.
- [105] Y.-C. Liang, C.-C. Wang, C.-C. Kei, Y.-C. Hsueh, W.-H. Cho, and T.-P. Perng, "Photocatalysis of Ag-loaded TiO₂ nanotube arrays formed by atomic layer deposition," *J. Phys. Chem. C*, vol. 115, pp. 9498–9502, 2011.
- [106] P. Hoyer, "Semiconductor nanotube formation by a two-step template process," *Adv. Mater.*, vol. 8, pp. 857–859, 1996.
- [107] R. A. Caruso, J. H. Schattka, A. Greiner, "Titanium dioxide tubes from sol-gel coating of electrospun polymer fibers," *Adv. Mater.*, vol. 13, pp. 1577–1579, 2001.
- [108] J. H. Jung, H. Kobayashi, K. J. C. van Bommel, S. Shinkai, and T. Shimizu, "Creation of novel helical ribbon and double-layered nanotube tio₂ structures using an organogel template," *Chem. Mater.*, vol. 14, pp. 1445–1447, 2002.
- [109] Wikipedia. *Photocatalysis*. [Online]. Available: <http://en.wikipedia.org/wiki/Photocatalysis>
- [110] Z. Liu, X. Zhang, S. Nishimoto, M. Jin, D. A. Tryk, T. Murakami, and A. Fujishima, "Highly ordered tio₂ nanotube arrays with controllable length for photoelectrocatalytic degradation of phenol," *J. Phys. Chem. C*, vol. 112, pp. 253–259, 2008.
- [111] H. Tang, K. Prasad, R. Sanjines, P. E. Schmid, and F. Levy, "Electrical and optical properties of TiO₂ anatase thin films," *J. Appl. Phys.*, vol. 75 , pp. 2042–2047, 1994.
- [112] A. Fujishima and K. Honda, "Electrochemical photolysis of water at a semiconductor electrode," *Nature*, vol. 238, pp. 37–38, 1972.
- [113] T. Hisanaga, K. Harada, and K. Tanaka, "Photocatalytic degradation of organochlorine compounds in suspended TiO₂," *J. Photochem. Photobiol. A: Chem.*, vol. 54, pp. 113–118, 1990.

- [114] K. Tanaka, S. M. Robledo, T. Hisanaga, R. Ali, Z. Ramli, and W. A. Bakar, "Photocatalytic degradation of 3,4-xylyl N-methylcarbamate (MPMC) and other carbamate pesticides in aqueous TiO₂ suspensions," *J. Mol. Catal. A: Chem.*, vol. 144, pp. 425–430, 1999.
- [115] E. Pelizzetti, M. Borgarello, E. Borgarello, and N. Serpone, "Photocatalytic degradation of polychlorinated dioxins and polychlorinated biphenyls in aqueous suspensions of semiconductors irradiated with simulated solar light," *Chemosphere*, vol. 17, pp. 499–510, 1988.
- [116] A. I. Kontos, V. Likodimos, T. Stergiopoulos, D. S. Tsoukleris, P. Falaras, I. Rabias, G. Papavassiliou, D. Kim, J. Kunze, and P. Schmuki, "Self-organized anodic TiO₂ nanotube arrays functionalized by iron oxide nanoparticles," *Chem. Mater.*, vol. 21, pp. 662–672, 2009.
- [117] F. Sabin, T. Turk, and A. Vogler, "Photo-oxidation of organic compound in the presence of titanium dioxide: Determination of the efficiency," *J. Photochem. Photobiol. A: Chem.*, vol. 63, pp. 99–106, 1992.
- [118] Z. Liu, X. Zhang, S. Nishimoto, T. Murakami, and A. Fujishima, "Efficient photocatalytic degradation of gaseous acetaldehyde by highly ordered TiO₂ nanotube arrays," *Environ. Sci. Technol.*, vol. 42, pp. 8547–8551, 2008.
- [119] C. Wei, W.-Y. Lin, Z. Zainai, N. E. Williams, K. Zhu, A. P. Kruzic, R. L. Smith, and L. Rajeshwar, "Bactericidal activity of TiO₂ photocatalyst in aqueous media: Toward a solar-assisted water disinfection system," *Environ. Sci. Technol.*, vol. 28, pp. 934938, 1994.
- [120] K. Sunada, Y. Kikuchi, K. Hashimoto, and A. Fujishima, "Bactericidal and detoxification effects of TiO₂ thin film photocatalysts," *Environ. Sci. Technol.*, vol. 32, pp. 726–728, 1999.
- [121] H. Sakai, R. Baba, K. Hashimoto, Y. Kubota, and A. Fujishima, "Selective killing of a single cancerous T24 cell with TiO₂ semiconducting microelectrode under irradiation," *Chem. Lett.*, vol. 24, pp. 185–186, 1995.
- [122] J. H. Park, S. Kim, and A. J. Bard, "Novel carbon-doped TiO₂ nanotube arrays with high aspect ratios for efficient solar water splitting," *Nano Lett.*, vol. 6, pp. 24–28, 2006.
- [123] Y. Yin, Z. Jin, and F. Hou, "Enhanced solar water-splitting efficiency using core/sheath heterostructure CdS/TiO₂ nanotube arrays," *Nanotechnology*, vol. 18, pp. 495608–495613, 2007.

- [124] J. H. Park and O. O. Park, "Photoelectrochemical water splitting at titanium dioxide nanotubes coated with tungsten trioxide," *Appl. Phys. Lett.*, vol. 89, pp. 163106–163108, 2006.
- [125] Z. Zhang, Md. F. Hossain, and T. Takahashi, "Photoelectrochemical water splitting on highly smooth and ordered TiO₂ nanotube arrays for hydrogen generation," *Int. J. Hydrogen Energy*, vol. 35, pp. 8528–8535, 2010.
- [126] W. Nam and G. Y. Han, "Preparation and characterization of anodized Pt–TiO₂ nanotubes arrays for water splitting," *J. Chem. Eng. Jpn.*, vol. 40, pp. 266–269, 2007.
- [127] N. Lu, X. Quan, J. Li, S. Chen, H. Yu, and G. Chen, "Fabrication of boron-doped TiO₂ nanotube array electrode and investigation of its photoelectrochemical capability," *J. Phys. Chem. C*, vol. 111, pp. 11836–11842, 2007.
- [128] S. K. Mohapatra, K. S. Raja, V. K. Mahajan, and M. Misra, "Efficient photoelectrolysis of water using TiO₂ nanotube arrays by minimizing recombination losses with organic additives," *J. Phys. Chem. C*, vol. 112, pp. 11007–11012, 2008.
- [129] J. Gong, Y. Lai, and C. Lin, "Electrochemically multi-anodized TiO₂ nanotube arrays for enhancing hydrogen generation by photoelectrocatalytic water splitting," *Electrochim. Acta*, vol. 55, pp. 4776–4782, 2010.
- [130] K. Shankar, G. K. Mor, H. E. Prakasam, S. Yoriya, M. Paulose, O. K. Varghese, and C. A. Grimes, "Highly-ordered TiO₂ nanotube arrays up to 220 μm in length: Use in water photoelectrolysis and dye-sensitized solar cells," *Nanotechnology*, vol. 18, pp. 065707–065717, 2007.
- [131] N. K. Allam, C.-W. Yen, R. D. Near, and M. A. El-Sayed, "Bacteriorhodopsin/TiO₂ nanotube arrays hybrid system for enhanced photoelectrochemical water splitting," *Energy Environ. Sci.*, vol. 4, pp. 2909–2914, 2011.
- [132] C. Das, P. Roy, M. Yang, H. Jha, and P. Schmuki, "Nb doped TiO₂ nanotubes for enhanced photoelectrochemical water-splitting," *Nanoscale*, vol. 3, pp. 3094–3096, 2011.
- [133] D. Eder, M. Motta, and A. H. Windle, "Iron-doped Pt–TiO₂ nanotubes for photocatalytic water splitting," *Nanotechnology*, vol. 20, pp. 055602–055607, 2009.
- [134] Z. Zhang and P. Wang, "Optimization of photoelectrochemical water splitting performance on hierarchical TiO₂ nanotube arrays," *Energy Environ. Sci.*, vol. 5, pp. 6506–6512, 2012.

- [135] N. K. Allam, and C. A. Grimes, "Effect of rapid infrared annealing on the photoelectrochemical properties of anodically fabricated TiO₂ nanotube arrays," *J. Phys. Chem. C*, vol. 113, 7996–7999, 2009.
- [136] J. A. Seabold, K. Shankar, R. H. T. Wilke, M. Paulose, O. K. Varghese, C. A. Grimes, and K.-S. Choi, "Photoelectrochemical properties of heterojunction CdTe/TiO₂ electrodes constructed using highly ordered tio₂ nanotube arrays," *Chem. Mater.*, vol. 20, pp. 5266–5273, 2008.
- [137] R. Abe, T. Takata, H. Sugihara, and K. Domen, "Photocatalytic overall water splitting under visible light by TaON and WO₃ with an IO₃⁻/I⁻ shuttle redox mediator," *Chem. Commun.*, pp. 3829–3831, 2005.
- [138] M. P. Dare-Edwards, J. B. Goodenough, A. Hamnett, K. R. Seddon, and R. D. Wrigh, "Sensitisation of semiconducting electrodes with ruthenium-based dyes," *Faraday Discuss. Chem. Soc.*, vol. 70, pp. 285–298, 1980.
- [139] B. O'Regan and M. Grätzel, "A low-cost, high-efficiency solar cell based on dye-sensitized colloidal TiO₂ films," *Nature*, vol. 353, pp. 737–740, 1991.
- [140] P. Roy, D. Kim, K. Lee, E. Spiecker, and P. Schmuki, "TiO₂ nanotubes and their application in dye-sensitized solar cells," *Nanoscale*, vol. 2, pp. 45–59, 2010.
- [141] H. Tang, K. Prasad, R. Sanjinbs, P. E. Schmid, and F. Levy, "Electrical and optical properties of TiO₂ anatase thin films," *J. Appl. Phys.*, vol. 75, pp. 2042–2047, 1994.
- [142] J. H. Park, T.-W. Lee, and M. G. Kang, "Growth, detachment and transfer of highly-ordered TiO₂ nanotube arrays: Use in dye-sensitized solar cells," *Chem. Commun.*, pp. 2867–2869, 2008.
- [143] A. Ghicov, S. P. Albu, R. Hahn, D. Kim, T. Stergiopoulos, J. Kunze, C.-A. Schiller, P. Falaras, and P. Schmuki, "TiO₂ nanotubes in dye-sensitized solar cells: Critical factors for the conversion efficiency," *Chem. Asian J.*, vol. 4, 520–525, 2009.
- [144] D. Kim, A. Ghicov, S. P. Albu, and P. Schmuki, "Bamboo-type TiO₂ nanotubes: Improved conversion efficiency in dye-sensitized solar cells," *J. Am. Chem. Soc.*, vol. 130, pp. 16454–16455, 2008.
- [145] H. Tsuchiya, N. Tokuoka, S. Honda, Y. Shinkai, Y. Shimizu, and S. Fujimoto, "TiO₂ nanotube layers with metallic nanoparticles," *J. Phys. Conf. Series*, vol. 165, pp. 012037–012042, 2009.
- [146] R. Hahn, T. Stergiopoulos, J. M. Macak, D. Tsoukleris, A. G. Kontos, S. P. Albu, D. Kim, A. Ghicov, J. Kunze, P. Falaras, and P. Schmuki, "Efficient solar energy

- conversion using TiO₂ nanotubes produced by rapid breakdown anodization – A comparison,” *Phys. Status Solidi RRL*, vol. 1, 135–137, 2007.
- [147] N. K. Shrestha, J. M. Macak, F. Schmidt-Stein, R. Hahn, C. T. Mierke, B. Fabry, and P. Schmuki, “Magnetically guided titania nanotubes for site-selective photocatalysis and drug release,” *Angew. Chem.*, vol. 121, pp. 987–990, 2009.
- [148] Y. Y. Song, P. Roy, I. Paramasivam, and P. Schmuki, “Voltage-induced payload release and wettability control on TiO₂ and TiO₂ nanotubes,” *Angew. Chem.*, vol. 122, pp. 361–364, 2010.
- [149] F. Schmidt-Stein, R. Hahn, J. F. Gnichwitz, Y. Y. Song, N. K. Shrestha, A. Hirsch, and P. Schmuki, “X-ray induced photocatalysis on TiO₂ and TiO₂ nanotubes: Degradation of organics and drug release,” *Electrochem. Commun.*, vol. 11, pp. 2077–2080, 2009.
- [150] Y. Y. Song, F. Schmidt-Stein, S. Bauer, and P. Schmuki, “Amphiphilic TiO₂ Nanotube arrays: An actively controllable drug delivery system,” *J. Am. Chem. Soc.*, vol. 131, pp. 4230–4232, 2009.
- [151] G. K. Mora, M. A. Carvalhoa, O. K. Varghesea, M. V. Pishkoa, and C. A. Grimes, “A room-temperature TiO₂-nanotube hydrogen sensor able to self-clean photoactively from environmental contamination,” *J. Mater. Res.*, vol. 19, pp. 628–634, 2004.
- [152] P. Hu, G. Du, W. Zhou, J. Cui, J. Lin, H. Liu, D. Liu, J. Wang, and S. Chen, “Enhancement of ethanol vapor sensing of TiO₂ nanobelts by surface engineering,” *ACS Appl. Mater. Interfaces*, vol. 2, pp. 3263–3269, 2010.
- [153] Q. Zheng, B. Zhou, J. Bai, L. Li, Z. Jin, J. Zhang, J. Li, Y. Liu, W. Cai, and X. Zhu, “Self-organized TiO₂ nanotube array sensor for the determination of chemical oxygen demand,” *Adv. Mater.*, vol. 20, pp. 1044–1049, 2008.
- [154] L.-C. Jiang and W.-D. Zhang, “Electrodeposition of TiO₂ nanoparticles on multiwalled carbon nanotube arrays for hydrogen peroxide sensing,” *Electroanalysis*, vol. 21, pp. 988–993, 2009.
- [155] H. F. Lu, F. Li, G. Liu, Z.-G. Chen, D.-W. Wang, H.-T. Fang, G. Q. Lu, Z. H. Jiang, and H.-M. Cheng, “Amorphous TiO₂ nanotube arrays for low-temperature oxygen sensors,” *Nanotechnology*, vol. 19, pp. 405504, 2008.
- [156] M.-H. Seo, M. Yuasa, T. Kida, J.-S. Huh, K. Shimano, N. Yamazoe, “Gas sensing characteristics and porosity control of nanostructured films composed of TiO₂ nanotubes,” *Sens. Actuators B*, vol. 137, pp. 513–520, 2009.

- [157] I. D. Kim, A. Rothschild, B. H. Lee, D. Y. Kim, S. M. Jo, H. L. Tuller, "Ultrasensitive chemiresistors based on electrospun TiO₂ nanofibers," *Nano Lett.*, vol. 6, pp. 2009–2013, 2006.
- [158] M. Sánchez, R. Guirado, and M. E. Rincón, "Multiwalled carbon nanotubes embedded in sol-gel derived TiO₂ matrices and their use as room temperature gas sensors," *J. Mater. Sci. - Mater. Electron.*, vol. 18, pp. 1131–1136, 2007.
- [159] S.-J. Bao, C. M. Li, J.-F. Zang, X.-Q. Cui, Y. Qiao, J. Guo, "New nanostructured TiO₂ for direct electrochemistry and glucose sensor applications," *Adv. Funct. Mater.*, vol. 18, pp. 591–599, 2008.
- [160] Z. Li, H. Zhang, W. Zheng, W. Wang, H. Huang, C. Wang, A. G. MacDiarmid, and Y. Wei, "Highly sensitive and stable humidity nanosensors based on LiCl doped TiO₂ electrospun nanofibers," *J. Am. Chem. Soc.*, vol. 130, pp. 5036–5037, 2008.
- [161] N. Kılınç, E. Şennik, D. Atilla, A. G. Gürek, Z. Z. Öztürk, and V. Ahsen, "TiO₂ nanotube/phthalocyanine hybrid structure for VOC sensor application," *IMCS 2012 – The 14th International Meeting on Chemical Sensors*, pp. 1557–1558, 2012.
- [162] M.-H. Seo, M. Yuasa, T. Kida, Y. Kanmura, J.-S. Huh, N. Yamazoe, and K. Shimano, "Gas sensor using noble metal-loaded TiO₂ nanotubes for detection of large-sized volatile organic compounds," *J. Ceram. Soc. Jpn.*, vol. 119, pp. 884–889, 2011.
- [163] J. M. Macak, K. Sirotna, and P. Schmuki, "Self-organized porous titanium oxide prepared in Na₂SO₄/NaF electrolytes," *Electrochim. Acta*, vol. 50, pp. 3679–3684, 2005.
- [164] S. P. Albu, A. Ghicov, S. Aldabergenova, P. Drechsel, D. LeClere, G. E. Thompson, J. M. Macak, and P. Schmuki, "Formation of double-walled TiO₂ nanotubes and robust anatase membranes," *Adv. Mater.*, vol. 20, pp. 4135–4139, 2008.
- [165] L.-B. Xiong, J.-L. Li, B. Yang, and Y. Yu, "Ti³⁺ in the surface of titanium dioxide: Generation, properties and photocatalytic application," *J. Nano Mat.*, vol. 2012, pp. 831524, 2011.
- [166] R. Asahi, T. Morikawa, T. Ohwaki, K. Aoki, Y. Taga, "Visible-light photocatalysis in nitrogen-doped titanium oxides," *Science*, vol. 293, pp. 269–271, 2001.
- [167] X. Chen and C. Burda, "Photoelectron spectroscopic investigation of nitrogen-doped titania nanoparticles," *J. Phys. Chem. B*, vol. 108, pp. 15446–15449, 2004.

- [168] R. Hahn, A. Ghicov, J. Salonen, V.-P. Lehto, and P. Schmuki, "Carbon doping of self-organized TiO₂ nanotube layers by thermal acetylene treatment," *Nanotechnology*, vol. 18, pp. 105604–105607, 2007.
- [169] A. Ghicov, J. M. Macak, H. Tsuchiya, J. Kunze, V. Haeublein, L. Frey, and P. Schmuki, "Ion implantation and annealing for an efficient N-doping of TiO₂ nanotubes," *Nano Lett.*, vol. 6, pp. 1080–1082, 2006.
- [170] A. Ghicov, B. Schmidt, J. Kunze, and P. Schmuki, "Photoresponse in the visible range from Cr doped TiO₂ nanotubes," *Chem. Phys. Lett.*, vol. 433, pp. 323–326, 2007.
- [171] S. T. Aruna, S. Tirosh, and A. Zaban, "Nanosize rutile titania particle synthesis via hydrothermal method without mineralizers," *J. Mater. Chem.*, vol. 10, pp. 2388–2391, 2000.
- [172] J. M. Macak, B. G. Gong, M. Hueppe, and P. Schmuki, "Filling of TiO₂ nanotubes by self-doping and electrodeposition," *Adv. Mater.*, vol. 19, pp. 3027–3031, 2007.
- [173] A. Benoit, I. Paramasivam, Y. C. Nah, P. Roy, and P. Schmuki, "Decoration of TiO₂ nanotube layers with WO₃ nanocrystals for high-electrochromic activity," *Electrochem. Commun.*, vol. 11, pp. 728–732, 2009.
- [174] P. Roy, D. Kim, I. Paramasivam, and P. Schmuki, "Improved efficiency of TiO₂ nanotubes in dye sensitized solar cells by decoration with TiO₂ nanoparticles," *Electrochem. Commun.*, vol. 11, pp. 1001–1004, 2009.
- [175] N. K. Shrestha, M. Yang, Y. C. Nah, I. Paramasivam, and P. Schmuki, "Self-organized TiO₂ nanotubes: Visible light activation by Ni oxide nanoparticle decoration," *Electrochem. Commun.*, vol. 12, pp. 254–257, 2010.
- [176] J. M. Macak, P. J. Barczuk, H. Tsuchiya, M. Z. Nowakowska, A. Ghicov, M. Chojak, S. Bauer, S. Virtanen, P. J. Kulesza, and P. Schmuki, "Self-organized nanotubular TiO₂ matrix as support for dispersed Pt/Ru nanoparticles: Enhancement of the electrocatalytic oxidation of methanol," *Electrochem. Commun.*, vol. 7, pp. 1417–1422, 2005.
- [177] I. Paramasivam, J. M. Macak, A. Ghicov, P. Schmuki, "Enhanced photochromism of Ag loaded self-organized TiO₂ nanotube layers," *Chem. Phys. Lett.*, vol. 445, pp. 233–237, 2007.
- [178] I. Paramasivam, J. M. Macak, and P. Schmuki, "Photocatalytic activity of TiO₂ nanotube layers loaded with Ag and Au nanoparticles," *Electrochem. Commun.*, vol. 10, pp. 71–75, 2008.

- [179] J. M. Macak, F. Schmidt-Stein, and P. Schmuki, "Efficient oxygen reduction on layers of ordered TiO₂ nanotubes loaded with Au nanoparticles," *Electrochem. Commun.*, vol. 9, pp. 1783–1787, 2007.
- [180] I. Paramasivam, A. Avhale, A. Inayat, A. Bosmann, P. Schmuki, and W. Schwieger, "MFI-type (ZSM-5) zeolite-filled TiO₂ nanotubes for enhanced photocatalytic activity," *Nanotechnology*, vol. 20, pp. 225607–225611, 2009.
- [181] Y. Y. Song, H. Hildebrand, and P. Schmuki, "Optimized monolayer grafting of 3-aminopropyltriethoxysilane onto amorphous, anatase and rutile TiO₂," *Surf. Sci.*, vol. 604, pp. 346–353, 2010.
- [182] E. Balaur, J. M. Macak, H. Tsuchiya, P. Schmuki, "Wetting behaviour of layers of TiO₂ nanotubes with different diameters," *J. Mater. Chem.*, vol. 15, pp. 4488–4491, 2005.
- [183] F. Schmidt-Stein, J. F. Gnichwitz, J. Salonen, R. Hahn, A. Hirsch, and P. Schmuki, "Electrochemical wettability control on conductive TiO₂ nanotube surfaces modified with a ferrocene redox system," *Electrochem. Commun.*, vol. 11, pp. 2000–2003, 2009.
- [184] G. K. Mor, O. K. Varghese, M. Paulose, and C. A. Grimes, "Transparent highly ordered TiO₂ nanotube arrays via anodization of titanium thin films," *Adv. Func. Mater.*, vol. 15, pp. 1291–1296, 2005.
- [185] N. Kılınç, E. Şennik, and Z.Z. Öztürk, "Fabrication of TiO₂ nanotubes by anodization of Ti thin films for VOC sensing," *Thin Solid Films*, vol. 520, pp. 953–958, 2011.
- [186] J. Wang and Z. Lin, "Anodic formation of ordered TiO₂ nanotube arrays: Effects of electrolyte temperature and anodization potential," *J. Phys. Chem. C*, vol. 113, pp. 4026–4030, 2009.
- [187] S. Berger, J. Kunze, P. Schmuki, D. LeClere, A. T. Valota, P. Skeldon, G. E. Thompson, "A lithographic approach to determine volume expansion factors during anodization: Using the example of initiation and growth of TiO₂-nanotubes," *Electrochim. Acta*, vol. 54, pp. 5942–5948, 2009.
- [188] S. Berger, J. M. Macak, J. Kunze, and P. Schmuki, "High-efficiency conversion of sputtered Ti thin films into TiO₂ nanotubular layers," *Electrochem. Solid-State Lett.*, vol. 11, pp. C37–C40, 2008.
- [189] V. Galstyan, A. Vomiero, I. Concina, A. Braga, M. Brisotto, E. Bontempi, G. Faglia, and G. Sberveglieri, "Vertically aligned TiO₂ nanotubes on plastic substrates for flexible solar cells," *Small*, vol. 7, pp. 2437–2442, 2011.

- [190] W. Yu-De, C. Zhan-Xian, L. Yan-Feng, Z. Zhen-Lai, and W. Xing-Hui, "Electrical and gas-sensing properties of WO_3 semiconductor material," *Solid-State Electron.*, vol. 45, pp. 639–644, 2001.
- [191] B. Orel, U. Opara Krašovec, U. Lavrenčič Štangar, and P. Judeinstein, "All sol-gel electrochromic devices with Li^+ ionic conductor, WO_3 electrochromic films and SnO_2 counter-electrode films," *J. Sol-Gel Sci. Technol.*, vol. 11, pp. 87–104, 1998.
- [192] A. K. Prasad, and P. I. Gouma, " MoO_3 and WO_3 based thin film conductimetric sensors for automotive applications," *J. Mater. Sci.*, vol. 38, pp. 4347–4352, 2003.
- [193] I. Paramasivam, Y.-C. Nah, C. Das, N. K. Shrestha, and P. Schmuki, " WO_3/TiO_2 nanotubes with strongly enhanced photocatalytic activity," *Chem. Eur. J.*, vol. 16, pp. 8993–8997, 2010.
- [194] Y.-C. Nah, N. K. Shrestha, D. Kim, and P. Schmuki, "Electrochemical growth of self-organized TiO_2 – WO_3 composite nanotube layers: Effects of applied voltage and time," *J. Appl. Electrochem.*, vol. 43, pp. 9–13, 2013.
- [195] B. Lu, X. Li, T. Wang, E. Xie, and Z. Xu, " WO_3 nanoparticles decorated on both sidewalls of highly porous TiO_2 nanotubes to improve UV and visible-light photocatalysis," *J. Mater. Chem. A*, vol. 1, pp. 900–3906, 2013.
- [196] L. Cheng, X. Zhang, B. Liu, H. Wang, Y. Li, Y. Huang, and Z. Du, "Template synthesis and characterization of WO_3/TiO_2 composite nanotubes," *Nanotechnology*, vol. 16, pp. 1341–1345, 2005.
- [197] H. L. Tsai, M. K. H. Leung, G. S. Li, and D. C. Y. Leung, " WO_3 doping effects on the photoelectrocatalytic activity of TiO_2 nanotube film prepared by an anodization process," *Mater. Res. Soc. Symp. Proc.*, vol. 1258, 2010.
- [198] J. H. Park, O. O. Park, and S. Kim, "Photoelectrochemical water splitting at titanium dioxide nanotubes coated with tungsten trioxide," *Appl. Phys. Lett.*, vol. 89, pp. 163106, 2006.
- [199] Y. R. Smith, B. Sarma, S. K. Mohanty, and M. Misra, "Formation of TiO_2 – WO_3 nanotubular composite via single-step anodization and its application in photoelectrochemical hydrogen generation," *Electrochem. Commun.*, vol. 19, pp. 131–134, 2012.

CHAPTER 3

GROWTH AND CHARACTERIZATION OF TiO₂ NANOTUBES FROM SPUTTERED Ti FILM ON Si SUBSTRATE

Nanoscale Research Letters 2012, 7:388

reprinted with permission

NANO EXPRESS

Open Access

Growth and characterization of TiO₂ nanotubes from sputtered Ti film on Si substrate

Karumbaiah N Chappanda¹, York R Smith², Swornitra K Mohanty³, Loren W Rieth¹, Prashant Tathireddy¹ and Mano Misra^{2,3*}

Abstract

In this paper, we present the synthesis of self-organized TiO₂ nanotube arrays formed by anodization of thin Ti film deposited on Si wafers by direct current (D.C.) sputtering. Organic electrolyte was used to demonstrate the growth of stable nanotubes at room temperature with voltages varying from 10 to 60 V (D.C.). The tubes were about 1.4 times longer than the thickness of the sputtered Ti film, showing little undesired dissolution of the metal in the electrolyte during anodization. By varying the thickness of the deposited Ti film, the length of the nanotubes could be controlled precisely irrespective of longer anodization time and/or anodization voltage. Scanning electron microscopy, atomic force microscopy, diffuse-reflectance UV-vis spectroscopy, and X-ray diffraction were used to characterize the thin film nanotubes. The tubes exhibited good adhesion to the wafer and did not peel off after annealing in air at 350 °C to form anatase TiO₂. With TiO₂ nanotubes on planar/stable Si substrates, one can envision their integration with the current micro-fabrication technique large-scale fabrication of TiO₂ nanotube-based devices.

Keywords: TiO₂ nanotubes, Si substrate, Room temperature

Background

TiO₂ is a material of great interest due its low cost, stability, and interesting electrical and optical properties [1]. TiO₂ nanotubes (T-NT), compared to TiO₂ films, have a large surface area-to-volume ratio. Synthesis of these tubes via electrochemical anodization has been studied extensively over the past decade [2]. Due to their interesting electrical and optical properties, TiO₂ nanotubes are shown to have various applications such as harvesting solar energy [3], charge storage [4], and sensors [5,6]. However, these applications have been demonstrated by anodizing Ti foil, which is the limiting factor for commercialization since synthesis of T-NT on Ti foil limits the integration onto wafer-scale devices, which is required for large-scale production. Current semiconductor fabrication techniques use micro/nano-scale precision, which requires planar/stable substrates such as Si

wafer for manufacturing compact and powerful devices. Commonly used titanium foils are mechanically flexible, rendering them prone to bending which inhibits the ability to achieve the micro/nano-scaled precision. Hence, stable/planar substrates are required for integrating T-NT with the current semiconductor fabrication techniques for manufacturing compact and powerful T-NT-based devices. Growth of T-NT on stable/planar substrates such as glass and Si deposited by sputtering has been previously demonstrated [7,8]. However, in their synthesis of T-NT, low temperatures (0 °C) with a maximum voltage of 35 V were used, limiting the diameter of the tubes. Most of the micro-electro-mechanical systems (MEMS) and nano-electro-mechanical systems (NEMS) require a thin non-conductive layer to electrically isolate the device from the substrate and in order to define an electrical path to the device. Similarly, it is possible that a non-conductive layer isolating the tubes from the substrate is required in T-NT-based MEMS/NEMS. The T-NT synthesized per the method presented here generates nanotubes that are isolated from the substrate, which could prove advantageous while fabricating T-NT-based devices.

* Correspondence: mano.misra@utah.edu

²Metallurgical Engineering Department, University of Utah, 135 South 1460 East, WBB 00412, Salt Lake City, UT 84112, USA

³Chemical Engineering Department, University of Utah, 50 South Central Campus Dr, MEB 3290, Salt Lake City, UT 84112, USA

Full list of author information is available at the end of the article

Here, we present for the first time, the synthesis of T-NT from thin Ti film on Si wafer at room temperature and at high anodization potentials up to 60 V. Direct current (D.C.)-sputtered thin Ti film, along with an organic electrolyte with approximately 6.5 pH, was used for the synthesis of the tubes. A 100-nm-thick layer of thermally grown SiO₂ was used to electrically isolate the synthesized T-NT to demonstrate one of the suitability of the tubes for integration with the current MEMS/NEMS devices. The T-NTs were longer than the deposited film thickness, indicating selective electrochemical oxidation/dissolution of Ti by the organic electrolyte. The T-NT did not peel off from the substrate, exhibiting good adhesion even after annealing in air at high temperature. In order to extend the utility of T-NT to make compact and powerful strain gauges [9], sensors [5,6], and drug delivery systems [10], integration of these devices with electronic circuits is required, which in turn is incumbent on a substrate being compatible with the current semiconductor fabrication techniques. With the use of Si as substrate, as typically exemplified in the current semiconductor industry, T-NT-based devices have a great potential for large-scale production and commercialization.

Methods

Thin film deposition

Clean n-type (100) Si wafer with resistivity of 1 to 5 Ω cm were used as the substrates for T-NT growth. Wafers were subjected to water vapor-free thermal oxidation at 1,000 °C to form 100 nm of dry SiO₂. Ti film 650 nm thick was then deposited on the wafer by D.C. sputtering in a Denton Discovery 18 sputter system (Denton, Moorestown, NJ, USA). Ti target of 99.2% to

99.7% purity purchased from Kurt. J. Lesker (East Sussex, UK) was used for sputtering. The sputter chamber was pumped down to pressures < 2 μTorr. The Si substrate was heated to 200 °C, and the same temperature was maintained during sputtering [7]. Argon gas was pumped into the chamber as the plasma source. The argon gas flow was set such that the pressure in the chamber during sputtering is about 2 mTorr. After sputtering, the wafer was cooled down to room temperature in vacuum to minimize the formation of native TiO₂.

T-NT synthesis

TiO₂ nanotubes were synthesized at room temperature via electrochemical anodization. Figure 1 shows the schematic of the experimental setup used for the T-NT synthesis. Si wafer with approximately 650-nm-thin Ti film was diced into 1 × 2-cm-sized pieces. Ethylene glycol (89.5 wt%, from Fisher Scientific, Waltham, MA, USA), deionized (DI) water (10 wt%), and ammonium fluoride (0.5 wt%, from Fisher Scientific) were used as the anodizing electrolyte [11]. The Ti film was degreased with acetone and isopropanol alcohol followed by rinsing in DI water. The Ti film was connected to the positive terminal of the voltage supply via alligator clips to form the anode. The Si is electrically isolated due to the thermally grown SiO₂, and hence, the Si substrate does not take part in electrochemical reactions that occur during anodization. One-millimeter-thick platinum foil with 1 cm² area was connected to the negative terminal of the voltage source to form the cathode. Polyimide tape was used to mask the non-Ti portion of the diced substrate to prevent any reaction between the electrolyte and the substrate. The gap between the electrodes was 2 cm. Only about 1 cm² of the diced Ti/SiO₂/Si

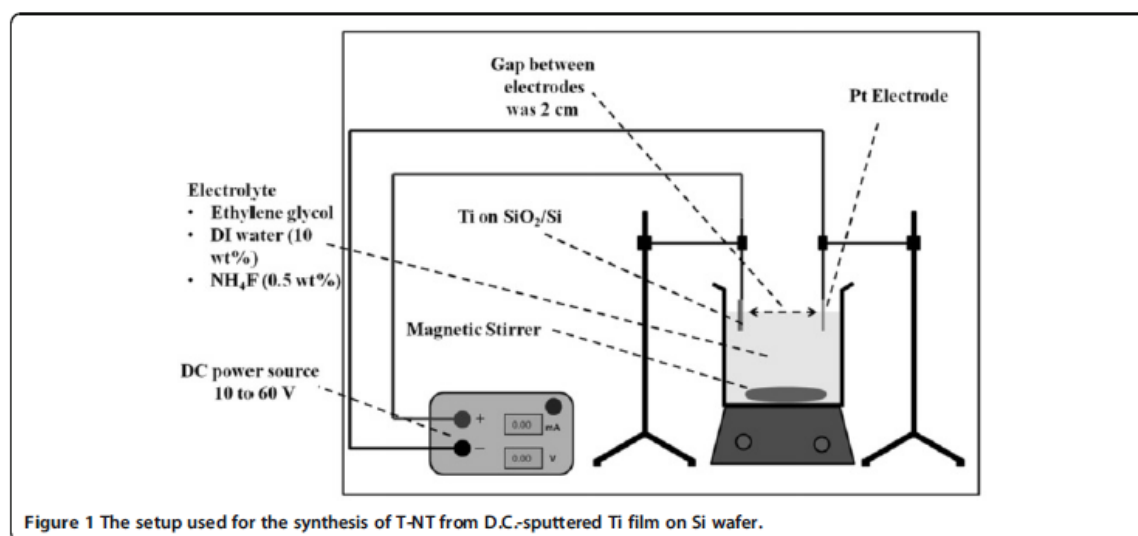


Figure 1 The setup used for the synthesis of T-NT from D.C.-sputtered Ti film on Si wafer.

substrate was subjected to anodization. Magnetic stirring was used to supply fresh electrolyte to the anodization site. A magnetic stirrer 2 cm long at 90 rpm was used to stir about 100 ml of the electrolyte. The rotation rate was chosen so that undesired vibrations due to stirring during anodization were minimum. The anodization voltage was ramped up at the rate of 1 V/s. The anodization was carried out at voltages varying from 10 to 60 V (D.C.). After anodization, the tubes were again cleaned in acetone and isopropanol alcohol followed by rinsing in DI water. The samples were then dried in air. The tubes were annealed in air at 350 °C for 2 h. The temperature was ramped up at a rate of 1.15 °C/min.

Characterization

Scanning electron microscopy (SEM) micrographs from FEI NanoNova SEM (FEI Co., Hillsboro, OR, USA) were used to characterize the diameter and length of the tubes, along with its structural morphology. Bruker Dimension ICON-PT atomic force microscopy (AFM) micrographs (Bruker AXS, Madison, WI, USA), along with the SEM micrographs, were used to study the effect of anodization time on the tubes' surface morphology. AFM micrographs using the PeakForce QNM (Bruker AXS) technique were obtained using ultra sharp AFM tips (10 nm diameter). The AFM micrographs were obtained at three different regions, and the average value was used for the roughness. Diffuse-reflectance UV-vis spectroscopy (UV-3600, Shimadzu, Kyoto, Japan) was used to characterize the band gap of the material. X-ray diffraction, utilizing the Philips X'Pert X-ray diffraction (XRD) system (Philips, Amsterdam, Netherlands), with incidence angles ranging from 20° to 80° was used for identification of crystalline phases and determination of stress in the nanotubes.

Results and discussions

SEM micrographs of TiO₂ nanotubes formed by anodization of sputtered Ti film are shown in Figure 2. From the top-view micrograph (Figure 2a), the surface appears to have a nano-porous/non-tubular structure. As pointed in the figure, pronounced grains of the sputtered film can be seen. Anodization starts at points of high electric field strength (hot spots) formed at grain boundaries. Upon milling the porous portions of the film, tubular-structured tubes can be seen (Figure 2b), and the grains of the sputtered film are not visible. Similarly, from the cross-section micrograph (Figure 2c), non-tubular and the tubular portions of the tubes can be seen. The porous/non-tubular portions consisted of about few tens of nanometer, as pointed in the figure. Self-aligned T-NT arrays interconnected along the side-walls via thin enclosing membranes can also be observed from the top and side view (pointed in Figure 2b,c). The

interconnecting membranes on the side of the nanotubes may be due to the addition of water to the anodizing electrolyte [12]. Figure 2d shows the base of the T-NTs, which was obtained by peeling off from the wafer. The bottom of the tubes show a random distribution of pentagonal and hexagonal patterns, which is also observed when T-NT is synthesized on Ti foils. T-NT growth via electrochemical anodization is the result of Ti oxidation and selective electric-field-assisted chemical etching of oxide. The steps taking place during electrochemical anodization are summarized as follows. Ti reacts with water to form a thin layer of TiO₂ in the presence of the electric field. TiO₂ reacts with fluoride ions from ammonium fluoride in the presence of electric field and is selectively etched in a direction defined by the electric field, exposing the underlying metallic Ti to the electrolyte. Again, the exposed Ti metal undergoes oxidation followed by etching. This continues until all the Ti metal is oxidized and selectively etched, resulting in a tubular structure. The synthesis of T-NT from Ti by electrochemical anodization is reviewed in detail in the literature [2]. The formation of the non-tubular nanoporous portion of the T-NT is due to the presence of native TiO₂ and/or the pronounced grain boundaries. The term native TiO₂ refers to a thin (10 to 30 nm) TiO₂ layer formed due to exposure of the sputtered film to atmosphere and is present before subjecting the sample to anodization. Native TiO₂ prevents the traditional formation of the tubes; however, the electrolyte etches the native TiO₂ at electric field 'hot spots' formed at the pronounced grain boundaries. Upon reaching the metallic Ti, regular tube formation is observed. Similar porous structure formation has been observed in anodizing mechanically polished Ti foil [13] as well as in template-based two-step anodization process [14]. To corroborate that the formation of non-tubular structure was influenced by the oxidized TiO₂, a control experiment was performed by heating the Ti film in air at 200 °C for 15 min to thicken the TiO₂ layer, followed by anodization. From the SEM micrographs, a significant increase in the thickness of the non-tubular oxidized layer was observed (Figure 2e). Hence, exposure of the film to air and high temperatures was minimized to reduce native TiO₂ formation in the T-NT synthesis method. Also, it is noted that the Si substrate or the substrate thickness has no effect on the synthesis of the nanotubes since it is chemically, as well as electrically, isolated during anodization. The sole purpose of the substrate is to provide a mechanical support for the sputtered thin films, and the Ti film was directly biased for anodization. Polyimide tape was used with the purpose of chemically isolating the substrate from the anodizing electrolyte. It was observed that Si would roughen with long exposure to the fluoride ions of the anodization electrolyte (1 h).

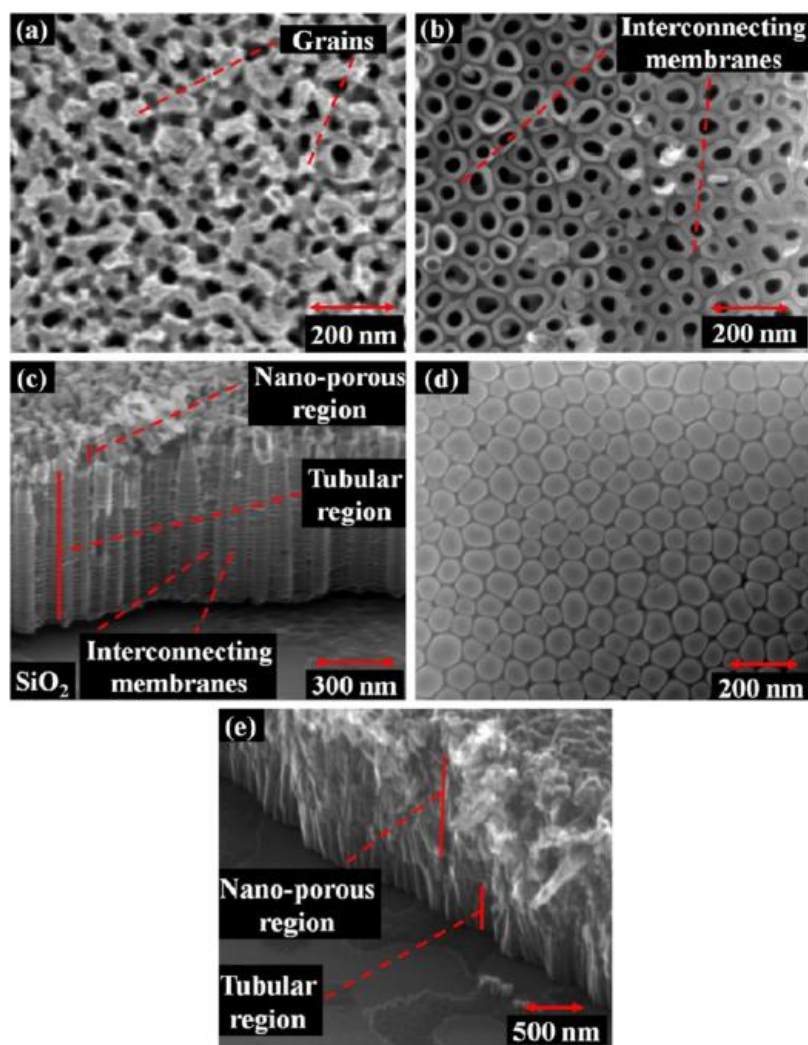
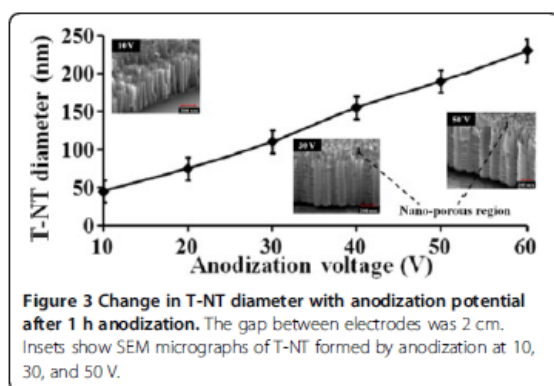


Figure 2 SEM micrographs. The T-NT formed by anodization of 650-nm-thick, D.C.-sputtered Ti at 20 V for 1 h. (a) Top view of the T-NT. (b) Top view after milling about 400 nm of the T-NT top surface. (c) Side view showing the length and outer diameter of the tubes (imaged at 60° tilt). (d) Bottom of the tube after peeling from the wafer. (e) The increase in the nano-porous region due to the presence of thermally induced native TiO₂ (1- μ m-thick film).

However, no observable change in the TiO₂ nanotube formation was observed in the absence of the polyimide tape.

Figure 3 shows the variation in the mode average diameter of the nanotubes with the anodization potential annotated with some inset SEM micrographs of T-NT formed at 10, 30, and 50 V, illustrating the change in the tube diameter/morphology. Ordered tube formation is observed at 10 V and above. However, relatively more uniform/ordered tube formation is observed at 20 V and higher. From the SEM micrographs, it can be seen that

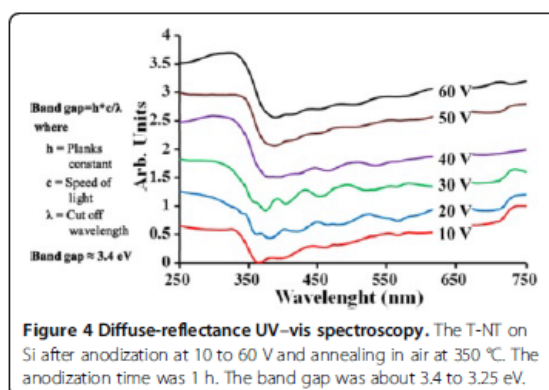
with the increase in voltage, the diameter as well as the thickness of the tube walls increases, which is similar to the T-NT synthesized on Ti foil [2]. The nanotubes' outer diameter increased linearly from about 45 to 230 nm with increase in anodization voltage from 10 to 60 V. The nanotubes formed at all voltages have a non-tubular/nano-porous region, as seen in Figure 2. However, the non-tubular region is relatively thin (10 to 30 nm) and is not clearly visible in the inset side-view SEM micrographs in Figure 3. It was consistently observed that the tube length was about 1.4 times longer



than the thickness of the deposited Ti film. The nanotubes were longer than the thickness of the Ti film due to the addition of oxygen atoms during anodization. Similar change in the film thickness due to oxidation can be observed in the case of Si [15]. The tubes did not elongate further irrespective of longer anodization time. Anodization potential also did not have any effect on the length of the tubes. This is because the length of the nanotube is limited by the thickness of the sputtered film, which is the source of the Ti atoms. The nanotube diameter and nanotube formation rate depend on the electric field strength and, hence, changes with anodization potential [2]. However, the length of the tube is mainly dependant on the supply of Ti available for anodization. The top surface of the tubes (few tens of nanometer) had smaller tube diameter compared to the lower portion of the tubes and showed a tapering structure. This may be due to anodization of the film during voltage ramp-up phase [16] and/or the effect of native titanium oxide. No visibly perceptible physical changes were seen after the annealing stage, thus demonstrating the high-temperature stability of the synthesized films.

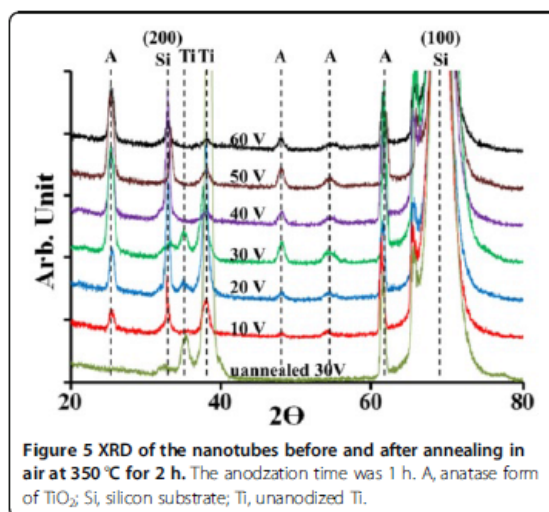
Figure 4 shows the diffuse-reflectance UV-vis spectroscopy of the tubes after annealing. The tubes showed maximum absorbance edge at wavelengths around 365 to 380 nm, corresponding to a band gap of 3.4 to 3.25 eV. One absorption band with increasing visible light absorbance tail may be due to the oxygen vacancies in TiO₂ [17]. The analysis was performed to confirm that the optical absorption characteristic is similar to that of T-NT synthesized on titanium foils [18].

Figure 5 shows the XRD patterns of the nanotubes before and after annealing. XRD showed that prior to annealing, irrespective of the anodization potential, the tubes were mostly amorphous with the occurrence of high-intensity 2θ peaks at 35°, 38° showing the presence of Ti, and a peak at 62° showing traces of anatase TiO₂, a high-intensity peak at 69° showing the presence of single crystal (100) Si, and a low-intensity peak at 33°



indicating (200) Si, which may be due to the stress induced in (100) Si by the sputtered film. Annealed samples showed a strong presence of anatase TiO₂ with 2θ peaks at 25°, 48°, 54°, 55°, and 62° along with low-intensity peaks present at 35° and 38° for traces of Ti metal, which was not anodized. With increase in anodization voltage, a decrease in the Ti peak intensity is observed. Annealing in air supplemented the oxidation of unanodized Ti, which reduced the Ti peak intensity. Annealed samples also showed an increase in intensity of (200) Si peak, which indicates an increase in stress induced in Si primarily due to annealing. X-ray diffraction analysis confirms the formation of TiO₂ anatase phase, which may be required for certain titania-based application. There was no noticeable stress-induced shifts in the anatase TiO₂ peaks, confirming stability of the synthesized substrate-based T-NT.

The surface of the nanotubes was characterized using AFM and SEM micrographs. Figure 6a shows the change



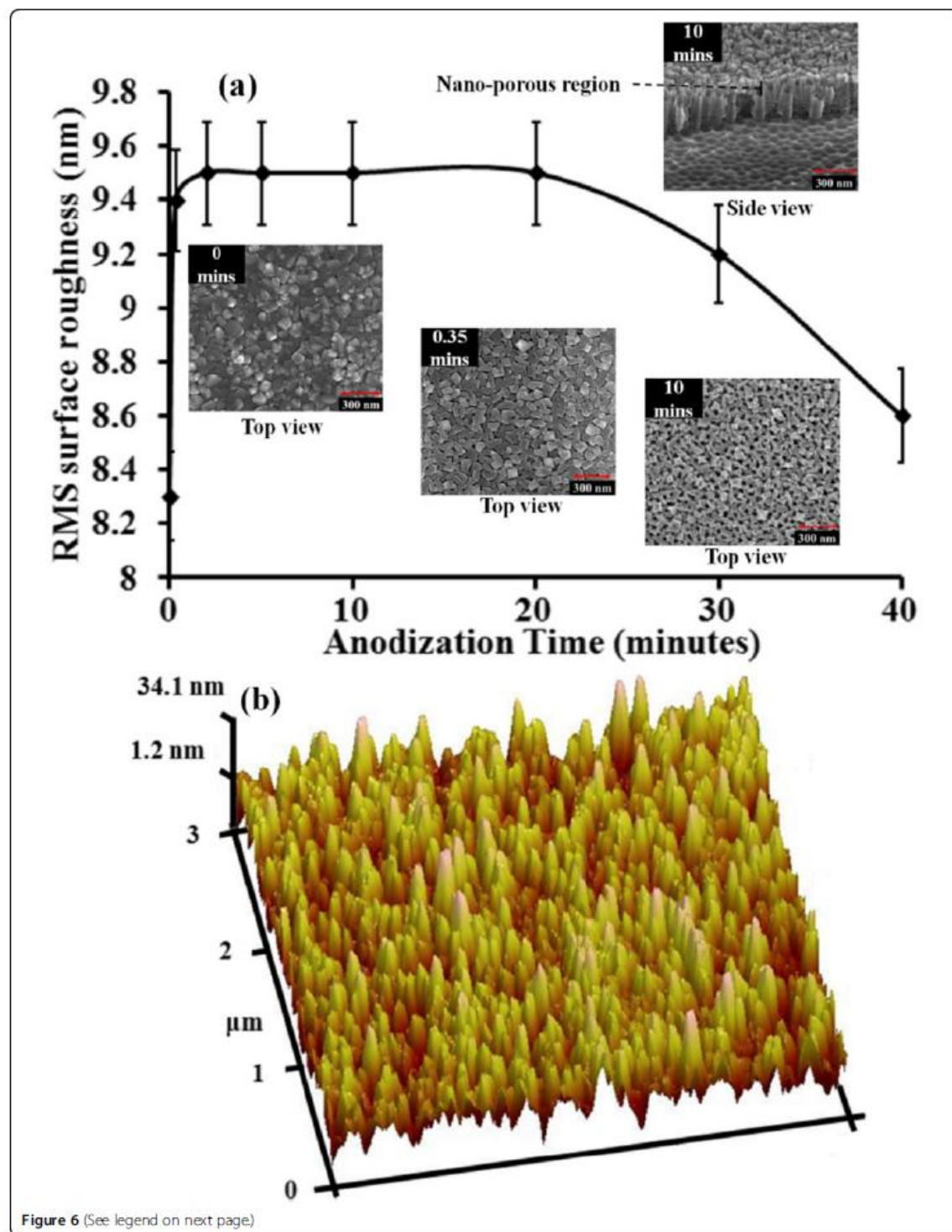


Figure 6 (See legend on next page.)

(See figure on previous page.)

Figure 6 Change in the root mean square surface roughness of the tubes with anodization time. (a) The samples were anodized at 20 V. Inset SEM micrographs showing the change in surface morphology after anodizing for 0, 0.35, and 10 min. (b) AFM image of the Ti film surface after anodization at 20 V for 10 min. The sputtered film thickness was about 650 nm.

in the root mean square (RMS) roughness of the film surface with anodization time obtained from AFM micrographs. The anodization of the film was carried out at 20 V. Magnetic stirring was used to ensure uniform/faster nanotube formation rate. In the absence of stirring of the electrolyte, the nanotube formation rate would reduce [19,20]. After anodization for 20 s, it can be seen that there is a rapid change in surface roughness as the tubes begin to form, and on further anodization, very little change in surface roughness is observed for up to 20 min. However, from cross-sectional SEM micrographs, it was seen that after 2 min of anodization, formation of regular nanotubes was observed underneath the non-tubular region similar to that seen in Figure 2. After 20 min, the surface roughness decreases. One possible mechanism for this is the pit formation via etching at the grain boundaries because of the occurrence of electric field hot spots at the grain boundaries. After the initial pit formation through the already present native TiO₂, the electric field is more concentrated at the bottom of the pits, which attracts reactive fluoride ions to the region. This results in etching selectively occurring at the bottom of the pits (high surface roughness during this stage). However, over time, when the nanotube length is considerably long (200 to 400 nm), the availability of the reactive fluoride ions within the tubes is more than what is required for nanotube formation. This results in undesired etching of the tube walls towards the upper region of the nanotubes (resulting in lower surface roughness). Once the Ti film is completely anodized, the nanotubes are electrically isolated from the anode, resulting in the annihilation of electric hot spots across the film. In the absence of the electric field hot spots, slow isotropic etching of the T-NT/native TiO₂ takes place, which also results in the decline of the RMS surface roughness. The surface roughness is mainly due to the pronounced grains of the sputtered film along with the nano-porous layer. Also, the measurement of the change in the film roughness is limited by the depth up to which the AFM tip can probe. The value provided by the AFM micrographs is only relative value and does not reflect the true roughness of the film. A similar change in the roughness of the film due to anodization can be confirmed from the inset SEM micrographs in Figure 6a. It may also be noted that Figure 6b shows a sample AFM image of the nanotubes' surface formed by anodizing for 10 min. It is noted that the nanotubes formed have

a non-tubular region along with tubular structure similar to the nanotubes seen in Figure 2. However, the non-tubular layer is relatively thin (10 to 30 nm) and is not clearly visible in the inset side-view SEM micrographs. However, from the top-view inset SEM micrographs, nano-porous region similar in morphology to that observed in Figure 2a, which is due to the native TiO₂ and pronounced surface grains, is seen.

Conclusions

TiO₂ nanotube arrays were successfully synthesized on Si wafer by anodization of D.C.-sputtered Ti film in an organic electrolyte. Due to the presence of native titania and pronounced surface grains, formation of nano-porous TiO₂ layer on top of self-aligned T-NT arrays was observed. From the SEM micrographs of T-NT viewed from the side and those of milled T-NT, the regular formation of nanotubes below the nano-porous layer was deduced. The diameter of the nanotubes varied linearly from 45 to 240 nm with an increase in anodization voltage from 10 to 60 V, respectively. SEM micrographs showed that the length of T-NT was about 1.4 times the thickness of the sputtered Ti film irrespective of the anodization voltage or longer anodization time. XRD characterization showed that unannealed tubes, irrespective of the anodization voltage/time, formed amorphous TiO₂ nanotubes, and upon annealing in air at 350 °C, anatase phase TiO₂ nanotubes was formed. AFM and SEM micrographs showed that on complete anodization of the film, the electrolyte etches TiO₂, resulting in tubes with thinner walls. It can be concluded that the T-NT formed on Si wafer has similar properties to T-NT formed on foil via various characterizations tools, giving rise to potential applications demonstrated by T-NT synthesized on Ti foil. Upon combining the use of well-established semiconductor fabrication techniques used in the semiconductor industry, integration of T-NT in MEMS devices and subsequent large-scale commercialization looks promising.

Competing interests

The authors declare that they have no competing interests.

Acknowledgment

The work presented here was supported by the Utah Science and Technology Research (USTAR) initiative.

Author details

¹Electrical and Computer Engineering Department, University of Utah, 50 South Central Campus Dr, MEB 3280, Salt Lake City, UT 84112, USA.

²Metallurgical Engineering Department, University of Utah, 135 South 1460

East, WBB 00412, Salt Lake City, UT 84112, USA. ³Chemical Engineering Department, University of Utah, 50 South Central Campus Dr, MEB 3290, Salt Lake City, UT 84112, USA.

Authors' contributions

The experiments and characterization presented in this work were carried by KNC. The experiments were designed by KNC and YRS. KNC, YRS, SKM, LWR, PT and MM analyzed and discussed the results obtained from the experiments. The manuscript was prepared by KNC and YRS, and SKM, LWR, PT and MM helped with draft editing. All authors read and approved the final manuscript.

Received: 15 May 2012 Accepted: 12 July 2012

Published: 12 July 2012

References

- Tang H, Prasad K, Sanjines R, Schmid PE, Levy F: **Electrical and optical properties of TiO₂ anatase thin films.** *J Appl Phys* 1994, **75**:2042–2047.
- Roy P, Berger S, Schmuki P: **TiO₂ nanotubes: synthesis and applications.** *Angew Chem Int Ed* 2011, **50**:2904–2939.
- Misra M, Raja KS: **On Solar Hydrogen & Nanotechnology.** In *Ordered titanium dioxide nanotubular arrays as photoanodes for hydrogen generation.* Vayssieres L. Chichester: John Wiley & Sons; 2010.
- Zhang G, Huang C, Zhou L, Ye L, Li W, Huang H: **Enhanced charge storage by the electrocatalytic effect of anodic TiO₂ nanotubes.** *Nanoscale* 2011, **3**:4174–4181.
- Mor GK, Varghese OK, Paulose M, Grimes CA: **A self-cleaning room temperature titania-nanotube hydrogen gas sensor.** *Sens Lett* 2003, **1**:42–46.
- Mun K-S, Alvarez SD, Choi W-Y, Sailor MJ: **A stable, label-free optical interferometric biosensor based on tio₂ nanotube arrays.** *ACS Nano* 2010, **4**:2070–2076.
- Mor GK, Varghese OK, Paulose M, Grimes CA: **Transparent highly ordered TiO₂ nanotube arrays via anodization of titanium thin films.** *Adv Funct Mater* 2005, **15**:1291–1296.
- Macak JM, Tsuchiya H, Berger S, Bauer S, Fujimoto S, Schmuki P: **On wafer TiO₂ nanotube-layer formation by anodization of Ti-films on Si.** *Chem Phys Lett* 2006, **428**:421–425.
- Asthana A, Shokuhfar T, Gao Q, Heiden P, Friedrich C, Yassar RS: **A study on the modulation of the electrical transport by mechanical straining of individual titanium dioxide nanotube.** *Appl Phys Lett* 2010, **97**:072107.
- Song Y-Y, Schmidt-Stein F, Bauer S, Schmuki P: **Amphiphilic TiO₂ nanotube arrays: an actively controllable drug delivery system.** *J Am Chem Soc* 2009, **131**:4230–4232.
- Smith YR, Subramanian V: **Heterostructural composites of TiO₂ Mesh/TiO₂ nanoparticles photosensitized with CdS: a new flexible photoanode for solar cells.** *J Phys Chem C* 2011, **115**:8376–8385.
- Song Y-Y, Schmuki P: **Modulated TiO₂ nanotube stacks and their use in interface sensors.** *Electrochemical Commun* 2010, **12**:579–582.
- Li S, Zhang G, Guo D, Yu L, Zhang W: **Anodization fabrication of highly ordered TiO₂ nanotubes.** *J Phys Chem C* 2009, **113**:12759.
- Zhang Z, Hossain MF, Takahashi T: **Photoelectrochemical water splitting on highly smooth and ordered TiO₂ nanotube arrays for hydrogen generation.** *Int J Hydrogen Energy* 2010, **35**:8528.
- Deal BE, Grove AS: **General relationship for the thermal oxidation of silicon.** *J Appl Phys* 1965, **36**:3770.
- Mor GK, Varghese OK, Paulose M, Mukherjee N, Grimes CA: **Fabrication of tapered, conical-shaped titania nanotubes.** *J Mater Res* 2003, **18**:2588–2593.
- Mahajan VK, Misra M, Raja KS, Mohapatra SK: **Self-organized TiO₂ nanotubular arrays for photoelectrochemical hydrogen generation: effect of crystallization and defect structures.** *J Phys D: Appl Phys* 2008, **41**:125307.
- Lu N, Quan X, Li JY, Chen S, Yu H-T, Chen G-H: **Fabrication of boron-doped TiO₂ nanotube array electrode and investigation of its photoelectrochemical capability.** *J Phys Chem C* 2007, **111**:11836–11842.
- Hassan FMB, Nanjo H, Kanakubo M, Ishikawa I, Nishioka M: **Effect of ultrasonic waves on the formation of TiO₂ nanotubes by electrochemical anodization of titanium in glycerol and NH₄F.** *J Surf Sci Nanotechnol* 2009, **7**:84–88.
- Mohapatra SK, Misra M, Mahajan VK, Raja KS: **A novel method for the synthesis of titania nanotubes using sonoelectrochemical method and its application for photoelectrochemical splitting of water.** *J Catal* 2007, **246**:362–369.

doi:10.1186/1556-276X-7-388

Cite this article as: Chappanda *et al.*: Growth and characterization of TiO₂ nanotubes from sputtered Ti film on Si substrate. *Nanoscale Research Letters* 2012 **7**:388.

Submit your manuscript to a SpringerOpen® journal and benefit from:

- Convenient online submission
- Rigorous peer review
- Immediate publication on acceptance
- Open access: articles freely available online
- High visibility within the field
- Retaining the copyright to your article

Submit your next manuscript at ► springeropen.com

CHAPTER 4

SITE-SPECIFIC AND PATTERNED GROWTH OF TiO₂

NANOTUBE ARRAYS FROM E-BEAM

EVAPORATED THIN TITANIUM

FILM ON Si WAFER

Nanotechnology 23 (2012) 385601 (8pp)

reprinted with permission

Site-specific and patterned growth of TiO₂ nanotube arrays from e-beam evaporated thin titanium film on Si wafer

Karumbaiah N Chappanda^{1,4}, York R Smith^{2,4}, Mano Misra^{2,3} and Swomitra K Mohanty³

¹ Electrical and Computer Engineering Department, University of Utah, Salt Lake City, UT 84112, USA

² Metallurgical Engineering Department, University of Utah, UT 84112, USA

³ Chemical Engineering Department, University of Utah, UT 84112, USA

E-mail: s.k.mohanty@utah.edu


Received 9 June 2012, in final form 26 July 2012

Published 4 September 2012

Online at stacks.iop.org/Nano/23/385601

Abstract

Growth of TiO₂ nanotubes on thin Ti film deposited on Si wafers with site-specific and patterned growth using a photolithography technique is demonstrated for the first time. Ti films were deposited via e-beam evaporation to a thickness of 350–1000 nm. The use of a fluorinated organic electrolyte at room temperature produced the growth of nanotubes with varying applied voltages of 10–60 V (DC) which remained stable after annealing at 500 °C. It was found that variation of the thickness of the deposited Ti film could be used to control the length of the nanotubes regardless of longer anodization time/voltage. Growth of the nanotubes on a SiO₂ barrier layer over a Si wafer, along with site-specific and patterned growth, enables potential application of TiO₂ nanotubes in NEMS/MEMS-type devices.

 Online supplementary data available from stacks.iop.org/Nano/23/385601/mmedia

(Some figures may appear in colour only in the online journal)

1. Introduction

Micro-electro mechanical systems (MEMS) and nano-electro mechanical systems (NEMS) have been shown to have a wide range of applications in sensors [1] and accelerometers [2], as well as in medical devices [3]. MEMS/NEMS devices have been commercialized due their compact size, low power, high reliability, high sensitivity and low cost. TiO₂ nanotubes (T-NTs) synthesized via electrochemical anodization, which were first investigated by Zwilling *et al* [4, 5], have been studied extensively over the past decade, with particular focus on their electrical and optical properties [6, 7]. The advantage of using an array of nanotube-type structures is the large surface area to volume ratio. TiO₂ nanotubes, in particular, have been demonstrated in many applications such as harvesting solar energy [7, 8], solar-hydrogen generation [9, 10], charge storage [11],

sensors [12, 13], hydrogen storage [14], biosensing [15] and biomedical implants [16]. These applications have traditionally been demonstrated via T-NTs synthesized by electrochemically anodizing Ti foil in a fluorinated acidic or organic electrolyte. Electrochemical anodization is not only a scalable process, but also enables highly controllable growth of the T-NT geometry at the nanoscale. Synthesis of T-NTs on curved Ti substrates such as wires [17, 18] and meshes [19, 20] has also been reported, demonstrating the flexibility of the anodization process for various Ti substrates. There is currently no commercially available T-NT based device, which may be due to a lack of fabrication techniques to make such devices on a large scale as well as packaging limitations for integration into MEMSs/NEMSs. One of the requirements for fabricating compact T-NT based devices is the need for a stable/planar substrate similar to the ones used in MEMS and NEMSs. The titanium foils commonly used in nanotube synthesis are mechanically flexible, making them more prone to bending, limiting the integration of T-NTs with

⁴ These authors contributed equally.

microfabrication techniques. Growth of T-NTs on thin Ti films (400–1000 nm) deposited onto conducting glass via radio frequency sputtering has been reported [21]. Anodization of thin Ti foil deposited on Si substrates via DC sputtering has also been reported [22, 23]; however, low temperatures ($\leq 0^\circ\text{C}$) and voltages ($\leq 35\text{ V}$) are required for growth.

Simply demonstrating the growth of T-NTs at room temperature and/or at high voltages on planar/Si stable substrates is not sufficient, and integration of photolithography (which is the most common step used for fabricating MEMSs/NEMSs) with the T-NT synthesis is required if devices with T-NTs are to be realized. Moreover, integration of T-NTs in NEMS/MEMS based devices requires a barrier layer (e.g. SiO_2) between the nanotubes and the Si substrate to define the electrical path through the device rather than through the bulk of the substrate.

Here for the first time we demonstrate integration of the synthesis of T-NTs with a photolithography technique. The growth of stable TiO_2 nanotubes at room temperature with anodization voltages from 10 to 60 V (DC) in an organic electrolyte using thin Ti film deposited by e-beam evaporation on a Si wafer substrate is demonstrated. The tubes are electrically isolated from the Si substrate via a layer of thermally grown SiO_2 making them more suitable for integration of the T-NTs in NEMS/MEMS based devices. The T-NTs were longer than the deposited film thickness showing selective electric field-assisted chemical dissolution of Ti by the electrolyte ($\text{pH} \sim 6.6$). With the use of simple photolithography techniques, we also for first time report site-specific and patterned growth of the T-NTs. By synthesizing T-NTs on Si wafer, and through the use of microfabrication technology, it is possible to integrate the electronic circuits required to make more compact and sensitive strain gauges [24], hydrogen sensors [12] and drug delivery systems [25]. Through the use of current microfabrication techniques and well-established electrochemical anodization methods, T-NT based micro/nanoscaled devices have great potential for commercialization.

2. Experimental methods

2.1. Deposition of Ti on a Si wafer

Clean n-type (5–10 $\Omega\text{ cm}$) Si(100) wafer was used as the substrate for T-NT growth. The wafer was then thermally oxidized at 1000°C for 10 min to form a 100 nm SiO_2 layer. Ti film was then deposited on the wafer by e-beam evaporation in a Denton SJ20C e-beam evaporator. Ti pellets of 99.95% purity were used for evaporation. The evaporation was carried at pressures of $< 1\ \mu\text{Torr}$. Ti films of varying thickness of 350–1000 nm were deposited at a rate between 2 and 3 \AA s^{-1} . After evaporation the wafer was cooled down to room temperature in vacuum ($< 1\ \mu\text{Torr}$) to minimize the formation of native TiO_2 .

2.2. Anodization e-beam deposited Ti films

TiO_2 nanotubes were formed by an electric field-assisted anodization technique at room temperature. The wafers were

diced into $1\text{ cm} \times 2\text{ cm}$ sized pieces, of which 1 cm^2 was subject to anodization. The anodizing electrolyte consisted of ethylene glycol (Fisher), DI water (10 wt%) and ammonium fluoride (0.5 wt%, Fisher) [20, 26]. The prepared electrolyte was aged for at least 36 h before using it for anodization. The Ti film was cleaned with acetone and isopropanol alcohol followed by rinsing in DI water to remove any organic contaminants. The back side of the Si substrate was masked with Kapton tape to prevent any reaction between the electrolyte and the SiO_2/Si . Platinum foil with 1 cm^2 area and 1 mm thick was used as the cathode. The gap between the electrodes was 2 cm. The electrolyte was magnetically stirred during the anodization. For every run the anodization potential was ramped at a rate of 1 V s^{-1} . The anodization was carried out at voltages varying from 10 to 60 V (DC). After the anodization the nanotubes were rinsed with DI water and dried in air. The nanotubes were annealed in stagnant air at 500°C for 2 h with a temperature ramp rate of $1.5^\circ\text{C min}^{-1}$.

2.3. Site-specific growth of TiO_2 nanotubes

Two photolithography steps were used to achieve site-specific and patterned growth. The steps are depicted in figure 1. Ti was deposited 350 nm to $1\ \mu\text{m}$ thick on clean Si wafer with 100 nm thermally grown dry SiO_2 in a similar way to that stated before. The Ti was then patterned using photolithography to form the Ti electrodes. Ammonium hydroxide (30% concentration) and hydrogen peroxide (30% concentration) at a ratio (volume) of 1:2 were used as the etchant for patterning the Ti film. Shipley's S1813 positive photoresist was used for the lithography. The photoresist was spun on the wafer at 2000 rpm. The thickness of the photoresist was about $2\ \mu\text{m}$. 'Light field' Cr based masks were used to pattern the Ti on the substrate. The masks were designed using a Heidelberg Micro PG 101 (pattern generator) system. Using another photolithography step, photoresist was deposited and a pattern was created such that a window was created in the photoresist exposing a small region on the bridge connecting the two electrodes. The developed photoresist was hard baked at 120°C for two minutes. The photoresist was used to mask the Ti film during anodization to achieve site-specific growth of the nanotubes down to areas of 0.01 mm^2 . The anodization was carried out in a dark room to prevent exposure of the photoresist to UV light.

2.4. Characterization

The nanotubes before and after annealing were characterized by scanning electron microscopy (SEM) micrographs from an FEI NanoNova SEM, and an x-ray diffraction technique using a Philips X'Pert XRD system. SEM was used to characterize the length and diameter of the tubes. X-ray diffraction was used for identification and determination of the crystalline phases of the nanotubes. X-ray diffraction with incidence angle ranging from 20° to 80° was used.

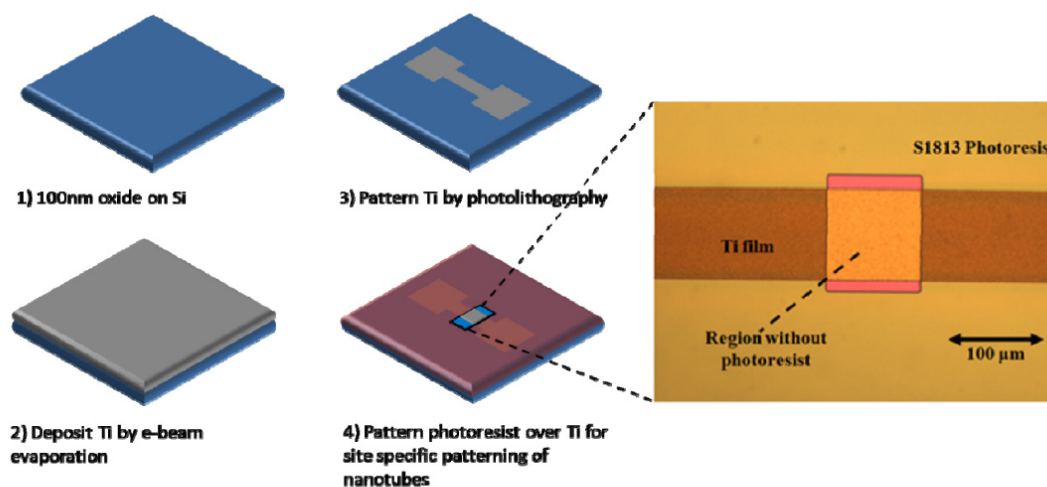
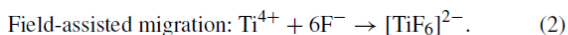
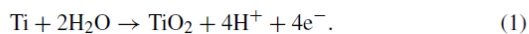


Figure 1. The fabrication steps used for site-specific growth of TiO_2 nanotubes. The right optical image shows the region with exposed Ti film via patterned photoresist before anodization.

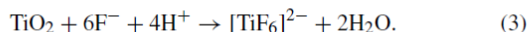
3. Results and discussion

Titania nanotube growth via electrochemical anodization is the result of a competition between electrochemical oxide formation and field-assisted/chemical oxide dissolution, which can generally be summarized by the following reactions [27].

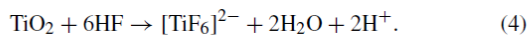
Field-assisted oxidation:



Field-assisted dissolution:



Chemical dissolution:



The field-assisted reactions (equations (1)–(3)) drive the Ti/TiO₂ interface deeper into the Ti foil, which results in an increase in length of the nanotubes, while chemical dissolution (equation (4)) decreases the length of the nanotubes [27]. In this study, an organic electrolyte with near neutral pH (pH ~ 6.6) was used to limit chemical dissolution. Further details on the mechanism of T-NT formation via anodization of Ti are available in the literature [6, 28, 29].

Scanning electron micrographs (SEMs) of various T-NTs formed by anodization on thin Ti film are shown in figure 2. From the top view (figure 2(a)), the surface appears to have more of a porous structure and a non-uniform tubular structure. Removal of ~30 nm of the non-uniform porous top layer via Ar ion milling reveals a tubular morphology below (figure 2(b)). The cross section of the T-NT film (figure 2(c)) shows that the T-NTs have interconnected sidewalls. The interconnected ripples on the sides on the nanotubes can be attributed to the water content of the electrolyte causing small oscillation in current during the anodization process [30].

Figure 2(d) shows the bottoms of the T-NTs after peeling off from the wafer. The bottoms of the tubes form in a hexagonal pattern, which is also observed when T-NTs are formed on Ti foils at high anodization potentials [31]. The formation of a nanoporous layer on top of the T-NTs may be a result of the deposition technique (i.e. e-beam deposition). Metal films deposited by the e-beam technique generally form poly-crystalline films consisting of several grains, which are more pronounced at the topmost layer of the film. The sizes of the grains vary based on several deposition conditions (e.g., vacuum, distance between the substrate and the metal source, e-beam current, amount of material present in the evaporation crucible, etc). Weickert *et al* [32] anodized DC sputtered film in a similar electrolyte, and observed a nanoporous layer very similar to the observation made by us. A similar observation of a nanoporous layer was made when thin Ti film was anodized (using different electrolytes from the ones used by us) by Stergiopoulos *et al* [33] (glycerol and ammonium fluoride as electrolyte), by Yu-xin *et al* [34] (aqueous/non-organic HF solution as electrolyte) and by Yang *et al* [35] (aqueous solutions mixed with highly corrosive Na₂SO₄/NaF/citric acid as electrolyte). However, it is seen that with the use of highly reactive electrolytes such as aqueous HF (which etch the Ti/TiO₂ at a faster rate), the nanoporous layer is present initially but is eventually etched away (due to undesired etching) during anodization exposing the tubular structure (seen in anodization time based studies [34]). Please note that the term ‘undesired etching’ refers to etching of Ti/TiO₂ in directions other than the ones defined by the electric field. However, Sohn *et al* [25] and Smith *et al* [20] anodized Ti foil using the same type of electrolyte and no nanoporous layer was observed. Therefore, a thin, native TiO₂ surface layer along with a pronounced grain structure may be the result of this top layer morphology.

An approach for understanding the formation of the top nanoporous structure is summarized as follows. Titania

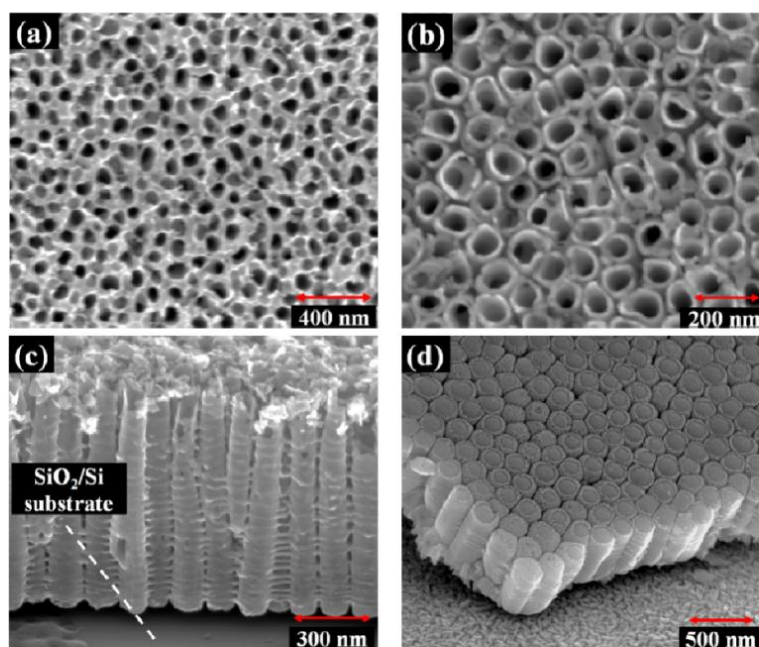


Figure 2. (a) Top view SEM of the T-NTs formed by anodization of 1 μm Ti film at 40 V, (b) after argon ion milling to remove the top layer, (c) side view of the nanotubes imaged at 60° tilt anodized at 30 V for 1 h, (d) image of the bottoms of the tubes after peeling from the wafer (60 V, anodized for 30 min, 350 nm Ti sample).

nanotube formation depends on the local electric field and solution diffusion rate [29]. After the initial oxide formation during the anodization process (equation (1)), due to the discontinuous surface, the electric field is not uniformly spread over the surface and becomes localized at the grains as the strongest electric field occurs at the bottom of the grains [36]. The current during anodization reduces and stabilizes rapidly, implying that an initial oxide layer is already formed. The initial oxide layer formed is smooth as the surface of the deposited film has low surface roughness, of the order of a few nanometers [37]. Previous reports show that anodization of a specially processed Ti foil smoothed via mechanical polishing resulted in a nanoporous layer [38] with ordered arrays of nanotubes forming below. This layered feature of the nanotubes is also observed in template-assisted anodization of T-NTs [38], which involves a two-step anodization process. After the first anodization step, nanotubes are formed without a nanoporous layer. These nanotubes are removed to form a dimpled surface formed by the bottoms of the nanotubes. This template is then subjected to a second anodization at a different potential to form nanotubes with a top, porous layer. During the second anodization step, the electric field becomes concentrated at the bottoms of the dimples where locally etching occurs faster resulting in a porous top layer. A similar mechanism applies to the formation of T-NTs on e-beam sputtered films.

Films were anodized at various potentials from 10 to 60 V. Figure 3 shows the change in the diameter of the nanotubes with anodization potential with some

inset SEM micrographs of TiO_2 nanotubes. Poor ordered nanotube formation is observed at 10 V, while at anodization potentials of 20 V and greater more uniform/ordered nanotube formation is achieved. SEM images of T-NTs formed by anodization at 10–60 V are shown in the supplementary information, figure S1 (available at stacks.iop.org/Nano/23/385601/mmedia). From the SEM images it can be seen that with the increase in voltage the diameters of the nanotubes increase, which is commonly observed on other Ti films under similar conditions [31]. The thickness of the nanotube walls also increased with anodization potential. The nanotubes' outer diameter linearly increased from 40 to 230 nm with increase in anodization voltage from 10 to 60 V with about 10% variation in tube diameter. Over several runs, it was observed that the nanotube length was about 1.4 times longer than the thickness of the deposited Ti film. Moreover, the nanotube length did not increase for longer anodization times nor did the anodization potential have any effect on the length of the nanotubes. However, the rate of nanotube formation was increased with increased anodization potential. The nanotubes were longer than the thickness of Ti film, which could be due to the addition of oxygen atoms during anodization. The nanotubes' length was not reduced due to minimal undesired etching by the electrolyte. It has been reported that the use of a low pH electrolyte results in shorter nanotube length (shorter than the thickness of the deposited film) due to undesired etching [22, 39]. During our initial studies, it was observed that a low pH electrolyte (pH \sim 1.5) at room temperature does not result in synthesis of nanotubes. In aqueous solutions,

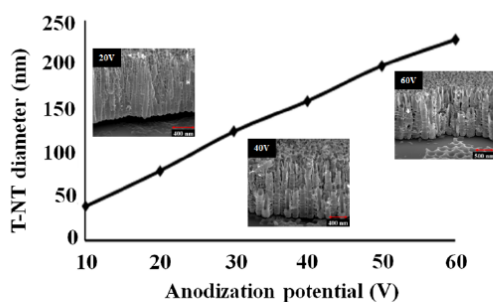


Figure 3. Change in nanotube diameter with anodization potential for 1 h on 1 μm Ti films. Insets show SEM micrographs of T-NT formed by anodization at 20, 40 and 60 V.

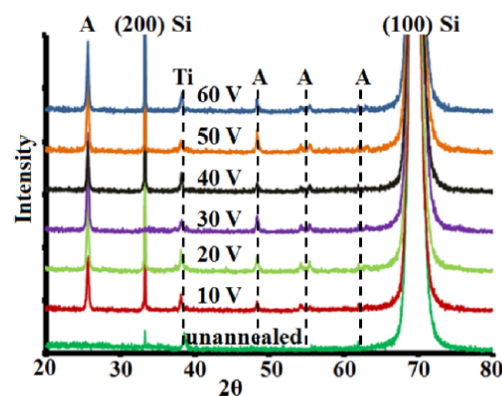
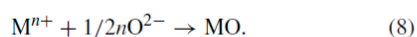
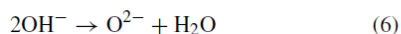


Figure 4. The XRD patterns of the nanotubes before and after annealing at various potentials for one hour on 1 μm Ti films. 'A' indicates the anatase phase of TiO_2 , 'Si' indicates peaks for silicon and 'Ti' labels peaks associated with the underlying titanium.

hydroxyl ions are a source of oxygen for oxide formation, given by the reactions [28]



Since a thin film was the source of Ti, the growth rate of the nanotubes was higher when compared to Ti foils. For example, anodization of Ti foils (0.2 mm thickness) at 20 V for 1 h in the same electrolyte results in nanotubes of ~ 500 nm [26], whereas anodization of a 1000 nm Ti film under similar conditions results in nanotubes of ~ 1400 nm in length. This may be due to the difference in the morphology of thin film versus foil. It is well known that thin films have more defects and are less dense compared to commercially available Ti foil. Due to the difference in density and higher number of defects (the etch rates depend on the crystal orientation), the nanotubes may form at a faster rate.

The top surfaces of the tubes (few tens of nm) had smaller tube diameters compared to the lower portions of the tubes and showed a tapering structure. This may be due to the anodization of the film during the voltage ramp up phase [40] and/or may be due to the effect of native titania. Post-anodization, the samples were washed with DI water, dried in air and then subjected to calcination. No visible physical changes (i.e., film delaminating) were observed before and after annealing the nanotubes, demonstrating the stability of the developed films.

Figure 4 shows the XRD patterns of the nanotubes before and after annealing. The XRD showed that before annealing the tubes are amorphous with the presence of a 2 theta degree peak at 38° showing the presence of Ti, and a high intensity peak at 69° showing the presence of the underlying (100) single crystal Si. Annealed samples were shown to be predominantly anatase phase TiO_2 with 2 theta degree peaks at 25° , 48° , 54° , 55° and 62° along with a low intensity peak present at 38° for traces of Ti metal which was not anodized. Also a 2 theta peak at 33° was detected showing the presence of (200) Si which may be due to stress induced by

the evaporated Ti film. X-ray diffraction analysis confirmed the formation of predominantly anatase phase titania, while there were no noticeable stress induced shifts in the anatase TiO_2 peaks confirming stable T-NTs. From the cross-sectional SEM images (figures 2(c) and S1 available at stacks.iop.org/Nano/23/385601/mmedia), it is observed that the entire thickness of the evaporated Ti film is anodized to form T-NTs. The detected Ti may be present at the very bottom in the crevices between the tubes which are electrically isolated by surrounding T-NTs and hence not be anodized. From the inset SEM micrographs in figure 3 it can be observed that in regions on the Si substrate where the nanotubes were peeled off (during SEM sample preparation), crater like structures are present which may be the metallic un-anodized Ti. Mor *et al* [21] showed that the underlying, non-continuous residual metallic Ti can be fully anodized/eliminated by a two-step deposition technique. In the first deposition step, Ti metal is deposited over the entire substrate. During the second deposition, Ti metal is deposited in regions which will be exposed to the electrolyte during anodization. A two-step deposition method is required for full metal anodization as the etching of Ti is higher at the metal–air–electrolyte junction compared to the metal–electrolyte junction due to non-uniform electric field. The required thickness of the first deposited Ti film depends on the anodization voltage (a minimum of 400 nm for 10 V) to minimize the non-uniform electric field distribution. However, integration of a two-step deposition technique in our work to eliminate the underlying metallic Ti and achieve site-specific growth was not examined and is part of future work.

To obtain site-specific growth of the TiO_2 nanotubes, photoresist was used to mask regions of the thin titanium film. A schematic of the fabrication steps used to mask specific Ti regions is provided in figure 1. For the patterning of the film, 350 nm to 1 μm thick Ti films were used. Square Ti pads of varying size were first investigated. Figure 5 shows SEM micrographs of site-specific grown nanotubes with the top view of the nanotubes on a typical pad with Ti metal

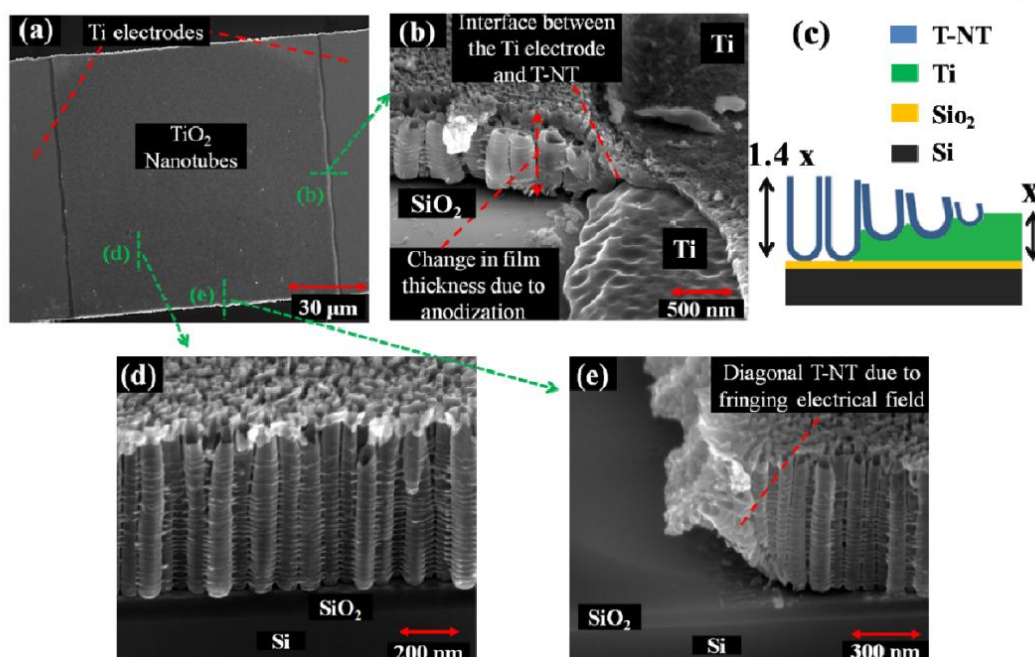


Figure 5. SEM micrographs of site-specific nanotubes. (a) Top view of the nanotubes with self-aligned Ti electrodes of 650 nm deposited film anodized at 20 V for 1 h. The lines labeled '(b)', '(d)' and '(e)' correspond to regions where SEM micrographs were acquired. (b) The interface between the nanotubes and the Ti electrodes, showing the increase in thickness due to anodization, imaged at 60° tilt (350 nm Ti film anodized at 60 V for 1 h). (c) Schematic representation of the interface between the nanotubes and the Ti electrode after removal of the photoresist. (d) Cross sections of the nanotubes in the central region and (e) nanotubes at the edge after anodization of the patterned Ti film. Anodization was carried out at 20 V for 1 h on 650 nm Ti film.

contacts as depicted in figure 5(a). Successful site-specific growth of ordered T-NTs on regions as low as 0.01 mm² in area was achieved. The interface between the nanotubes and the Ti electrode after removal of the photoresist is shown in figure 5(b). The T-NT length in site-specific regions was also observed to be about 1.4 times the thickness of the evaporated Ti film, similar to when larger Ti areas are anodized. From SEM analysis it can also be seen that the Ti electrode is in contact along the base and sidewalls of the nanotubes forming an electrical contact. At the interface defined by the photoresist, the nanotubes do not end abruptly as a defined step. It can be observed (figure 5(b)) that the nanotubes continue to grow beyond the photoresist interface due to the electrolyte going underneath the photoresist as a result of capillary action. This results in a gradual decrease in nanotube length further away from the photoresist interface as depicted in figure 5(c). An inverse trend for the underlying Ti can be observed, in that the Ti metal becomes thicker closer to the photoresist interface. The cross sections of the T-NT (figure 5(d)) nanotubes in the central portion of the nanotube site show similar T-NT morphology for larger Ti pads when anodized. At the vertical walls of the patterned film the nanotubes have a diagonal orientation (figure 5(e)), which is in the orientation of the fringing electric field. It is observed that the nanotube morphology does not change with site-specific growth with the exception of

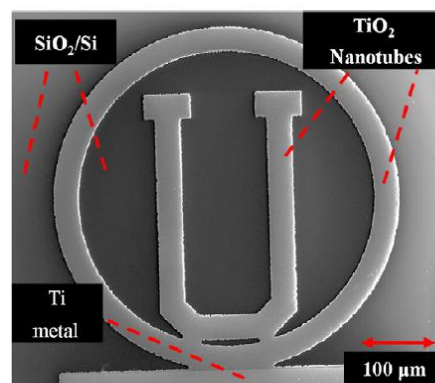


Figure 6. Patterned growth of nanotubes resembling the letter 'U' with 25 μm pattern size feature on a 650 nm deposited film. A two-step photolithography technique was utilized. Anodization was carried out at 30 V for 1 h.

the photoresist interface. Photolithographic techniques were applied for patterned growth of T-NTs in a 25 μm feature in the shape of a 'U' (figure 6). Closer magnification reveals that the nanotubes formed are similar when larger Ti areas are anodized.

In most of the sensors demonstrated using T-NTs, the change in electrical signal is measured as the output [12, 13]. Electrical resistance measurement of the site-specific grown (0.01 mm^2) T-NTs via self-aligned Ti electrodes showed only thermal noise and was beyond the measuring capability of the Keithley 4200 SCS (semiconductor characterization system). The nanotubes are interconnected along the side walls via thin (5–10 nm) membranes which may be the reason for the high electrical resistance. Therefore site-specific grown T-NTs (with interconnecting membranes) with an electrical conduction path length of $100 \mu\text{m}$ and width of $100 \mu\text{m}$ resulted in only thermal noise. This resulted in the need for T-NTs in regions of less than 0.01 mm^2 with an electrical conduction path shorter than $100 \mu\text{m}$. However, in regions smaller than 0.01 mm^2 no T-NT formation was observed. This may be due to the photolithographic technique used and the high electric field applied to a relatively small area. Further studies are underway to understand the role of masking and growth of T-NTs on smaller areas. Another constraint to successful formation of T-NTs using photolithographic techniques is that the S1813 photoresist has a limit of about 1 h for anodization as it is slightly soluble in the anodizing electrolyte. Exposure to UV light increases the solubility of the photoresist in the electrolyte as well. Without a hard bake, the limit of photoresist is less than 30 min. Also, during the hard bake, the Ti film is exposed to ambient environment forming an even thicker titania surface layer. To confirm the effect of native TiO_2 on the nanotube formation, the Ti film was heated in ambient environment for about 10 min at 200°C followed by anodization. From the cross-sectional SEM micrographs it was observed that the non-tubular portion (top nanoporous layer, *vide supra*) was much longer compared to that for the T-NTs synthesized from Ti films with only native TiO_2 . The thermally induced oxide is subsequently comparable in thickness to that of the underlying Ti layer. The thicker oxide layer hinders the dissolution of Ti species and ordered nanotube formation is only realized below the oxide layer. As a result, special care should be taken to minimize native TiO_2 formation.

4. Conclusion

TiO_2 nanotube arrays were successfully grown on Si wafer by e-beam evaporation of Ti film followed by anodization in an organic electrolyte. A nanoporous layer on top of the nanotubes was observed due to the presence of native titania and grains from the evaporated film. Upon milling the top region of the titania nanotubes, regular nanotube formation below the nanoporous layer was observed. The diameter of the nanotubes increased linearly from about 40 to 240 nm with increase in anodization voltage from 10 to 60 V. SEM imaging showed that the length of the nanotubes was limited by the thickness of the Ti film and upon anodizing the titania nanotube length was about 1.4 times the thickness of the deposited Ti film in this study. XRD showed that the unannealed nanotubes were mostly amorphous and formed anatase phase TiO_2 upon annealing in air at 500°C ; they were demonstrated to be stable films. Site-specific growth of TiO_2

nanotubes in regions as small as 0.01 mm^2 with self-aligned Ti electrodes was achieved using two photolithography steps. The ability to synthesize T-NTs with site-specific and patterned growth through a simple anodization process opens new potential applications for T-NTs in wafer-scale devices. Through various characterization tools, it can be concluded that the T-NTs formed on Si wafer have similar properties to T-NTs formed on foil, giving rise to potential applications realized by foil based T-NTs. The site-specific and patterned growth of T-NTs by common techniques used in the semiconductor industry opens many potential avenues for the application of T-NTs in NEMS/MEMS devices and large-scale commercialization.

Acknowledgments

The work presented here was supported by the Utah Science and Technology Research (USTAR) initiative. The authors also declare no conflict of financial interest.

References

- [1] Bogue R 2007 MEMS sensors: past, present and future *Sensor Rev.* **27** 7–13
- [2] Luczak S, Oleksiuk W and Bodnicki M 2006 Sensing tilt with MEMS accelerometers *IEEE Sensors J.* **6** 1669–755
- [3] Rebello K J 2004 Applications of MEMS in surgery *Proc. IEEE* **92** 43–55
- [4] Zwilling V, Aucouturier M and Darque-Ceretti E 1999 Anodic oxidation of titanium and TA6V alloy in chromic media. An electrochemical approach *Electrochim. Acta* **45** 921–9
- [5] Zwilling V, Darque-Ceretti E, Boutry-Forveille A, David D, Perrin M Y and Ancouturier M 1999 Structure and physicochemistry of anodic oxide films on titanium and TA6V alloy *Surf. Interface Anal.* **27** 629–37
- [6] Roy P, Berger S and Schmuki P 2011 TiO_2 nanotubes: synthesis and applications *Angew. Chem. Int. Edn* **50** 2904–39
- [7] Mor G K, Varghese O K, Paulose M, Shankar K and Grimes C A 2006 A review on highly ordered, vertically oriented TiO_2 nanotube arrays: fabrication, material properties, and solar energy applications *Sol. Energy Mater. Sol. Cells* **90** 2011–75
- [8] Liu Z and Misra M 2010 Bifacial dye-sensitized solar cells based on vertically oriented TiO_2 nanotube arrays *Nanotechnology* **21** 125703
- [9] Misra M and Raja K S 2010 Ordered titanium dioxide nanotubular arrays as photoanodes for hydrogen generation *Solar Hydrogen and Nanotechnology* ed L Vayssieres (Chichester: Wiley)
- [10] Mohapatra S K, Mahajan V K and Misra M 2007 Double-side illuminated titania nanotubes for high volume hydrogen generation by water splitting *Nanotechnology* **18** 445705
- [11] Zhang G, Huang C, Zhou L, Ye L, Li W and Huang H 2011 Enhanced charge storage by the electrocatalytic effect of anodic TiO_2 nanotubes *Nanoscale* **3** 4174–81
- [12] Mor G K, Varghese O K, Paulose M and Grimes C A 2003 A self-cleaning room temperature titania-nanotube hydrogen gas sensor *Sensor Lett.* **1** 42–6
- [13] Banerjee S, Mohapatra S K and Misra M 2009 The detection of improvised nonmilitary peroxide based explosives using a titania nanotube array sensor *Nanotechnology* **20** 075502
- [14] Mishra A, Banerjee S, Mohapatra S K, Graeve O A and Misra M 2008 Synthesis of carbon nanotube– TiO_2 nanotubular material for reversible hydrogen storage *Nanotechnology* **19** 445607

- [15] Mun K-S, Alvarez S D, Choi W-Y and Sailor M J 2010 A stable, label-free optical interferometric biosensor based on TiO₂ nanotube arrays *ACS Nano* **4** 2070–6
- [16] Kar A, Raja K S and Misra M 2006 Electrodeposition of hydroxyapatite onto nanotubular TiO₂ for implant applications *Surf. Coating Technol.* **201** 3723–31
- [17] Kar A, Smith Y R and Subramanian V R 2009 Improved photocatalytic degradation of textile dye using titanium dioxide nanotubes formed over titanium wires *Environ. Sci. Technol.* **43** 3260–5
- [18] Liu Z and Misra M 2010 Dye-sensitized photovoltaic wires using highly ordered TiO₂ nanotube arrays *ACS Nano* **4** 2196
- [19] Liu Z, Subramanian V and Misra M 2009 Vertically oriented TiO₂ nanotube arrays grown on Ti meshes for flexible dye-sensitized solar cells *J. Phys. Chem. C* **113** 14028–3
- [20] Smith Y R and Subramanian V 2011 Heterostructural composites of TiO₂ mesh TiO₂ nanoparticles photosensitized with CdS: a new flexible photoanode for solar cells *J. Phys. Chem. C* **115** 8376–85
- [21] Mor G K, Varghese O K, Paulose M and Grimes C A 2005 Transparent highly ordered TiO₂ nanotube arrays via anodization of titanium thin films *Adv. Funct. Mater.* **15** 1291–6
- [22] Yu X, Li Y, Ge W, Yang Q, Zhu N and Zadeh K K 2006 Formation of nanoporous titanium oxide films on silicon substrates using an anodization process *Nanotechnology* **17** 808
- [23] Macak J M, Tsuchiya H, Berger S, Bauer S, Fujimoto S and Schmuki P 2006 On wafer TiO₂ nanotube-layer formation by anodization of Ti-films on Si *Chem. Phys. Lett.* **428** 421–5
- [24] Asthana A, Shokuhfar T, Gao Q, Heiden P, Friedrich C and Yassar R S 2010 A study on the modulation of the electrical transport by mechanical straining of individual titanium dioxide nanotube *Appl. Phys. Lett.* **97** 072107
- [25] Song Y-Y, Schmidt-Stein F, Bauer S and Schmuki P 2009 Amphiphilic TiO₂ nanotube arrays: an actively controllable drug delivery system *J. Am. Chem. Soc.* **131** 4230–2
- [26] Sohn Y S, Smith Y R, Subramanian V R and Misra M 2008 Electrochemically assisted photocatalytic degradation of methyl orange using anodized titanium dioxide nanotubes *Appl. Catal. B* **84** 372–8
- [27] Mohammadpour A, Waghmare P R, Mitra S K and Shankar K 2010 Anodic tipodal TiO₂ nanotubes *ACS Nano* **4** 7421–30
- [28] Raja K S, Gandhi T and Misra M 2007 Effect of water content of ethylene glycol as electrolyte for synthesis of ordered titania nanotubes *Electrochem. Commun.* **9** 1069–76
- [29] Raja K S, Misra M and Paramguru K 2005 Formation of self-ordered nano-tubular structure of anodic oxide layer on titanium *Electrochim. Acta* **51** 154–65
- [30] Song Y-Y and Schmuki P 2010 Modulated TiO₂ nanotube stacks and their use in interface sensors *Electrochem. Commun.* **12** 579–82
- [31] Mohapatra S K, Misra M, Mahajan V K and Raja K S 2007 Design of a highly efficient photoelectrolytic cell for hydrogen generation by water splitting: application of TiO_{2-x}C_x nanotubes as a photoanode and Pt/TiO₂ nanotubes as a cathode *J. Phys. Chem. C* **111** 8677–85
- [32] Weickert J, Palumbiny C, Nedelcu M, Bein T and Lukas Schmidt-Mende 2011 Controlled growth of TiO₂ nanotubes on conducting glass *Chem. Mater.* **23** 155–62
- [33] Stergiopoulos T, Valota A, Likodimos V, Speliotis T, Niarchos D, Skeldon P, Thompson G E and Falaras P 2009 Dye-sensitization of self-assembled titania nanotubes prepared by galvanostatic anodization of Ti sputtered on conductive glass *Nanotechnology* **20** 365601
- [34] Yu-xin T, Jie T, Yan-yan Z, Tao W, Hai-jun T and Ya-rong Z 2009 Preparation of TiO₂ nanotube on glass by anodization of Ti films at room temperature *Trans. Nonferrous Met. Soc. China* **19** 192–8
- [35] Yang D-J, Kim H-G, Cho S-J and Choi W-Y 2008 Vertically oriented titania nanotubes prepared by anodic oxidation on Si substrates *IEEE Trans. Nanotechnol.* **7** 131–4
- [36] Parkhutik V P and Shershulsky V I 1992 Theoretical modelling of porous oxide growth on aluminium *J. Phys. D: Appl. Phys.* **25** 1258–63
- [37] Cai K, Muller M, Bossert J, Rechtenbach A and Jandt K D 2005 Surface structure and composition of flat titanium thin films as a function of film thickness and evaporation rate *Appl. Surf. Sci.* **250** 252–67
- [38] Li S, Zhang G, Guo D, Yu L and Zhang W 2009 Anodization fabrication of highly ordered TiO₂ nanotubes *J. Phys. Chem. C* **113** 12759
- [39] Kang S H, Kim J-Y, Kim H S and Sung Y-E 2008 Formation and mechanistic study of self-ordered TiO₂ nanotubes on Ti substrate *J. Indust. Eng. Chem.* **14** 52–9
- [40] Mor G K, Varghese O J, Paulose M, Mukherjee N and Grimes C A 2003 Fabrication of tapered, conical-shaped titania nanotubes *J. Mater. Res.* **18** 2588–93

Supplementary Information

Site-Specific and Patterned Growth of TiO₂ Nanotube Arrays From E-Beam Evaporated Thin Titanium Film on Si Wafer

Karumbaiah N. Chappanda^{1,5}

York R. Smith^{2,5}

Mano Misra^{2,3}

Swomitra K. Mohanty,^{3,4}

¹Electrical & Computer Engineering Department, University of Utah, Salt Lake City, UT 84112, USA

²Metallurgical Engineering Department, University of Utah, UT 84112, USA

³Chemical Engineering Department, University of Utah, UT 84112, USA

⁴Corresponding author e-mail: s.k.mohanty@utah.edu

⁵These authors contributed equally

Figure S1, SEM micrographs showing the cross-section of T-NT anodized at 10-60V.....S2

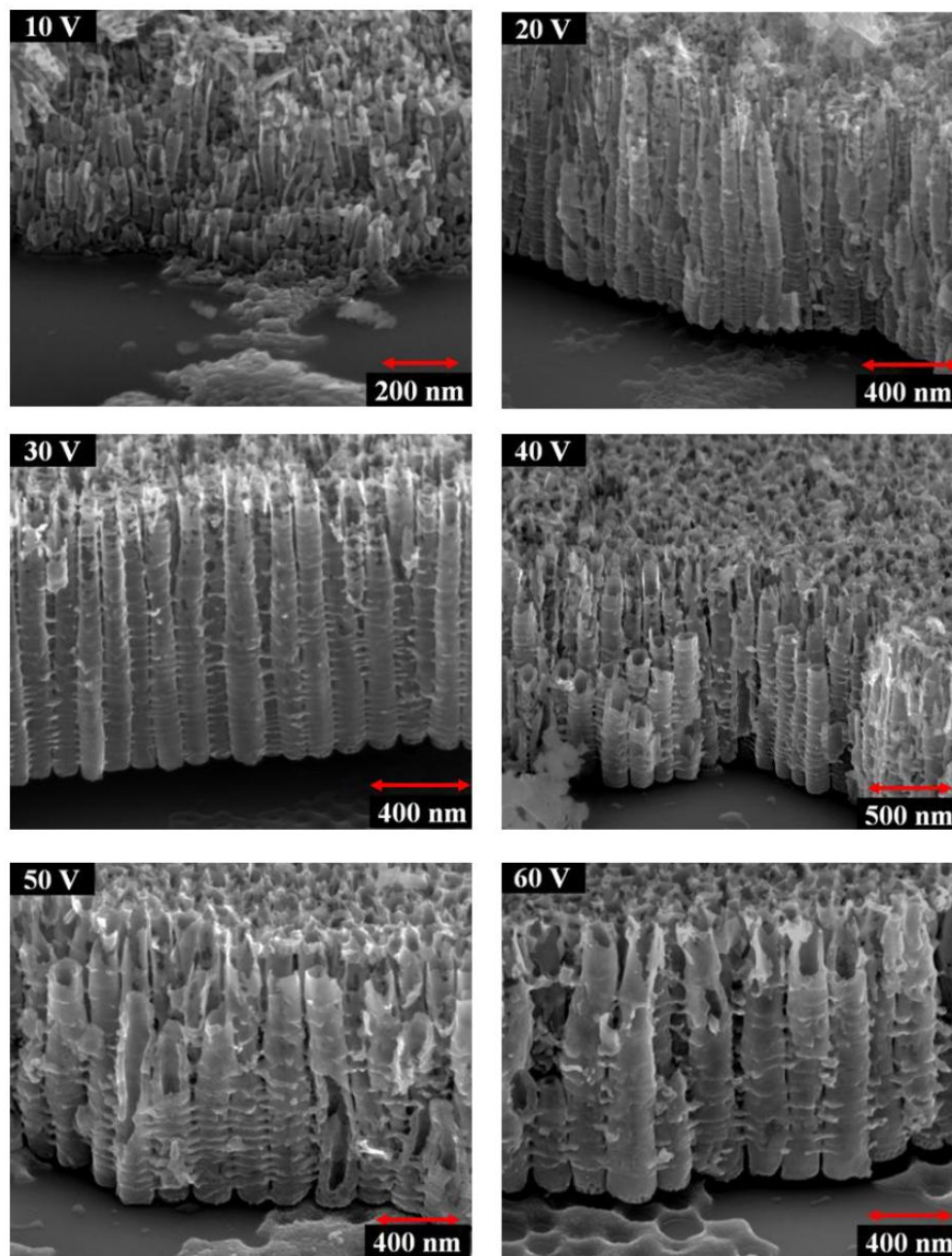


Figure S1: SEM micrographs showing the cross-section of T-NT anodized at 10-60V on 1 μm Ti film for one hour. (The SEM micrographs were obtained at different magnification in order to accommodate the length as well the morphology of the nanotubes).

CHAPTER 5

EFFECT OF SPUTTERING PARAMETERS ON THE MORPHOLOGY OF TiO₂ NANOTUBES SYNTHESIZED FROM THIN Ti FILM ON Si SUBSTRATE

5.1 Abstract

In this paper, we present the analysis of the properties of direct current (D.C.) magnetron sputtered Ti thin film that affect the morphology of TiO₂ nanotubes synthesized by electrochemical anodization. A Si wafer with thermally grown silicon dioxide was used as the substrate for deposition of Ti films. By varying the properties of the sputtered film, morphology of the anodized film can be varied from tubular to nanoporous TiO₂. Three sputtering parameters that affect the properties of the film were studied, which include sputtering power, process gas (argon) pressure, and substrate temperature. Anodization of these films was carried out at 30 V (D.C.) using an ethylene glycol based electrolyte. We show that the properties of thin films such as grain size and residual stress (biaxial) do not affect the morphology of the anodized film, and density alone influences the morphology of the anodized film. Most of the applications demonstrated by TiO₂ nanotubes require annealing at high temperatures (350–800°C) for calcination. Low residual stress in the thin film is required to prevent delaminating of the nanotubes from the substrate when exposed to high temperatures. We demonstrate that by varying the sputtering parameters, Ti films with low stress can be deposited, which is required to have stable TiO₂ nanotubes or nanoporous structure, based on the requirement of the application.

5.2 Introduction

In the recent decade, many applications such as sensors [1], [2], battery [3], [4], photocatalysis [5], photoelectrolysis [6], photovoltaics [6], [7], and capacitors [8], [9] using TiO₂ nanotubes (T-NT) have been demonstrated. One of the main drawbacks is that

these applications mainly have been demonstrated using T-NT synthesized from Ti foil. T-NT on foil limits the ability to integrate with the current high-precision microfabrication techniques to fabricate economical, sensitive, miniaturized, and low power T-NT-based devices, which is required for commercialization. One of the ways to approach this problem is by synthesis of T-NT from thin Ti films deposited on stable and planar substrates such as Si. Synthesis and characterization of T-NT from thin film on substrates such as glass [10], plastic [11], quartz [12], and silicon [13] have been previously demonstrated. Thin Ti film deposited by different techniques such as D.C. sputtering [14], radio frequency (RF) sputtering [15], thermal evaporation [15], and e-beam evaporation [16] have been used for synthesis of T-NT. However, very little work aimed at understanding the properties of these thin films that affect the morphology of the T-NT have been reported, and most of the work has mainly focused on understanding the growth mechanism of T-NT. Moreover, little work demonstrating applications such as solar cells [10], [11] and sensors [17], [18] has been reported using thin film based T-NT. Also, well-developed microfabrication processes such as photolithography were not used to fabricate these thin film T-NT-based devices, and hence, the advantages of microfabrication process such as miniaturization capability were not utilized, making them similar to T-NT synthesized on foil. In our previous work, we demonstrated integration of photolithography to achieve site-specific and patterned growth of T-NT on Si substrate with self-aligned electrodes establishing a platform for making miniaturized, highly sensitive, low power, and economical T-NT-based devices [16]. Some of the issues with thin films such as stiction, residual stress, and density of the film need to be addressed in order to synthesize stable T-NT on planar substrates before including

integrated circuits for making miniaturized low power devices. To our knowledge, no detailed study to understand the role of properties of thin film that influences the morphology of the nanotubes has been reported in the literature.

In this paper, we report a detailed analysis of deposition parameters of thin Ti film that affect the morphology of T-NT synthesized on Si substrate. A thin film was deposited on Si substrates via D.C. magnetron sputtering which is one of the commonly used thin film deposition techniques in the current semiconductor industry. By changing the sputtering parameters, the properties of the thin film change and are related to the morphology of the synthesized T-NT. We also demonstrate the synthesis of T-NT, semi-T-NT and nanoporous TiO₂ by simply varying the deposition parameters of the thin Ti film. Scanning electron microscopy (SEM) was used to study the morphology of the thin films before and after anodization. Laser interferometry was used to study the residual stress in the thin films.

5.3 Experimental procedure

5.3.1 Thin film deposition

Clean n-type (100) Si wafer with resistivity of 1–5 Ω .cm and with RMS roughness of less than 1 nm were used as substrates to study the synthesis of T-NT from thin film. Wafers were subjected to wet thermal oxidation at 1000 °C to form ~ 100 nm of silicon dioxide. The SiO₂ was grown to electrically isolate the T-NT from the substrate. The type of oxide (wet or dry) grown did not have any effect on the morphology of the T-NT. Ti films about 300–400 nm thick were then deposited on the wafer by D.C. magnetron sputtering in a Denton Discovery 18 sputter system. The sputter chamber was pumped

down to pressures $< 2 \mu\text{Torr}$. A Ti target of 99.97–99.98% purity purchased from Kurt J. Lesker was used for sputtering. Three sputtering parameters were varied to understand the relation between deposition parameters and the morphology of the anodized films. For the first set of runs, process gas (argon) pressure was varied from 2.5 to 7.5 mTorr, while the sputtering power was constant at 150 W, and the Si substrate was at ambient temperature. It should be noted that ambient temperature implies that the substrate was not externally heated, and the only heating that may have occurred was due to the sputtering process. During the second set of runs, the sputtering power was varied from 25 W to 500 W, while the argon pressure was constant at 7 mTorr, and the Si substrate was at ambient temperature. In the third set of the runs, the substrate temperature was varied from 100 to 300 °C, while the argon pressure was constant at 5 mTorr and the sputtering power was constant at 150 W. After sputtering, the wafer was cooled down to ambient temperature in a vacuum to minimize the oxidation of sputtered Ti film. The range of the sputtering parameters was chosen based on the capability of the sputtering system.

5.3.2 T-NT synthesis

The sputtered Ti thin films were subjected to electrochemical anodization at ambient temperature using an organic electrolyte to form T-NT. The experimental set-up used was similar to our previous work [14], [16]. A Si wafer with Ti film was diced into $1 \text{ cm} \times 2 \text{ cm}$ sized pieces. The organic electrolyte consisted of ethylene glycol (89.5 wt%, from Fisher Scientific), DI water (10 wt%), and ammonium fluoride (0.5 wt%, from Fisher Scientific) [19], [20]. The Ti film was cleaned with acetone and isopropanol alcohol

followed by rinsing in DI water. Polyamide tape was used to mask the non-Ti portion of the diced substrate to prevent any reaction between the electrolyte and the substrate. However, it was noticed that the absence of the polyamide tape did not affect the morphology of T-NT but only roughened the surface of the Si substrate in the regions without the SiO₂. The gap between the electrodes was 2.5 cm during anodization. Only about 1 cm² of the diced Ti/SiO₂/Si substrate was subjected to anodization. Magnetic stirring was used to supply fresh electrolyte to the anodization site. A 2 cm long magnetic stirrer at 90 RPM was used to stir ~100 ml of the electrolyte. The anodization voltage was ramped up at the rate of 1 V.s⁻¹. For all the runs, the anodization was carried out at 30 V (D.C.). After anodization the tubes were again cleaned in acetone and isopropanol alcohol, followed by rinsing in DI water. The samples were then dried in air and used for characterization studies.

5.3.3 Characterization

Scanning electron microscopy (SEM) micrographs were collected using an FEI NanoNova SEM. These micrographs were used to characterize qualitative density and the structural morphology of the thin film before and after anodization. All the top view micrographs were obtained at magnification of 200 000x, and the side view micrographs were obtained at magnification of 250 000x and 60° tilt. The residual stress of the Ti film was measured using laser interferometry (Tencor FLX-2320) by measuring the bow in the Si wafer before and after deposition of the Ti film. The average grain size of Ti film was measured using the stereology technique [21].

5.4 Results and discussions

5.4.1 Summary of sputtering process mechanism

The processes that occur during D.C. sputtering can be described and summarized as follows [22]. Sputtering equipment consists of a capacitively coupled plasma generating system [23]. The metal target (Ti in this case) forms the cathode and the substrate (Si) forms the anode of the electric circuit. The dielectric of the capacitor consists of a noble gas (noble gases can be used for reactive sputtering). When a high electric field is applied, dielectric break down occurs resulting in plasma (argon plasma). The ionized gas ions (positive Ar ions in this case) are accelerated toward the target metal. Argon ions upon striking the target may penetrate the target (implant), eject secondary electrons, reflect off from the target, or knock off (sputter) Ti atoms and occasional clusters of atoms. The sputtered Ti atoms condense on the substrate to form a thin film. As the Ti atoms approach the substrate, they undergo gas phase scattering with the ionized as well as the unionized Ar atoms resulting in a loss of energy. Ar ion implantation causes the target to heat up which radiatively and conventionally heats the substrate. The ejected secondary electrons along with the electrons produced due to ionization of the gas are accelerated toward the substrate which may further condense the film or sputter the already formed film, which is called the “atomic peening” effect [24], [25]. Atomic peening also contributes to the increase in the substrate temperature. Upon reaching the surface the gas phase Ti atoms form nucleation sites. These nuclei further attract gas phase Ti adatoms to form larger Ti chunks (islands). If the energy of the adatoms arriving on the substrate is sufficient enough, then these islands will merge together due to surface diffusion to form a uniform thin polycrystalline film. The morphology of the film, due to

the influence of the sputtering process, is described in detail using the Thornton model [26], [27].

5.4.2 Effect of gas pressure

Fig. 5.1 shows the SEM micrographs of the thin Ti film before and after anodization for the first set of sputtering experiments. The first set of runs implies that the films were sputtered at different argon pressure while the sputtered power was constant at 150 W and the substrate was at ambient temperature. The sputtering power 150 W was chosen as it is among the commonly used sputtering power, for studying thin film properties [28], [29]. Fig. 5.1 (a-1), (b-1), and (c-1) shows the top view SEM micrographs of the Ti film (before anodization) sputtered at 2.5 mTorr, 5 mTorr and 7.5 mTorr argon pressure, respectively. It can be observed that with the increase in the argon pressure, the average grain size increases (see Table 5.1 for values). Similar observations have been reported where the grain size of the sputtered film increases with increases in argon pressure [30]. With an increase in argon pressure there is more Ti gas phase scattering, resulting in higher energy loss along with lower surface diffusion to form larger grains. Fig. 5.1 (a-2), (b-2), and (c-2) shows the crosssectional SEM micrographs of the Ti film before anodization for the first set of runs. From the side view it can be observed that the film has a vertical column-like structure. This is because of the loss of adatom energy along with increased scattering (with pressure), where the adatoms adhere prominently to the initially formed islands. Also, there is an increase in the deviation of the adatoms from a perpendicular (to the substrate) trajectory due to the adatoms arriving in a scattered manner, causing the self-shadowing effect to increase. Due to these combined processes,

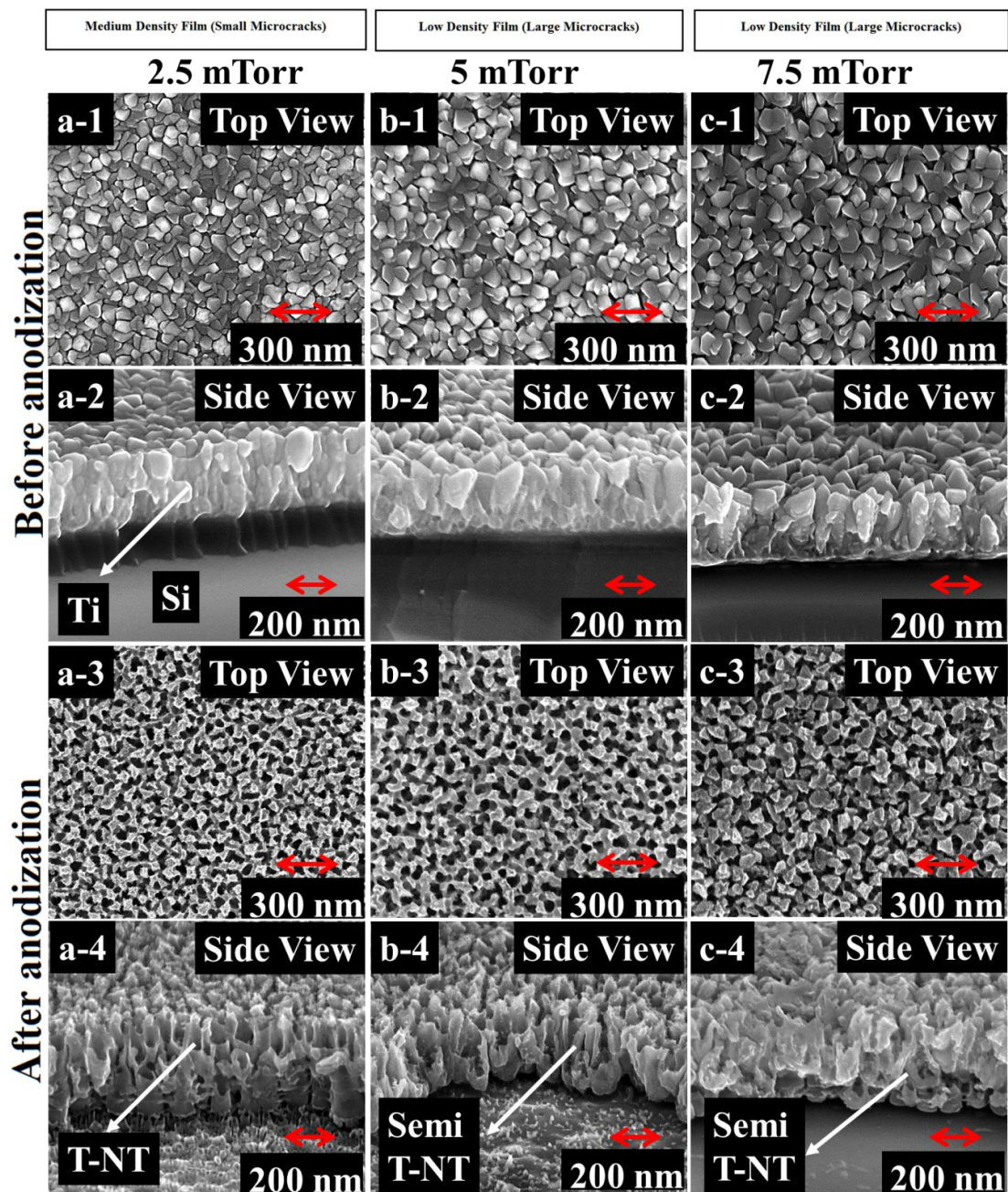


Figure 5.1: SEM micrographs of Ti sputtered on Si wafer before and after anodization for the first set of runs. The substrate was at ambient temperature and the sputter power was 150W while the argon pressure was varied from 2.5 mTorr to 7.5 mTorr. (a-1), (a-2), (a-3) and (a-4) show the top view (before anodization), side view (before anodization), top view (after anodization), and side view (after anodization) sputtered at 2.5 mTorr, respectively. Similarly, (b) and (c) show the top and side views of the films sputtered at 5 mTorr and 7.5 mTorr, respectively.

Table 5.1: Summary of the sputtering parameters and properties of the thin Ti film

Sputtering power (Watts)	Argon pressure (mTorr)	Substrate temperature (°C)	Film thickness (nm)	Average grain size (nm)	Residual stress (+MPa)	Tubularity
150	2.5	Ambient	340	58	200	T-NT
150	5	Ambient	310	65	170	Semi-T-NT
150	7.5	Ambient	310	72	140	Semi-T-NT
25	7	Ambient	335	62	80	Nanoporous
300	7	Ambient	340	70	120	Semi-T-NT
500	7	Ambient	310	80	140	T-NT
150	5	100	380	72	20	Semi-T-NT
150	5	200	380	75	90	T-NT
150	5	300	360	95	60	T-NT

the column-like structure increases with argon pressure. From the side view, the grain size of the film is not clearly visible, which may be due to the method used for SEM sample preparation. However, from the side view, it can also be observed that the defects present in thin film due to polycrystalline grains are relatively more pronounced in the upper portion of the thin film. This is because the grains at the bottom become more condensed than the grains in the upper portion of the film since the lower portion of the film undergoes a longer (timewise) peening effect. Secondary electrons push around the already deposited Ti atoms compared to the upper portion resulting in reduction of the pronounced grains/defects. Also from the side view, qualitatively, it can be observed that the density of the thin film decreases with increase in the argon pressure (see Table 5.1 for relative density). This is also due to increased gas phase scattering, decreased adatom energy for surface diffusion, and increased self-shadowing effect along with decreased peening effect. A similar change in the density of thin films with gas pressure is described by the Thornton model [26]. From the top view SEM micrographs, it can be observed that the gap/defects between the Ti grains increases with increase in gas pressure, affirming the decline in density of the films.

From the laser interferometry, it is observed that with the increase in the argon pressure, the residual stress (biaxial stress) in the film reduces (see Table 5.1 for values). The biaxial residual stress was measured by measuring the bow in the Si substrate before and after depositing the thin Ti films. Residual stress in thin films can be mainly classified as intrinsic and extrinsic stress [31], [32]. Extrinsic stress is mainly due to the difference in the thermal properties between the substrate and the material deposited by impurity contamination during deposition. Intrinsic stress is mainly caused by

microcracks and microdefects in the film. Since for the first set of runs, the sputtering power, and the substrate temperature were the same (any change in temperature due to sputtering would also be the same since the sputtering power was constant), and the depositions were carried out in a clean environment, the difference in the effect of extrinsic stress can be considered to be the same for all the sputtering runs carried out at different argon pressures. For PVD (physical vapor deposition) based deposition such as sputtering, the intrinsic stress in the film can be described using the grain boundary model (GMD) [33]. In this model, the film consists of Ti grains with different crystal orientation that share boundaries, and these grains attract each other due to interatomic forces resulting in stretching of the grains, which results in tensile stress. With the increase in the number of grains (for the same thickness of the film), the number of interatomic forces is higher, resulting in larger tensile residual stress. Therefore, as the argon pressure decreases, the number of grains increases causing the residual stress of the film to increase. Also, as the residual stress increases, the grains are much closer due to the interatomic forces, resulting in a denser film.

A detailed mechanism for synthesis of T-NT by electrochemical anodization can be found in the literature [34]–[36]. In short, the mechanism for tube formation can be summarized as cyclic oxidation of Ti and selective etching of TiO_2 by the electrolyte in the presence of an electric field. Fig. 5.1 (a-3), (b-3), (c-3) and Fig. 5.1 (a-4), (b-4), (c-4) shows the top view and the side view of the film after anodization. From the top view, it is observed that the tubes have a nanoporous layer and do not have tubular morphology all along the thickness of the anodized film. This may be due to the native TiO_2 (formed due to exposure to ambient atmosphere) as well as the pronounced grains at the surface of

the sputtered film as reported in our previous work on synthesis of T-NT from the thin Ti films [14], [16]. The initial T-NT formation begins at the grain boundaries where the electric field is the highest. After etching through the grain boundaries, pits are formed and the direction of the tube-growth/electric-field-assisted etching is defined. From the side view, it can be observed that the film sputtered at 2.5 mTorr argon pressure (Fig. 5.1 (a-4)) forms a tubular structure. At the 5 mTorr and 7.5 mTorr, it is observed that the anodized films have partial tubular morphology, resulting in semi-T-NT. Also, it can be observed that the tubular morphology relatively decreased with the increase in the argon pressure. Further, the T-NTs formed are interconnected by thin membranes, which are attributed to the water content in the electrolyte [37]. The difference in the morphology of the anodized film may be due to the difference in the density, residual stress, grain size, and/or defects in the film.

5.4.3 Effect of sputtering power

Fig. 5.2 shows the SEM micrographs of the sputtered Ti film before and after anodization for the second set of sputtering experiments. The second set of runs implies that the sputtering power was varied from 25–500 W while the substrate was at ambient temperature and the argon pressure was constant at 7 mTorr. From the first set of runs, it was observed that at argon pressures of 5 mTorr and greater, semi-T-NT was formed. Hence, 7 mTorr was chosen to see if T-NT can be formed by varying the sputtering power. Fig. 5.2 (a-1), (b-1), (c-1) shows the top view and Fig. 5.2 (a-2), (b-2) shows the side view of the Ti film (before anodization) sputtered at 25 W, 300 W, and 500 W, respectively. It should be noted that an order magnitude increase in sputtering power was

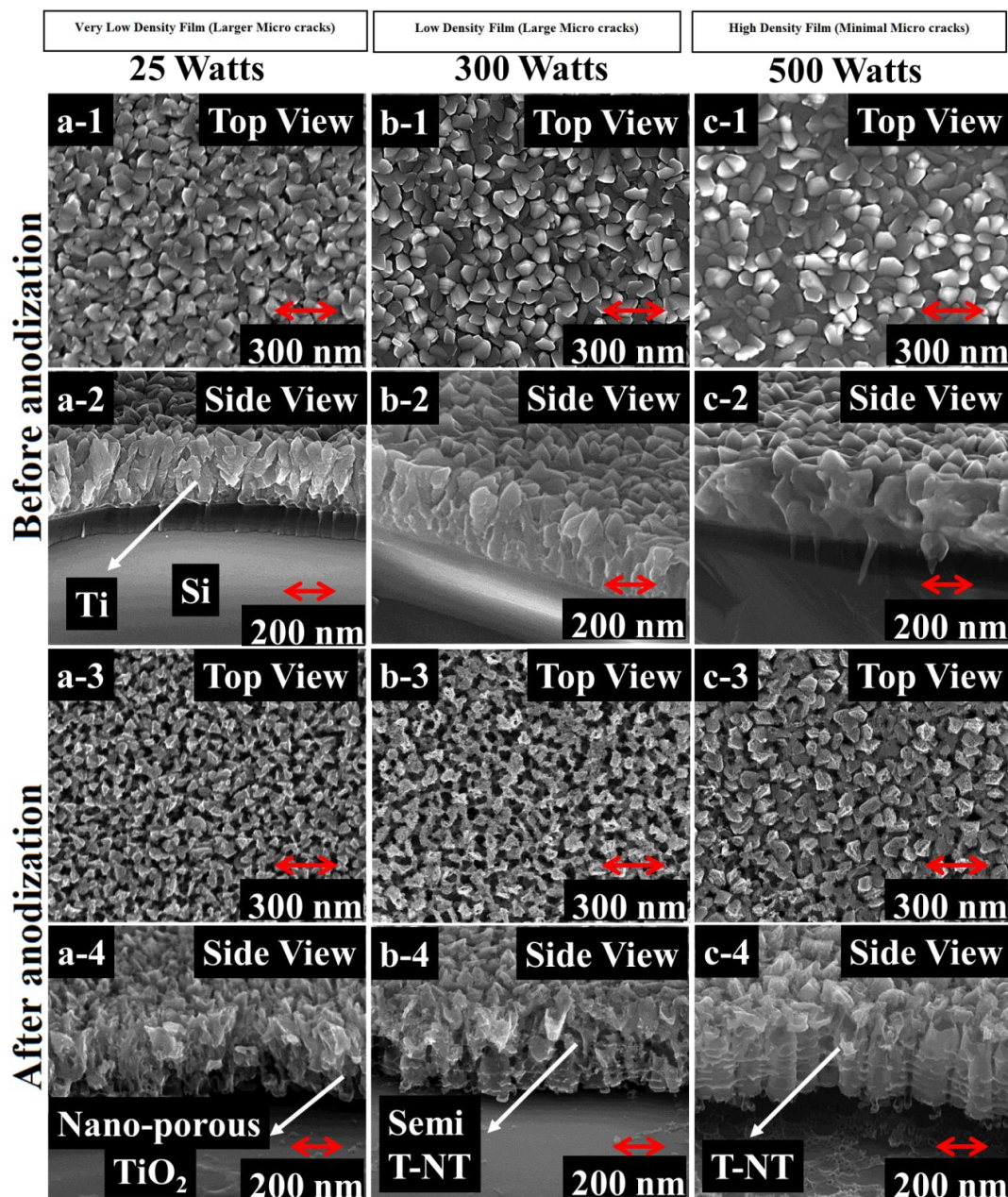


Figure 5.2: SEM micrographs of Ti sputtered on Si wafer before and after anodization for the second set of runs. The substrate was at ambient temperature and the argon pressure was constant at 7mTorr while sputtering power was varied from 25 W to 500 W. (a-1), (a-2), (a-3), and (a-4) show the top view (before anodization), side view (before anodization), top view (after anodization), and side view (after anodization) sputtered at 25 W, respectively. (b) and (c) show the top and side views of the films sputtered at 300 W and 500 W, respectively.

chosen since the first set of runs was sputtered at 150 W. Since the film was sputtered at the same Ar pressure, the gas phase scattering is considered to be the same. From the top view, it can be observed that with increase in the sputtering power, the grain size of the polycrystalline film increases (see Table 5.1 for values). This is because with the increase in the sputtering power, the energy with which ionized argon ions bombard the Ti target is higher, increasing the flux of the Ti atoms arriving at the surface of the substrate forming larger grains [38], [39]. From the side view, it can be observed (qualitatively) that with an increase in sputtering power the density of the films increases (see Table 5.1 for relative density). This is because with the increase in power, the energy of the gas phase Ti atoms increases resulting in higher surface diffusion, higher atomic peening, and a lower self-shadowing effect (there is less deviation from the perpendicular trajectory). Also, the Ar implantation is increased providing additional thermal energy for surface diffusion to form more dense and condensed film [26]. Similar observation of vertical column-like structures can also be noticed. However, the column-like structure reduces (eventually disappears) with the increase in power due to similar processes such as increased atomic peening and higher surface diffusion, which increase the density of the film. Also, similar observations of more numbers of defects in the upper portion (across the thickness) compared to the lower portion can be seen which may attributed to the atomic peening effect. It is observed that with an increase in sputtering power, the residual tensile stress in the film increases. This is because when sputtered at low power, though the grain size is smaller, there is lower densification of the film, resulting in films with more defects/gaps between grains. With the increase in defects/gaps in the film, the interatomic forces are not sufficient enough to have a significant stretching effect on the

grains, resulting in lower residual stress. With an increase in the sputtering power, there is an increase in the heating of the substrate from the target caused by Ar implantation in the Ti target, resulting in extrinsic stress. Also due to better densification of the film with an increase in power, the gap between the grains reduces sufficiently enough to cause/increase the interatomic forces resulting in the increase of tensile residual stress. Fig. 5.2 (a-3), (b-3), (c-3) shows the top view and Fig. 5.2 (a-4), (b-4), (c-4) shows the side view of the Ti film (after anodization) sputtered at 25 W, 300 W, and 500 W, respectively. From the top view, a nanoporous layer is present, similar to the observation made for the first set of runs. From the side view (Fig. 5.2 (a-4)) it is observed that at low sputtering power the anodized film has a nanoporous layer across the entire thickness of the sputtered film. At 300 W sputtering power (Fig. 5.2 (b-4)) it can be observed that semi-T-NT is formed. At 500 W sputtering (Fig. 5.2 (c-4)) it can be seen that the anodized film form very tubular T-NT. Comparing the results from the first set of runs, it was observed that films with smaller grain sizes resulted in tubular morphology upon anodization. However, in this set of runs, T-NT were formed from a film with a larger grain size. Therefore, it may be concluded that the grain size does not affect the morphology of the T-NT. However, the morphology of the top nanoporous layer is influenced by the grain size/surface roughness of the film. Similar influences of surface morphology on the T-NT surface have been reported [40], [41]. On comparing the first and second set of experimental runs, it seemed that the higher density and higher residual stress played an important role in the formation of the tubes.

5.4.4 Effect of substrate temperature

Fig. 5.3 shows the SEM micrographs of the sputtered Ti film before and after anodization for the third set of sputtering runs. The third set of runs implies that the substrate temperature was varied from 100 to 300 °C while the sputtering power was maintained constant at 150 W, and the argon pressure was constant at 5 mTorr. Fig. 5.3 (a-1), (b-1), (c-1) shows the top view and Fig. 5.3 (a-2), (b-2), (c-2) shows the side view of the Ti film (before anodization) sputtered with substrate temperatures at 100 °C, 200 °C, and 300 °C, respectively. From the top view, it can be seen that there is an increase in grain size with the increase in substrate temperature (Table 5.1). Similar observations have been reported where the grain size of the sputtered film increases with increases in substrate temperature [29]. However, with an increase in temperature of the substrate during sputtering, the defect/gap between the grains is reduced, resulting in denser film. This is because when the temperature of the substrate is increased, the grains on the substrate undergo surface diffusion, resulting in more uniform and denser film [26]. Similar changes in the density of the film with substrate temperature are described in the Thornton model [26] (see Table 5.1 for relative density). The energy for diffusion is provided in the form of heat from the substrate. Ti particles upon reaching the substrate move around and reorient themselves to reach the most stable orientation. However, certain vertical column-like structures can be found when the substrate temperature is 200 °C or less. At 300 °C, no noticeable column-like structure can be observed. Also, a greater number of defects in the upper portion (across the thickness) compared to the lower portion of the film are observed when the substrate temperature is 200 °C or less. This is because when the temperature is 200 °C or less, there is not sufficient energy for

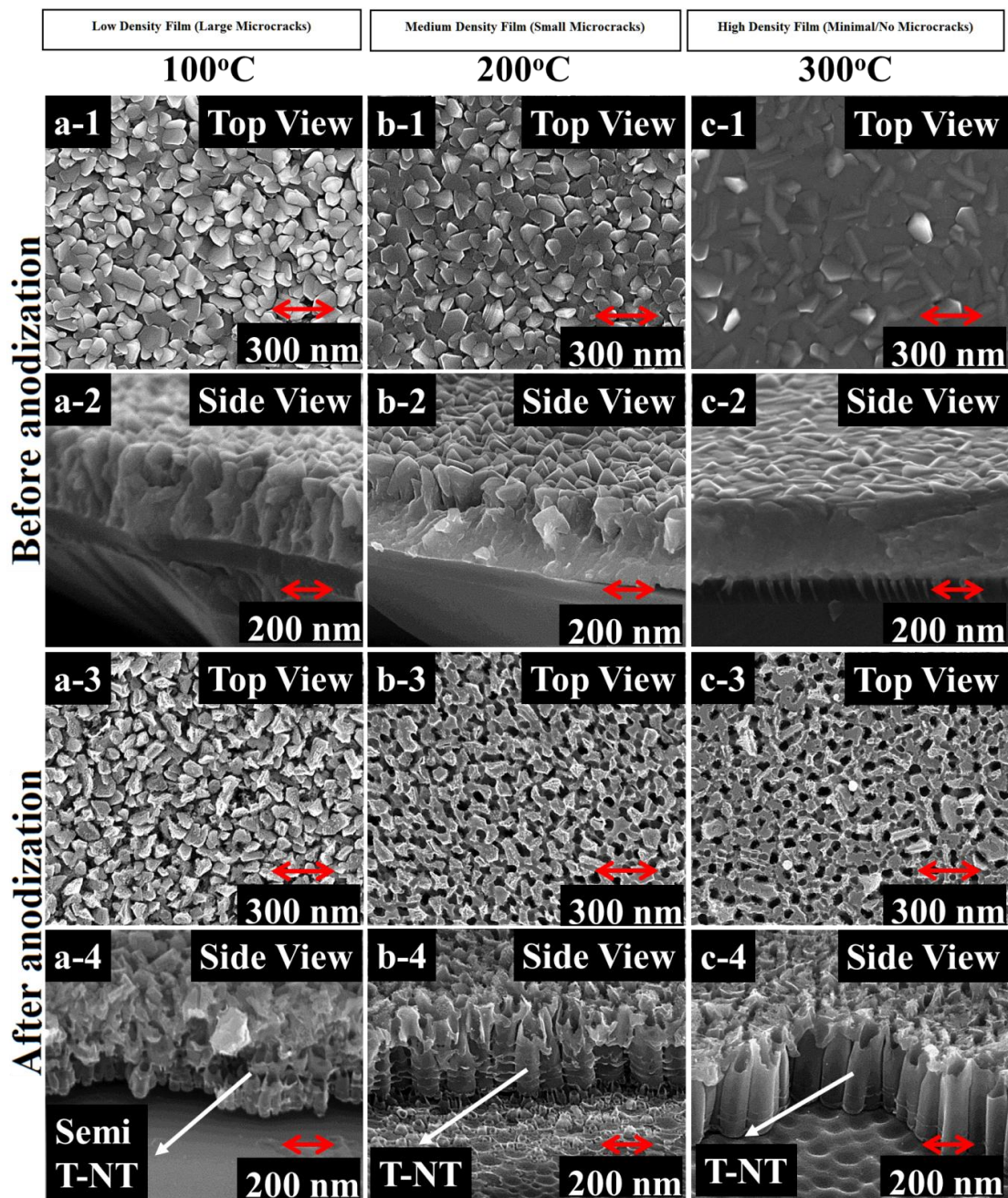


Figure 5.3: SEM micrographs of Ti sputtered on Si wafer before and after anodization for the third set of runs. The argon pressure was constant at 5 mTorr, and the sputtering power was constant at 150 W, while the substrate temperature was varied from 100 to 300 °C. (a-1), (a-2), (a-3), and (a-4) show the top view (before anodization), side view (before anodization), top view (after anodization), and side view (after anodization) sputtered at 100 °C, respectively. Similarly, (b) and (c) show the top and side views of the films sputtered at 200 °C and 300 °C, respectively.

the Ti particles to diffuse and completely reduce to a columnar-like structure, which forms due to the combination of gas phase scattering and self-shadowing effect. A minimum temperature of 250 °C is required for reorientation of Ti metal atoms [42]. It is observed that there is some relatively higher degree of diffusion occurring when compared to the film sputtered at ambient temperature, resulting in a denser film with a reduced number of defects (for the same sputtering power). With the substrate at higher temperature than room temperature, the difference in the thermal properties (expansion co-efficient) between the substrate and the thin film influences the residual stress. It should be noted that there is a nonlinear relationship between residual stress and substrate temperature. The parameters that affect the stress are the difference in thermal expansion between the substrate and the material deposited, as well as the diffusion/recrystallization property of the material. When sputtered at 100 °C the biaxial stress was $\sim +20$ MPa which constitutes a low stress film. At this temperature, there may be very little diffusion/reorientation of the Ti grains and the stress is mainly influenced by the difference in the thermal expansion co-efficient. When sputtered at 200 °C, there is some reorientation/diffusion occurring along with an increased difference in thermal expansion, which causes the stress to increase in the film. When sputtered at 300 °C, there is sufficient diffusion/reorientation occurring, which dominates the increased difference in thermal expansion, causing the stress to be lower than when sputtered at 200 °C but still higher than 100 °C. Fig. 5.3 (a-3), (b-3), (c-3) shows the top view and Fig. 5.3 (a-4), (b-4), (c-4) shows the side view of the Ti film after anodization of the sputtered film with substrate temperatures at 100 °C, 200 °C, and 300 °C, respectively. From the top view, a nanoporous layer is observed, similar to the first and second set of runs. From the side

view, it can be seen that when sputtered at 100 °C (Fig. 5.3 (a-3)) semi-T-NT is formed. At 200 °C and 300 °C T-NT is formed. Also, the tubularity relatively increases with increases in substrate temperature. At 300 °C, the T-NT formed contains interconnecting membranes with reduced length as well as thickness (Fig. 5.3 (c-4)). Also, a relatively long time (up to 12 hours) is required to cool the wafers to ambient temperature in a vacuum along with the higher energy budget required for heating the substrates and pump down, making this process (third run) less desirable.

5.4.5 Comparison of the three sputtering runs

Table 5.1 summarizes the characterized properties of the thin film. It can be seen that the grain size does not influence the tubularity of the anodized film. For example, by comparing two films, one sputtered at 150 W, 2.5 mTorr argon pressure and ambient substrate temperature resulted in average grain sizes of ~60 nm, and anodization of this film resulted in tubular morphology. In the other case, where the film was sputtered at 500 W, 7 mTorr argon power and ambient substrate temperatures resulted in average grain sizes of ~80 nm, and also had tubular T-NT morphology upon anodization. From the first set of runs, it was observed that with the increase in the average grain size, the tubularity decreased, and this trend is not consistent when comparing with the grain size and morphology of the titania formed for the second set of runs. A similar trend of biaxial residual stress having no effect on the morphology of the tubes can also be made. When comparing two samples, one sputtered at 150 W, 2.5 mTorr and ambient substrate temperature (340 nm film), and the other sputtered at 150 W, 5 mTorr and substrate at 200 °C (380 nm film), the residual stress was ~ +200 MPa and ~ +90 MPa, respectively.

However, both of the thin films after anodization resulted in a similar tubular morphology, showing that the residual stress does not have any significant influence on the resulting morphology of the anodized film. When comparing the qualitative density of the thin sputtered films, it can be observed that the morphology changes mainly with respect to density. Thin film deposited by sputtering forms a gas phase of metal that is physically deposited on the substrate. When deposition parameters such as sputtering power, argon pressure, and substrate temperature are changed, the gaps/defects in the film, change resulting in different film densities. When the density is low, the number of gaps/defects is high. The electric field, which determines the direction of T-NT growth, is highest initially at the wells in the defects; subsequently, pit formation becomes more concentrated at these wells. However, when a low density film is subjected to anodization, the defects may be comparable to the pits formed by anodization or sufficient enough to disturb/shift the concentration of the electric field in a random manner. As the direction of the electric field changes, the direction in which the electric-field assisted etching also may change resulting in nanoporous structures instead of tubular morphology. Hence, with the decrease in density, the number of defects increases. This may be causing an increase in the directional shifts of the electric field, which changes the anodized film to vary in morphology from tubular to semitubular to nanoporous film.

5.5 Conclusions

Tubular TiO₂ arrays to nanoporous TiO₂ were successfully synthesized on Si wafers by anodization of Ti film deposited by D.C. sputtering. Sputtering parameters such as

argon pressure, sputtering power, and substrate temperature were varied and found to influence the morphology of the anodized film. It was observed that factors such as grain size and residual stress of the thin film do not affect the morphology of the anodized film. The main factor affecting the morphology is the density of the film, rather. All the anodized films contained a nanoporous layer, which may be due to the presence of native titania and/or pronounced surface grains. When comparing different sputter deposition parameters, it can be concluded that higher sputtering power, lower gas pressure, and higher substrate temperatures, yield thin films with higher densities which are required for synthesizing tubular TiO_2 . When sputtered at lower power, lower substrate temperatures, and higher gas pressure, the deposited films have lower density, which results in fully nanoporous TiO_2 after anodization. However, with an increase in the gas pressure and sputtering power, the residual stress increases. This may result in unstable T-NT that may peel off easily from the substrate when subjected to high temperature calcinations (which is required for most of the T-NT-based applications). Also, sputter deposition of Ti at higher substrate temperatures is not economical due to the long pump down time of the sputtering chamber and heating budget. Therefore, based on the type of T-NT required, and/or based on the stability of the T-NT required, and/or cost effectiveness of the T-NT, appropriate sputtering parameters should be adopted. When combining the use of well-established semiconductor fabrication techniques used within industry and better understanding of the deposition parameters that affect the morphology of the anodized film, large-scale commercialization of T-NT-based devices looks promising.

5.6 References

- [1] G.K. Mor, O. K. Varghese, M. Paulose, K.G. Ong, and G. A. Grimes, "A room-temperature TiO₂-nanotube hydrogen sensor able to self-clean photoactively from environmental contamination," *J. Mater. Res.*, vol. 19, pp. 628–634, 2004.
- [2] Q. Zheng, B. Zhou, J. Bai, L. Li, Z. Jin, J. Zhang, J. Li, Y. Liu, W. Cai, and X. Zhu, "Self-organized TiO₂ nanotube array sensor for the determination of chemical oxygen demand," *Adv. Mater.*, vol. 20, pp. 1044–1049, 2008.
- [3] G. Du, Z. Guo, P. Zhang, Y. Li, M. Chen, D. Wexler, and H. Liu, "SnO₂ nanocrystals on self-organized TiO₂ nanotube array as three-dimensional electrode for lithium ion microbatteries," *J. Mater. Chem.*, vol. 20, pp. 5689–5694, 2010.
- [4] T. Djenizian, I. Hanzu, and P. Knauth, "Nanostructured negative electrodes based on titania for Li-ion microbatteries," *J. Mater. Chem.*, vol. 21, pp. 9925–9937, 2011.
- [5] N. K. Shrestha, M. Yang, I. Paramasivam, and P. Schmuki, "Visible-light-induced photocatalysis using self-organized TiO₂ nanotubes decorated with AgBr deposits," *Semicond. Sci. Technol.*, vol. 26, pp. 092002–092006, 2011.
- [6] K. Shankar, G. K. Mor, H. E. Prakasam, S. Yoriya, M. Paulose, O. K. Varghese, and G. A. Grimes, "Highly-ordered TiO₂ nanotube arrays up to 220 μm in length: Use in water photoelectrolysis and dye-sensitized solar cells," *Nanotechnology*, vol. 18, pp. 65707–65717, 2007.
- [7] W. Cheng, Y. Shen, G. Wu, F. Gu, J. Zhang, and L. Wang, "Preparation and properties of a phthalocyanine-sensitized TiO₂ nanotube array for dye-sensitized solar cells," *Semicond. Sci. Technol.*, vol. 25, pp. 125014–125017, 2010.
- [8] Y. Zhao, Y. Hu, Y. Li, H. Zhang, S. Zhang, L. Qu, G. Shi, and L. Dai, "Super-long aligned TiO₂/carbon nanotube arrays," *Nanotechnology*, vol. 21, pp. 505702–505708, 2010.
- [9] B. C. Kim, S. J. Kim, J. K. Chung, J. Chen, S. Y. Park and G. G. Wallace, "Charge storage in carbon nanotube–TiO₂ hybrid nanoparticles," *Synth. Met.*, vol. 162, pp. 650–654, 2012.
- [10] B. Y. Yu, A. Tsai, S.-P. Tsai, K.-T. Wong, Y. Yang, C.-W. Chu, and J.-J. Shyue, "Efficient inverted solar cells using TiO₂ nanotube arrays," *Nanotechnology*, vol. 19, pp. 255202–255206, 2008.
- [11] V. Galstyan, A. Vomiero, I. Concina, A. Braga, M. Brisotto, E. Bontempi, G. Faglia, and G. Sberveglieri, "Vertically aligned TiO₂ nanotubes on plastic

- substrates for flexible solar cells,” *Small*, vol. 7, pp. 2437–2442, 2011.
- [12] Y.-C. Liang, C.-C. Wang, C.-C. Kei, Y.-C. Hsueh, W.-H. Cho, and T.-P. Perng, “Photocatalysis of ag-loaded TiO₂ nanotube arrays formed by atomic layer deposition,” *J. Phys. Chem. C*, vol. 115, pp. 9498–9502, 2011.
- [13] J. M. Macak, H. Tsuchiya, S. Berger, S. Bauer, S. Fujimoto, and P. Schmuki, “On wafer TiO₂ nanotube-layer formation by anodization of Ti-films on Si,” *Chem. Phys. Lett.*, vol. 428, pp. 421–425, 2006.
- [14] K. N. Chappanda, Y. R. Smith, S. K. Mohanty, L. W. Rieth, P. Tathireddy, and M. Misra, “Growth and characterization of TiO₂ nanotubes from sputtered Ti film on Si substrate,” *Nanoscale Res. Lett.*, vol. 7, pp. 388–395, 2012.
- [15] G. K. Mor, O. K. Varghese, M. Paulose, and C. A. Grimes, “Transparent highly ordered TiO₂ nanotube arrays via anodization of titanium thin films,” *Adv. Funct. Mater.*, vol. 15, pp. 1291–1296, 2005.
- [16] K. N. Chappanda, Y. R. Smith, M. Misra, and S. K. Mohanty, “Site-specific and patterned growth of TiO₂ nanotube arrays from e-beam evaporated thin titanium film on Si wafer,” *Nanotechnology*, vol. 23, pp. 385601–385608, 2012.
- [17] G. K. Mor, O. K. Varghese, M. Paulose, K. G. Ong, and Grimes C. A., “Fabrication of hydrogen sensors with transparent titanium oxide nanotube-array thin films as sensing elements,” *Thin Solid Films*, vol. 496, pp. 42–48, 2006.
- [18] N. Kılınç N, E. Şennik, and Z. Öztürk, “Fabrication of TiO₂ nanotubes by anodization of Ti thin films for VOC sensing,” *Thin Solid Films*, vol. 520, pp. 953–958, 2011.
- [19] Y. R. Smith and V. Subramanain, “Heterostructural composites of TiO₂ mesh TiO₂ nanoparticles photosensitized with CdS: A new flexible photoanode for solar cells,” *J. Phys. Chem. C*, vol. 115, pp. 8376–8385, 2011.
- [20] Y. S. Sohn, Y. R. Smith, V. Subramanian, and M. Misra, “Electrochemically assisted photocatalytic degradation of methyl orange using anodized titanium dioxide nanotubes,” *Appl. Catal. B*, vol. 84, pp. 372–378, 2008.
- [21] H. J. G. Gundersen, “Stereology of arbitrary particles,” *J. Microsc.*, vol. 143, pp. 43–45, 1986.
- [22] S. A. Campbell, *The Science and Engineering of Microelectronic Fabrication*, 2nd ed., New York: Oxford Univ. Press, 1996, pp. 305–21.
- [23] B. S. Brownstein, D. B. Fraser, and J. F. O’Hanlon, “Characterization of an ultrahigh vacuum sputtering system,” *J. Vac. Sci. Technol. A*, vol. 11, pp. 694–

- 700, 1993.
- [24] M. Kobayashia, T. Matsuia, and Y. Murakami, "Mechanism of creation of compressive residual stress by shot peening," *Int. J. Fatigue*, vol. 20, pp. 351–357, 1998.
- [25] Y. Fu, H. Du, and S. Zhang, "Sputtering deposited TiNi films: Relationship among processing, stress evolution and phase transformation behaviors," *Surf. Coat. Technol.*, vol. 167, pp. 120–128, 2003.
- [26] J. A. Thornton, "Influence of apparatus geometry and deposition conditions on the structure and topography of thick sputtered coatings," *J. Vac. Sci. Technol.*, vol. 11, pp. 666–700, 1974.
- [27] O. Kluth, G. Schöpe, J. Hüpkes, C. Agashe, J. Müller, and B. Rech, "Modified Thornton model for magnetron sputtered zinc oxide: Film structure and etching behavior," *Thin Solid Films*, vol. 442, pp. 80–85, 2003.
- [28] V. Chawla, R. Jayaganthana, A. K. Chawla, and R. Chandra, "Morphological study of magnetron sputtered Ti thin films on silicon substrate," *Mater. Chem. Phys.*, vol. 111, pp. 414–418, 2008.
- [29] C.-P. Liu and H.-G. Yang, "Deposition temperature and thickness effects on the characteristics of dc-sputtered ZrN_x films," *Mater. Chem. Phys.*, vol. 86, pp. 370–374, 2004.
- [30] D. Song, A. G. Aberle, and J. Xia, "Optimisation of ZnO:Al films by change of sputter gas pressure for solar cell application," *Appl. Surf. Sci.*, vol. 195, pp. 291–296, 2002.
- [31] D.-J. Kim, J.-P. Maria, A. I. Kingon, and S. K. Streiffer, "Evaluation of intrinsic and extrinsic contributions to the piezoelectric properties of Pb(Zr_{1-x}Ti_x)O₃ thin films as a function of composition," *J. Appl. Phys.*, vol. 93, pp. 5568–5577, 2003.
- [32] R. Abermann and R. Koch, "The internal stress in thin silver, copper and gold films," *Thin Solid Films*, vol. 129, pp. 71–78, 1985.
- [33] F. A. Doljack and R. W. Hoffman, "The origins of stress in thin nickel films," *Thin Solid Films*, vol. 12, pp. 71–74, 1972.
- [34] P. Roy, S. Berger, and P. Schmuki, "TiO₂ nanotubes: Synthesis and applications," *Angew. Chem. Int. Edn.*, vol. 50, pp. 2904–2939, 2011.
- [35] K. S. Raja, T. Gandhi, and M. Misra, "Effect of water content of ethylene glycol as electrolyte for synthesis of ordered titania nanotubes," *Electrochem. Commun.*, vol. 9, pp. 1069–1076, 2007.

- [36] K. S. Raja, M. Misra, and K. Paramguru, "Formation of self-ordered nano-tubular structure of anodic oxide layer on titanium," *Electrochim. Acta*, vol. 51, pp. 154–165, 2005.
- [37] Y.-Y. Song and P. Schmuki, "Modulated TiO₂ nanotube stacks and their use in interface sensors," *Electrochem. Commun.*, vol. 12, pp. 579–582, 2010.
- [38] X. Yu, J. Ma, F. Jin, Y. Wang, X. Zhang, C. Cheng, and H. Ma, "Effects of sputtering power on the properties of ZnO:Ga films deposited by R.F. magnetron-sputtering at low temperature," *J. Cryst. Growth*, vol. 274, pp. 474–479, 2005.
- [39] J. Lee, D. Lee, D. Lim, and K. Yang, "Structural, electrical and optical properties of ZnO:Al films deposited on flexible organic substrates for solar cell applications," *Thin Solid Films*, vol. 515, pp. 6094–6098, 2007.
- [40] Y. R. Smith, B. Sarma, S. K. Mohanty, and M. Misra, "Single-step anodization for synthesis of hierarchical TiO₂ nanotube arrays on foil and wire substrate for enhanced photoelectrochemical water splitting," *Int. J. Hydrogen Energy*, vol. 32, pp. 2062–2069, 2013.
- [41] S. Li, G. Zhang, D. Guo, L. Yu, and W. Zhang, "Anodization fabrication of highly ordered TiO₂ nanotubes," *J. Phys. Chem. C*, vol. 113, pp. 12759–12765, 2009.
- [42] Y.-F. Chena, C.-Y. Lee, M.-Y. Yenga, and H.-T. Chiu, "The effect of calcination temperature on the crystallinity of TiO₂ nanopowders," *J. Cryst. Growth*, vol. 247, pp. 363–370, 2002.

CHAPTER 6

TiO₂-WO₃ COMPOSITE NANOTUBES FROM COSPUTTERED THIN FILMS ON Si SUBSTRATE FOR ENHANCED PHOTOELECTROCHEMICAL WATER SPLITTING

6.1 Abstract

TiO₂-WO₃-based systems for improved photoelectrochemical (PEC) activity have been widely researched. The novelty of this work is the synthesis of a TiO₂-WO₃ composite nanotube structure. The PEC tests demonstrate improved performance in water splitting application. Electrochemical anodization of Ti-W nanocomposite thin films deposited by simultaneous magnetron sputtering on Si substrate resulted in the formation of TiO₂-WO₃ nanotubular arrays. A change in the morphology of TiO₂-WO₃ composite nanotubes by varying the density of W in Ti-W composite thin films was observed. With tungsten density of less than or equal to 5.25×10^{18} of W atoms per cm³, the morphology of the composite nanotubes were similar to that of plain TiO₂ nanotubes, whereas a further increase in W density resulted in a nanoporous morphology. Ti-W composite thin films were deposited by simultaneous sputtering of Ti and W targets using D.C. and RF sputtering systems, respectively. Ti-W composite films were also deposited on Si substrates with 100 nm thick layer tin doped indium oxide (ITO) to examine the photoelectrochemical activity of the formed oxide composites. The TiO₂-WO₃ composite nanotubes with 1.05×10^{19} WO₃ molecules per cm³ proved to be optimal WO₃ density for this system, giving rise to a 40% increase in photocurrent at 0.5 V compared to plain TiO₂ nanotubes. The nanotubes were subjected to calcination at temperatures from 250–550°C for 2 hours in ambient atmosphere. The effect of nanotube length on photoelectrochemical performance by anodizing 500 nm thick Ti-W film was also studied.

6.2 Introduction

With the diminishing of fossil fuels, a lot of research is being done in generating alternative renewable fuels such as hydrogen [1], [2], biodiesel [3], [4], and solar cells [5]. Fossil fuels upon combustion emits CO₂ and CO, resulting in global warming [6]. Hence, there is more interest in generating zero-emission fuels such as hydrogen [7]. In addition, hydrogen is used as coolants in turbine generators [8], for production of ammonia [9], for recrystallization amorphous silicon [10], etc. Hydrogen is produced from various sources such as fossil fuels [11] and water [12]. Production of hydrogen from fossil fuel adds to the issue of global warming. Hence, a lot of work has been focused on production of hydrogen using cleaner methods such as photoelectrochemical water splitting [12–14] and photobiological water splitting [15]. Photoelectrochemical water splitting has been demonstrated via various photo active materials such as TiO₂ [12], [16], [17], Fe₂O₃ [18], WO₃ [19], GaPN [20], and GaAsPN [20]. TiO₂ has caught a lot of interest in the last decade when the ability to synthesis TiO₂ nanotubes (T-NT) from the Ti metal via electrochemical anodization was reported by Zwillings *et al.* [21], [22]. In addition, TiO₂ is a photocorrosion resistant, nontoxic, and environmentally friendly material, making it suitable for hydrogen generation via water splitting. In order to enhance the efficiency of the T-NT-based PEC cells, various approaches have been made to modify the electrical and optical properties. TiO₂ doped with carbon [23], niobium [17], nitrogen [24], sulphur [25], chromium [26], [27], antimony [26], nickel [27], and zinc [27] have been shown to have improved photocatalytic activity. Other approaches such as light assisted T-NT synthesis [28], and flame annealing of T-NT [29] have also been shown to enhance the photocurrents. Composite materials such as CdS–

TiO₂ [30], TiO₂-WO₃ [31], [32] and carbon nanotube/TiO₂ [33] have also been shown to have enhanced water splitting capabilities. However, these materials are not homogeneous composite and are materials deposited on the surface of the TiO₂ nanomaterials.

In this paper, we report the synthesis of TiO₂-WO₃ composite nanotubes (TW-NT) from thin films on the Si substrates for improving the photocatalytic activity. The nanotubes were synthesized by anodizing Ti-W composite film deposited by simultaneous sputtering of Ti and W targets on the silicon substrate. This method is economical, easy, and is similar to the one synthesised on foil. The composite nanotube is demonstrated to have a 40% increase in water splitting photocurrent in comparison to plain T-NT. Also, this method can be used for synthesis of any valve metal oxide/TiO₂-based composite nanotubes.

6.3 Experimental procedure

6.3.1 Thin film deposition

Clean n-type (100) Si wafer with resistivity of 1–5 Ωcm and RMS roughness of less than 1 nm were used as substrates for synthesizing the composite nanotubes. The wafers were subjected to wet thermal oxidation at 1 000 °C to form ~100 nm thick layer of SiO₂. W was simultaneously deposited via RF magnetron sputtering to form a composite Ti-W film. An RF sputtering system was utilized for depositing W since the sputter rate of RF sputtering systems are slower compared to DC sputtering systems, providing a better control on the low percentage of W. Ti and W targets of 99.2–99.7% purity purchased from Kurt. J. Lesker were used for sputtering. The sputtering was carried out at 2.5

mTorr Ar pressure. Ti was sputtered at 200 W while Tungsten was sputtered from 15–100 W to vary the Ti–W composition ratio. Below 15 W, the plasma would not ignite to sputter tungsten. About 100 nm ITO was deposited (100 W D.C. power, 2.5 mTorr argon pressure) as electrodes before depositing Ti–W film in the case of thin films used for PEC water splitting studies. For comparison of the PEC activity, plain Ti thin films (200 W D.C. power, 2.5 mTorr argon pressure) on Si substrate with no tungsten were also deposited on ITO/Si substrates. After sputtering, the wafer was cooled down to ambient temperature in a vacuum to minimize the oxidation of sputtered Ti–W films.

6.3.2 Nanotube synthesis

The Ti and Ti–W thin films were subjected to electrochemical anodization at ambient temperature using an organic electrolyte to form T-NT and TW-NT, respectively. The experimental set up used was similar to the set up used in our previous work [34], [35]. Si wafer with Ti–W or Ti film was diced into 1 cm × 2 cm sized pieces. The organic electrolyte consisted of ethylene glycol (89.5 wt%, from Fisher Scientific), DI water (10 wt%), and ammonium fluoride (0.5 wt%, from Fisher Scientific) [36], [37]. The Ti film was cleaned with acetone and isopropanol alcohol followed by rinsing in DI water. The Ti film was connected to the positive terminal of the voltage source to form the anode. A platinum foil with 1 cm² area was connected to the negative terminal of the voltage source as the cathode. Polyamide tape was used to mask the non-Ti portion of the diced substrate to prevent any reaction between the electrolyte and the substrate. The gap between the electrodes was 2.5 cm. Only about 1 cm² of the diced Ti–W/SiO₂/Si substrate was subjected to anodization under magnetic stirring of approximately 100 ml

of electrolyte. The anodization voltage was ramped up at the rate of $1 \text{ V}\cdot\text{s}^{-1}$. The anodization was carried out at 30 V (D.C.) and maintained until the current dropped to zero. After anodization, the tubes were thoroughly rinsed in DI water. The samples were then dried in air and used for characterization studies. In case of samples used for PEC testing, ammonium hydroxide (30% concentration) and hydrogen peroxide (30% concentration) at a ratio (volume) of 1:2 were used to etch a portion of Ti–W film in the diced samples, exposing the underlying ITO film which was then connected to the positive terminal of the voltage source before being subjected to anodization. These samples were anodized at 20 V (D.C.) and were used for PEC cells. The anodized films used for PEC were subjected to calcination in stagnant air from 250–550 °C for 2 hours.

6.3.3 Characterization and testing

Scanning electron microscopy (SEM) micrographs from FEI NanoNova SEM were used to study the change in the structural morphology of the anodized thin film with change in W density in Ti–W composite film. All the top view micrographs were obtained at 200 000x magnification, and the side view micrographs were obtained at 250 000x magnification and 60° tilt. X-ray diffraction was used for identification and determination of the crystalline phases of the nanotubes using a Rigaku Miniflex XRD system. The x-ray diffraction incidence angle was ranged from 20° to 80°. Diffuse reflectance UV-vis spectroscopy was used to characterize the band gap of the T-NT and TW-NT using a Shimadzu UV-3600 UV-Vis-NIR spectrophotometer. Agilent 7500ce inductively coupled plasma mass spectrometer (ICP-MS) with quadrupole mass spectrometer and an octopole reaction system to preferentially remove polyatomic

interferences was used to analyze the atomic ratio of the tungsten and Ti before and after anodization. A 193 nm fluorine-neon laser ablation was used to generate the aerosol of the Ti–W films. The laser was scanned at 40 $\mu\text{m/s}$ at 3 pulses/s to limit the volume interaction of the laser to about 500 nm in depth. The W and Ti composition ratios were determined by comparing the counts per second with a standard sample (NIST 610 glass) with elements of known concentration. Kratos Axis Ultra DLD x-ray photoelectron spectrometer (XPS) was used to analyze the oxidation state of Ti–W anodized film. The photoelectrochemical activity of the composite anodes was examined under 1.5 AM irradiation with a Newport Solar Simulator (300 W Mercury lamp) in 0.5 M Na_2SO_4 (pH ~6.8). The photocurrent was monitored using PARSTAT 4 000 potentiostat where the composite films served as the photoanode, a platinum mesh as the cathode, and Ag/AgCl as the reference electrode.

6.4 Results and discussions

6.4.1 Synthesis of TiO_2 – WO_3 composite nanotubes

Fig. 6.1 shows the schematic set up used for depositing Ti–W films. The W deposition ranged from 5.25×10^{18} to 2.1×10^{19} atoms per cm^3 of Ti–W composite films. The composition ratio was determined using ICP MS. The equation used for calculating the atomic ratio is as follows [38].

$$c_E^{SM} = \frac{\left(\frac{i_E}{i_{IS}}\right)^{sm}}{\left(\frac{i_E}{i_{IS}}\right)^{std}} \left(\frac{c_E}{c_{IS}}\right)^{std} c_{IS}^{sm} \quad (1)$$

where c is concentration

E is element

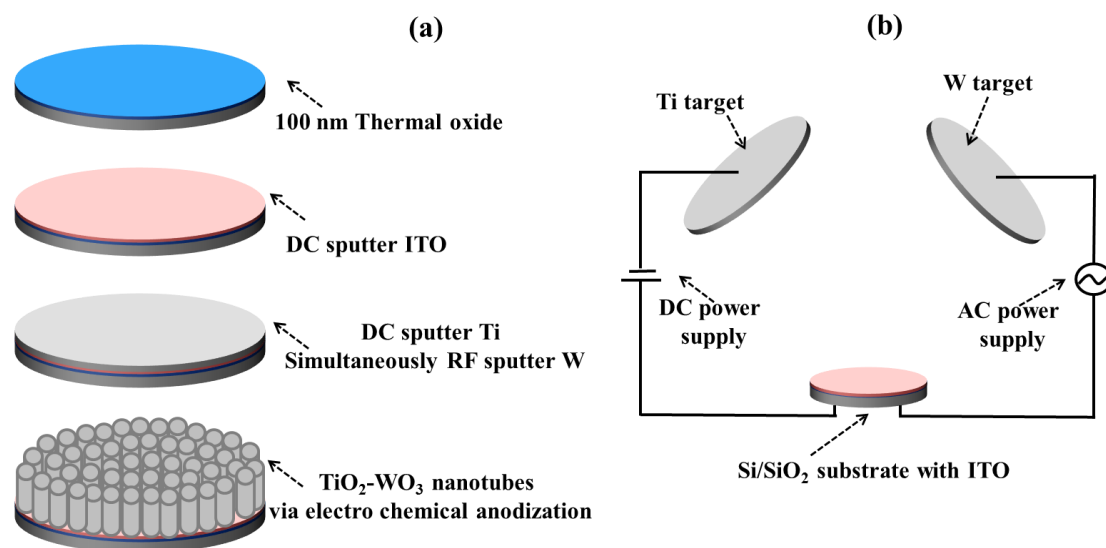


Figure 6.1: Schematic showing the experimental set up used for depositing W-Ti film and synthesis of the $\text{TiO}_2\text{-WO}_3$ composite nanotube. (a) Shows the process step used for synthesis of the $\text{TiO}_2\text{-WO}_3$ composite nanotube. (b) Shows the experimental set up used for deposition of Ti-W composite thin film achieved by simultaneously sputtering Ti (using D.C. magnetron sputtering system) and W (using RF magnetron sputtering system).

IS is element used as internal standard
I is intensity (in counts per second cps)
sm sample
std standard (NIST 610 glass)

The standard glass sample consisted of 443 ppm of Ti, 440 ppm of In, 122 ppm of W, and 69.9 atomic % SiO₂.

Table 6.1 shows the sputtering parameters used for depositing the composite film and the atomic ratio before and after anodization of the film. Fig. 6.2 shows the SEM micrographs of the top and side views of Ti–W films after anodization. From Fig. 6.2 (a) and (b) it can be observed that the anodized film has a tubular morphology similar to T-NT synthesized from thin Ti film. SEM micrographs are presented in Fig. 6.3 (c) for comparison. Increasing the W loading up to 1.2×10^{19} W atoms per cm³ in Ti–W film, resulted in a semitubular morphology. With a further increase in W loading the morphology of the anodized film results in a nanoporous type morphology as observed by Fig. 6.2 (e)-(h). The transition of a nanotubular morphology to a more nanoporous morphology with an increase in W loading is due to the difference in the electrochemical etch rate of Ti and W. Fluoride ions in the electrolyte electrochemically etch W at a slower rate compared to Ti [39], [40]. Due to the difference in etch rate there is more etching of Ti and hence more of W remains in the anodized film. With the increase in W density in the Ti–W composite film, the morphology of the nanotube is more influenced/pronounced by the unetched W. When the atomic density of tungsten is less than 5.25×10^{18} atoms per cm³, the influence of the W is minimal on the morphology of the anodized film, having a tubular morphology as there is a sufficient amount of Ti

Table 6.1: Sputtering parameters used for depositing the Ti–W composite film and the Ti–W, and the atomic ratio before and after anodization.

DC sputtering power (Watts)	Rf sputtering power (Watts)	Argon pressure (mTorr)	W (atoms/cm³) Before anodization	W (atoms/cm³) After anodization
200	25	2.5	5.25×10^{18}	1.75×10^{19}
200	50	2.5	1.2×10^{19}	4×10^{19}
200	75	2.5	1.6×10^{19}	5.34×10^{19}
200	100	2.5	2.1×10^{19}	7×10^{19}

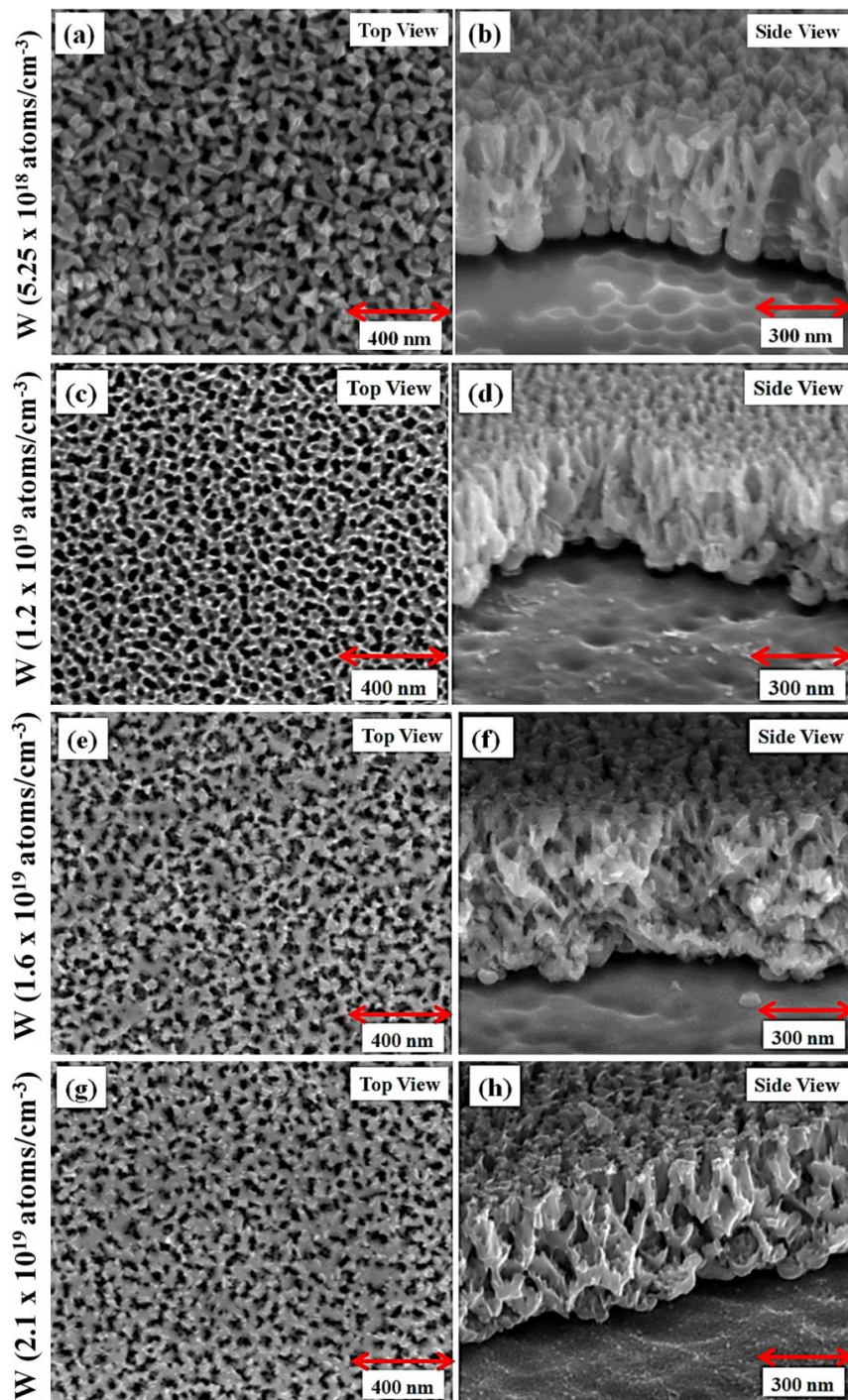


Figure 6.2: SEM micrographs showing the change in the morphology of anodized Ti-W film with the change in the W density. (a), (c), (e), and (g) show the top view of anodized film in which the W density is ranged from 5.25×10^{18} to 2.1×10^{19} atoms/cm³ of Ti-W composite film. (b), (d), (f), and (h) show the side view of anodized film in which the W density is ranged from 5.25×10^{18} to 2.1×10^{19} atoms/cm³ of Ti-W composite film. With an increase in W density, the morphology changes from a tubular to nanoporous morphology.

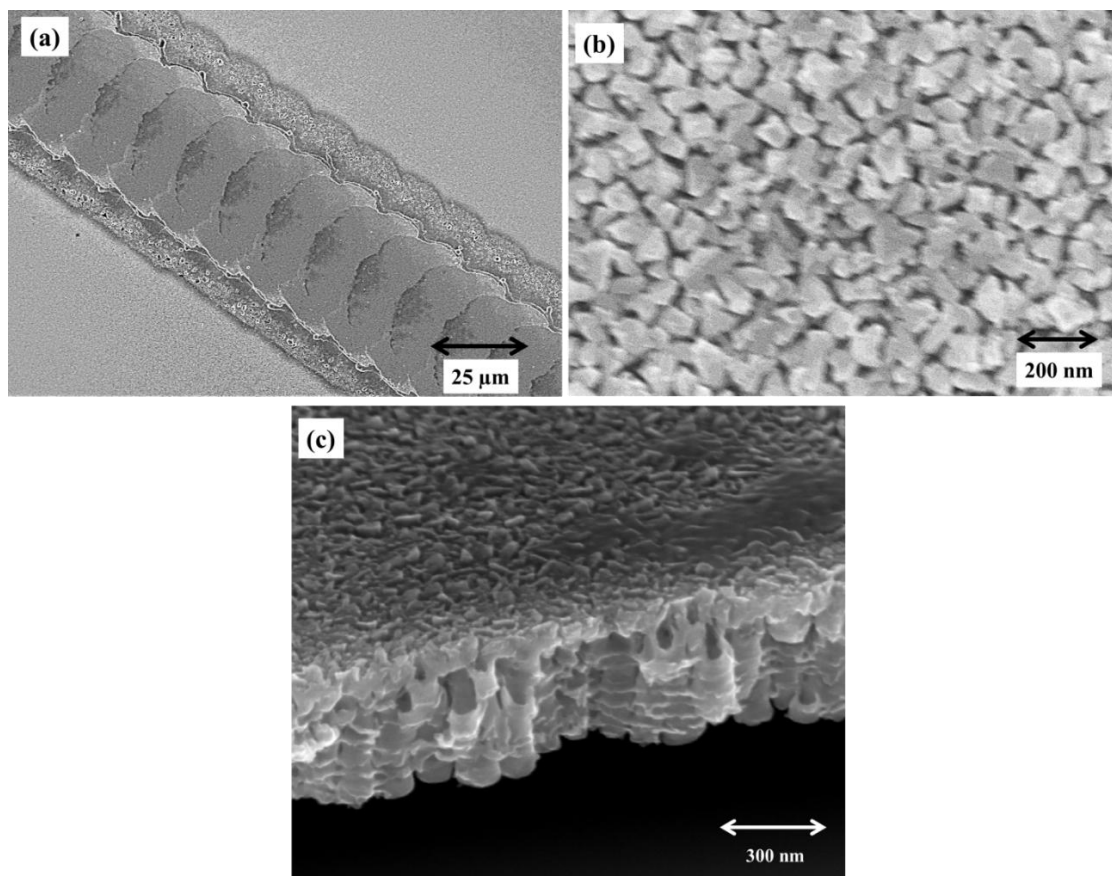


Figure 6.3: SEM micrographs as supporting data for PEC tests. (a) SEM micrographs of $\text{TiO}_2\text{-WO}_2$ nanotubes after laser ablation. It shows the nonuniform interaction of the laser with the sample. (b) shows the top view of SEM micrographs of the composite nanotubes after used for water splitting for 1 hour. (c) shows the side view of plain T-NT.

present to mask the nontubularity caused by W in the anodized film. Also, various reports have shown that with the anodization of W, the resulting morphology is porous and not tubular WO_3 [41]–[43]. The nontubularity is attributed to the difference in stress from the formation of WO_3 and solubility of W by the electrolyte [44]. Fig. 6.4 shows the ICP-mass spectrometry of Ti–W film before and after anodization (Ti-200W, tungsten-15W sample) and is compared with a standard sample (NIST 610 glass) with a known concentration of W, Ti, and In. The counts/s of the Ti–W sample were compared with the standard sample along with their sensitivity factor to determine the atomic ratio. The Ti–W atomic ratio varied from 20 000:1 before anodization to 6 000:1 after anodization. SEM micrographs of the T-NT sample after laser ablation are shown in Fig. 6.3 (a). During the ICP-MS measurements, the laser did not interact with the silicon dioxide substrate during generation of the aerosol, and hence no Si was detected. The indium detected was from the ITO deposited for the electrical connections. From the change in the concentration ratio, it can be concluded that the electrolyte etches Ti at a relatively faster rate compared to W and hence results in nontubular morphology with the increase in W atomic ratio. Hence, the presence of W (above 5.25×10^{18} atoms per cm^3) in the Ti–W films inhibits the anodized film from attaining tubular morphology similar to the morphology of plain Ti anodized film. Fig. 6.5 shows the XPS Ti–W film annealed at 350 °C. Using the peak position of physisorbed carbon as the correction factor, the binding energy peak of Ti $2p_{1/2}$ and $2p_{3/2}$ was found to be at about 464.3 and 458.9 eV, suggesting that the Ti is predominately at a Ti^{4+} oxidation state [45]. The oxidation state of tungsten could not be determined accurately because the 3p peak of Ti overlaps with the W 4f peak [46]. Due to the low concentration of W, no other W peak was visible in

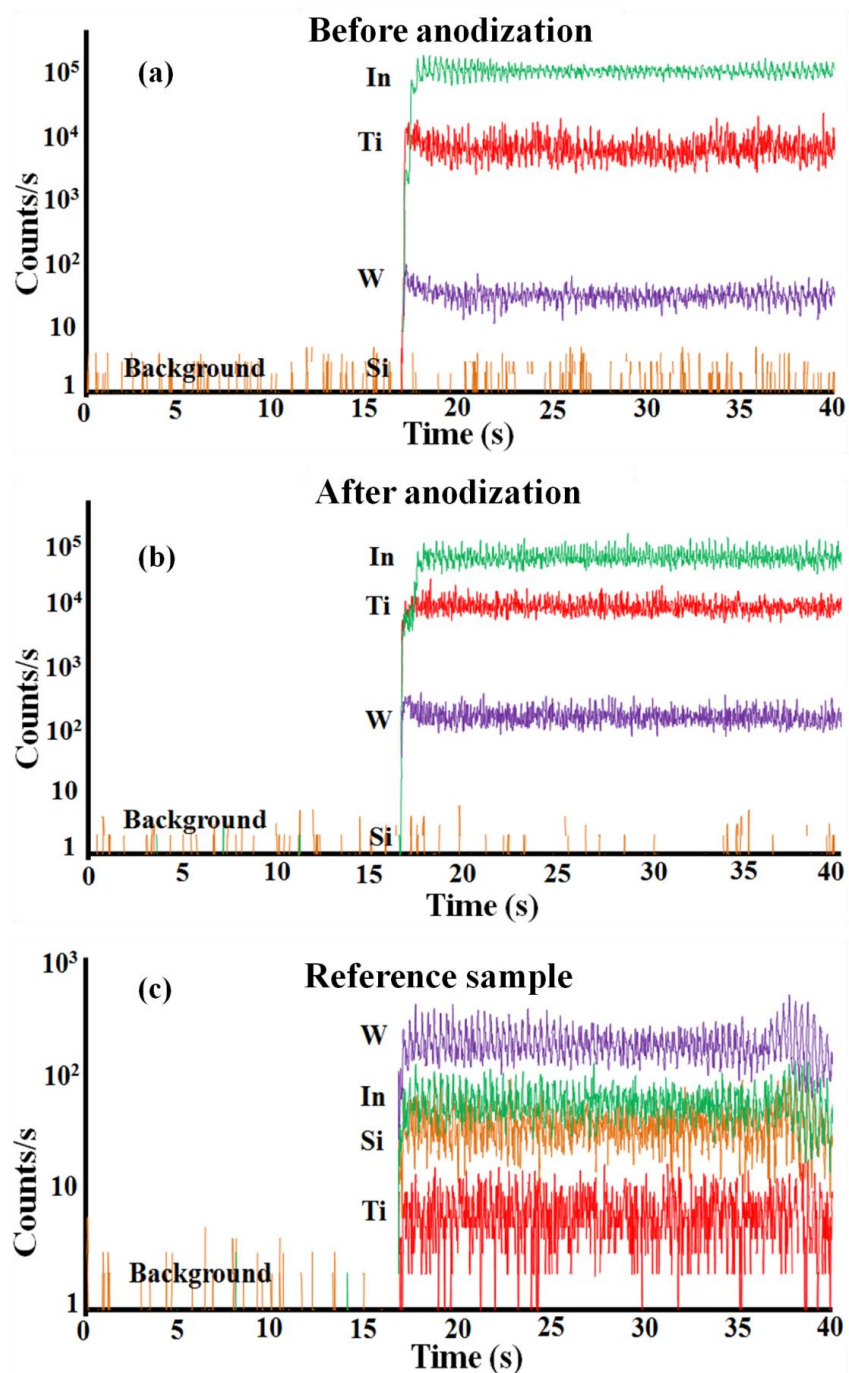


Figure 6.4: Inductively coupled plasma mass spectrometry (ICP-MS) of Ti-W composite film for calculating the Ti-W ratio. The Ti-W atomic ratio changed from 20 000:1 before anodization to 6 000:1 after anodization showing the difference in electrochemical etching of Ti and W. (a) ICP-MS of Ti-W composite film before anodization. (b) ICP-MS of Ti-W composite film after anodization. (c) ICP-MS of a standard sample whose concentration is known.

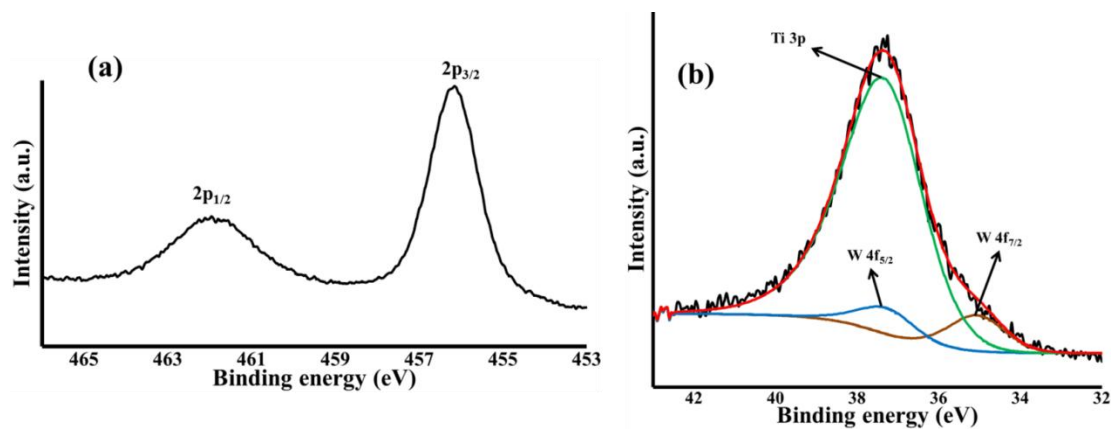


Figure 6.5: XPS of Ti–W anodized film. (a) Using the peak position of physisorbed carbon as the correction factor, the binding energy peak of Ti $2p_{3/2}$ was found to be at about 458.9 eV implying that the Ti has Ti^{4+} oxidation state. (b) Similarly, the binding energy peak W $4f_{5/2}$ and $4f_{7/2}$ was found to be at about 37.3 and 35.3 eV, respectively, implying that the tungsten has W^{6+} oxidation state.

the XPS spectrum. However, there was a considerable amount of nonlinearity observed in the overlapped peak showing the presence of a trace amount of W. Fig. 6.5 (b) shows the XPS spectrum of Ti 3p and W 4f overlapping peaks. The binding energy peaks of W $4f_{5/2}$ and $4f_{7/2}$ were found to be at about 37.3 and 35.3 eV, respectively, implying that the tungsten is predominately in the W^{6+} oxidation state. Using the XPS fit, the atomic percentage of W was found to be 1.6 atomic % which is significantly larger compared to ICP-MS results. Since XPS elemental probing depth is about 1–10 nm (depending on the sample), it only provides an elemental surficial composition. An important point to be noted is that the composite films were deposited using two sputtering systems. The thickness of the film was controlled by controlling the sputtering time. The process of stopping the sputtering process was done manually (using shutters controlled by switches), and there is a human error factor involved in accurately stopping both sputtering processes at the same time. This slight difference in stopping the sputtering process can have a significant difference in atomic percentages especially when probing depths ranging from 1–10 nm. Hence, the XPS technique is not an accurate tool to determine the atomic percentage for our case and is therefore only used for determining the oxidation states. Hence, a technique like ICP-MS was used to determine the Ti-W ratio which has larger depth probing capability. Also after anodization, the WO_3 percentages may be significantly different on the top portion of the nanotubes in comparison to the entire length of the nanotubes. In addition, from the literature, it has been reported that when W is calcinated at similar temperatures and environments, the oxidation state of W was been shown to be W^{6+} , confirming the oxidation state of W [47, 48]. From the top view SEM micrographs in Fig. 6.2, a nanoporous layer can be

observed; it is due to the influence of the native TiO_2 and WO_3 formed by exposure to the atmosphere as well as the presence of pronounced surface grains [34], [35]. Also, a significant influence on the morphology of the surficial nanoporous layer of the anodized films with the increase in W loading can be observed.

6.4.2 Water splitting using TiO_2 - WO_3 composite nanotube

From experimental runs, it was found that the optimum density of W is about 1.05×10^{19} WO_3 molecules per cm^3 for highest water splitting photocurrents. Fig. 6.6 shows the change in the photocurrent density with W loading after anodization for samples that were annealed at 350°C . The TW-NT showed the maximum photocurrent density of 0.42 mA cm^{-2} at 0.5 V for a W loading of 1.05×10^{19} atoms per cm^3 . The dark current (in the absence of light) irrespective of the W loading was very minimal (less than $5 \mu\text{A cm}^{-2}$), showing that the current density is mainly attributed to photoinduced charge carriers. In comparison with the T-NT, the TW-NT demonstrates a 40% increase in the photocurrent. The increase in photocurrent density is due to the properties of WO_3 . The band gap of WO_3 is $\sim 2.6 \text{ eV}$ compared to $\sim 3 \text{ eV}$ for TiO_2 , further utilizing the visible range photons. Also, WO_3 , when in contact with TiO_2 , increases the lifetime of the electron hole pair generated when the photoactive anode is illuminated with the solar spectrum [49]. During the morphology change with W loading studies, it was observed that the film would delaminate during anodization when the tungsten is at or above 2.1×10^{19} atoms per cm^3 (concentration before anodization). The film is further prone to delaminating when exposed to higher temperatures (during calcination). Beyond a certain W loading (3.15×10^{18} atoms per cm^3) photocurrent density is reduced which may be due to reduced

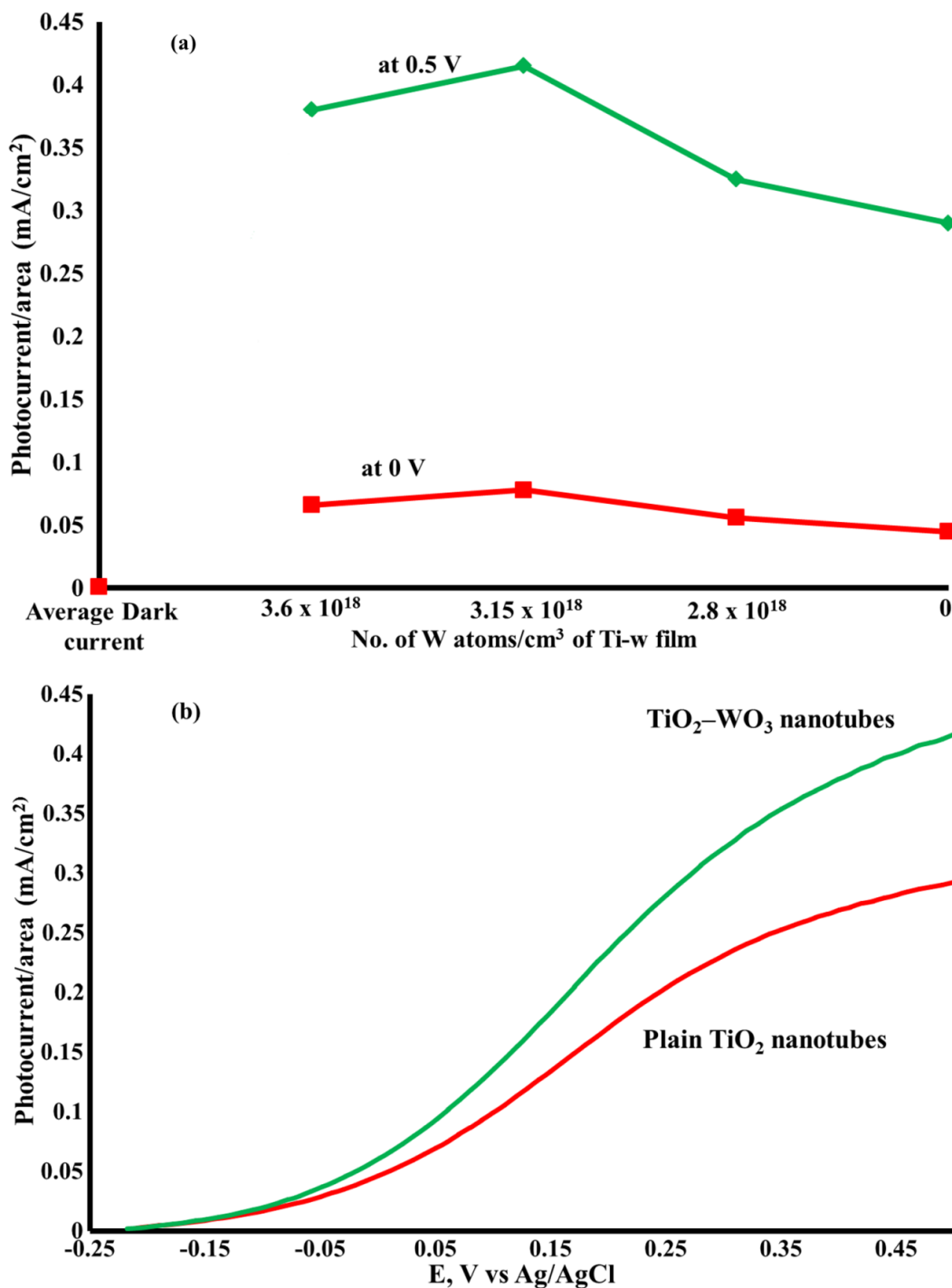


Figure 6.6: Shows the change in the photocurrent density of PEC cell with the change in the WO₃ density. (a) The PEC shows a 40% increase in the performance with 1.05×10^{19} WO₃ molecules per cm³ when compared to plain T-NT. The photocurrents were measured at 0.5 and 0 V. The calcinations temperature was 350 °C. (b) Shows the comparison of the photocurrents of optimized composite and plain nanotubes.

electrical contact with ITO from the unstable film. Currently, there are no reports on high aspect ratio WO_3 nanopores as generally the oxide films delaminate from the substrate due to a stress induced mismatch of the W/WO_3 surface [44]. To understand the effect of the electrical contact of the TW-NT to the ITO a study of the change in photocurrent with nanotube length was carried out. Fig. 6.7 shows the change in photocurrent with length of the nanotube. The length of the nanotube was varied by controlling the anodization time (0 to 20 mins). The thickness of the Ti-W film used was 500 nm and the calcination temperature was at 350 °C. From Fig. 6.7 it can be seen that photocurrent density was the highest when the length of the TW-NT is 200 nm. Upon completely anodizing the film, the nanotube length is 700 nm which is 1.4 times longer than the thickness of the Ti-W deposited film. This is due the oxidation of Ti and W during anodization [34], [35]. With the increase in the length of the nanotube (above 200 nm), the nanotubes are less stable and do not make good electrical contact with the ITO. With a decrease in the nanotube length (less than 200 nm) the electrical contact would improve but the photocurrent would reduce due to the decrease in the surface area to volume ratio. Therefore, there is a need for an optimal Ti-W thickness to be present for a stable oxide layer to form with high PEC performance. The change in the photocurrent density and stability of the oxide layer with calcination temperature was also examined. Fig. 6.8 shows the change in photocurrent with the annealing temperature. The lowest photocurrent density was observed when annealed at 250 °C and increased upon an increase in annealing temperature. This is because at 250 °C there is very little crystallization that occurs and the nanotubes are still amorphous. This can be confirmed from the XRD results in Fig. 6.9. When annealed at 350 °C and 450 °C, the TiO_2 forms the anatase polymorph, and

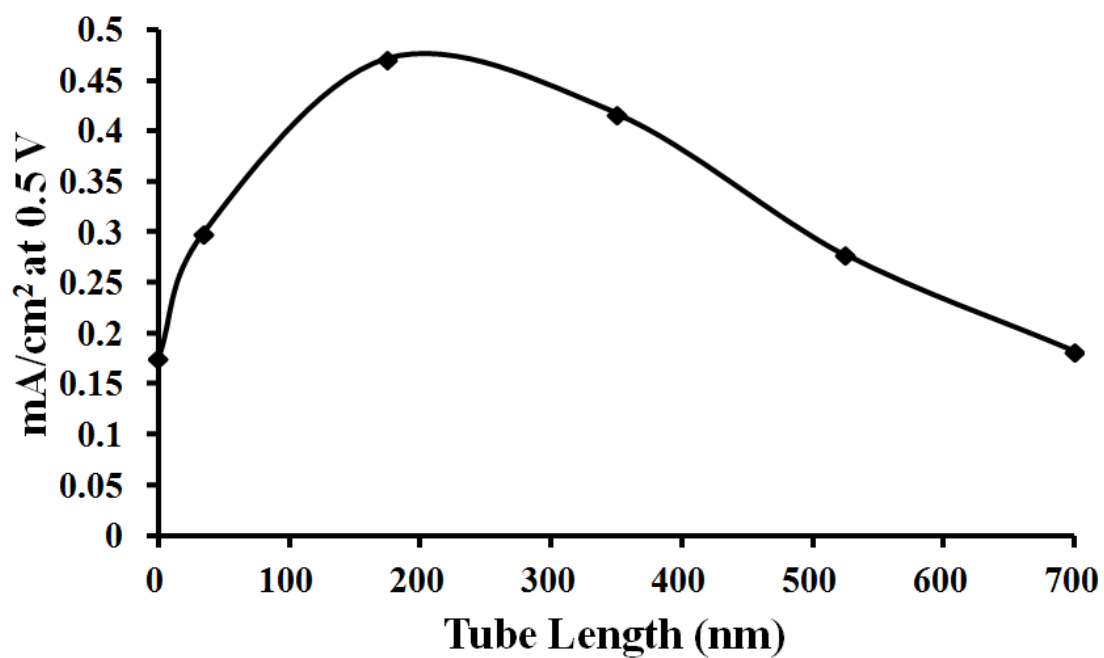


Figure 6.7: Shows the change in the photocurrent density of the PEC with the length of the composite nanotube. A 500 nm thick Ti-W film on anodizing such that the length of the TW-NT is 200 nm shows the highest photocurrent density. The photocurrent was measured at 0.5 V and calcination temperature was 350 °C. The nanotubes consisted of 1.05×10^{19} WO_3 molecules per cm^3 .

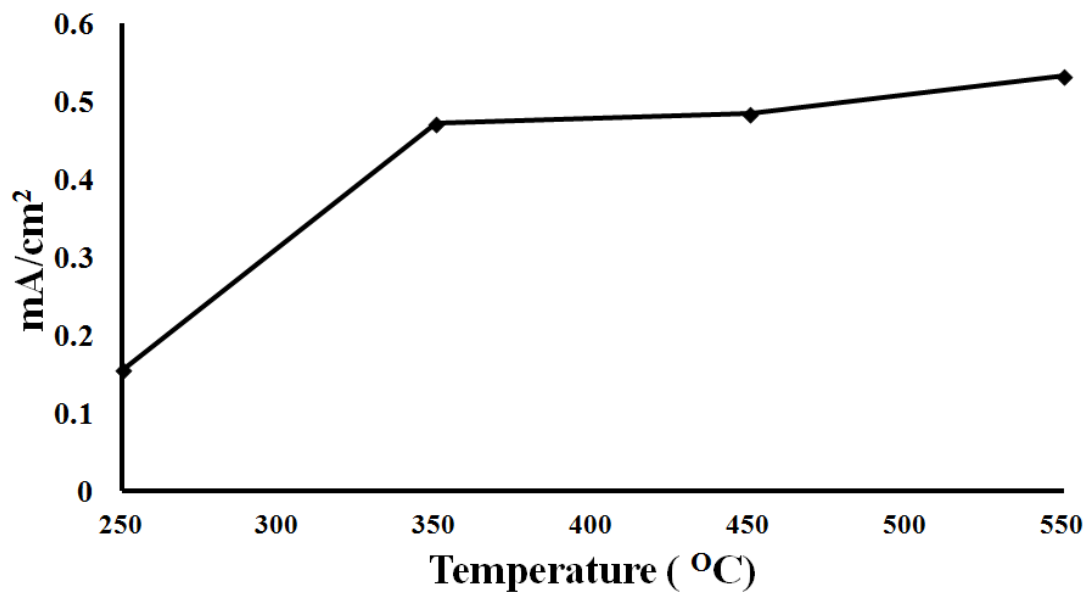


Figure 6.8: Shows the change in the photocurrent density of the PEC with annealing temperature. The photocurrent was measured at 0.5 V. The annealing time was 2 hours. The temperature was ramped at $1.15\text{ }^{\circ}\text{C min}^{-1}$. The nanotubes consisted of 1.05×10^{19} WO_3 molecules per cm^3 .

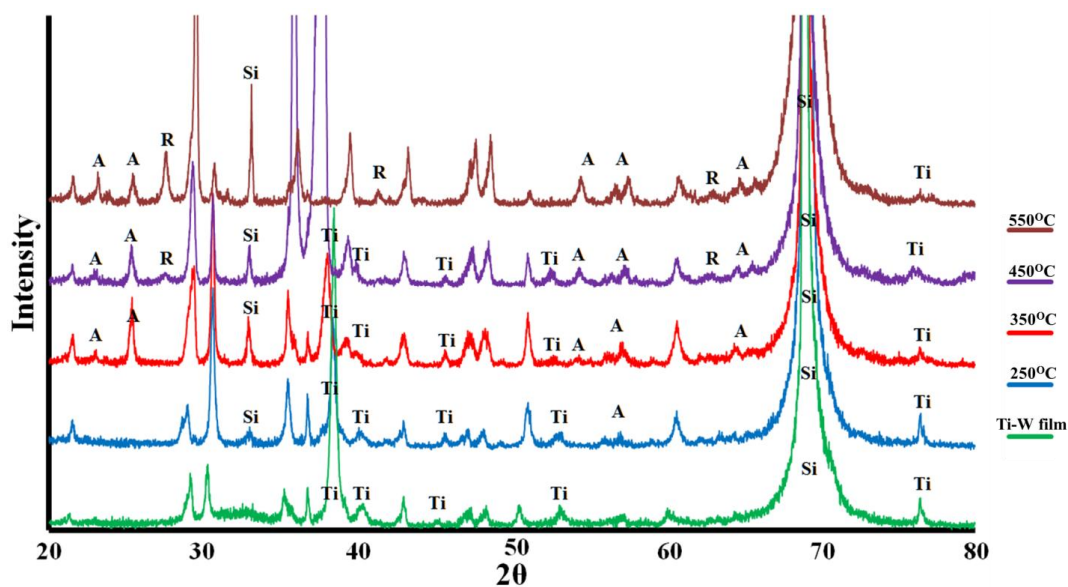


Figure 6.9: Shows the XRD of TW-NT samples annealed at 250 °C to 550 °C and unanodized Ti-W film. The unnamed peaks correspond to the presence of ITO and are not labeled as its crystalline phase is of no significance. ‘A’ implies anatase and ‘R’ implies rutile polymorphs of TiO₂. The nanotubes consisted of 1.05×10^{19} WO₃ molecules per cm³.

hence the photocurrent increases. When annealed at 550 °C, TiO₂ is partly transferred to the rutile polymorph [50] improving the photocurrent efficiency. The XRD results do not show any presence of WO₃ due to the low atomic percentage. Fig. 6.10 shows the diffuse reflectance UV-Vis spectroscopy of a sample annealed from 250 to 550 °C as well as that of plain TiO₂ annealed at 350 °C. For the samples annealed at 450 °C and below, the band gap is shown to be about 3.4 eV with the presence of the absorbance edge at 365 nm. However, when the sample is annealed at 550 °C, the band gap is 3 eV which is shown by the presence of the absorption edge at 410 nm. The reduced band gap is due to the formation of rutile TiO₂ [51], which are observed in the XRD peaks in Fig. 6.9. Hence, when annealed at 550 °C the photocurrent density is higher compared to samples annealed at lower temperature. This is due to the formation of rutile TiO₂ which has a lower band gap, increasing the absorption spectrum. The change in the band gap is not due to the presence of WO₃ since with a significant amount of WO₃, or with doping/alloying of WO₃ with TiO₂ the band gap would be less than 3 eV [47], [52]. From the UV-Vis spectroscopy results, it can also be seen that there is no absorption in the visible range (which should occur due to the presence of WO₃) due to a low concentration WO₃. Therefore, the increase in the photocurrent is mainly due to the hole affinity property of WO₃ which reduces the electron hole recombination. When annealed at temperatures above the 550 °C, the film delaminates decreasing the photocurrent. The samples were tested for 1 hour for photocurrent densities at 0.5 V and the performance of the photoanode did not change. A top view SEM micrograph of the composite nanotube after 1 hour of water splitting is shown in Fig. 6.3 (b). It was observed that there was no change in the morphology showing the stability of the nanotubes.

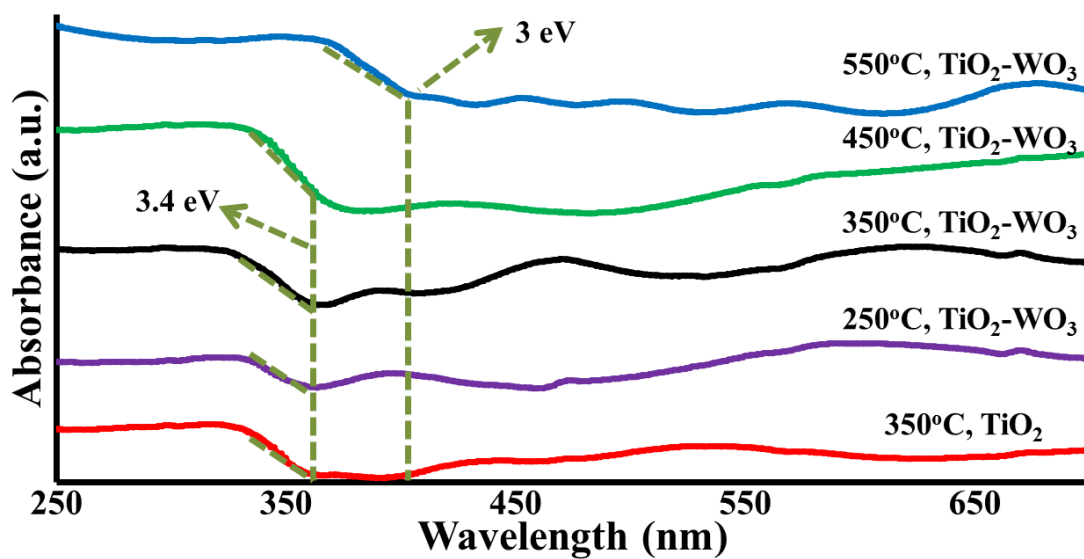


Figure 6.10: Shows the diffuse reflectance UV-Vis spectrum of the TW-NT annealed at temperatures from 250 to 550 °C and plain TiO₂ nanotubes annealed at 350 °C. Up to 450 °C, the band gap of TW-NT was 3.4 eV. When annealed at 550 °C the band gap reduced to 3 eV due to the formation of rutile TiO₂. The composite nanotubes consisted of 1.05×10^{19} WO₃ molecules per cm³.

6.5 Conclusions

Tubular TW-NT was successfully synthesized on a Si wafer by simultaneous sputtering Ti and W to form a Ti-W nanocomposite film followed by electrochemical anodization using an ethylene glycol based organic electrolyte. The change in morphology with the change in W density in the Ti-W composite was studied, and it was observed that with less than 5.25×10^{18} W atoms per cm^3 , the anodized film has a tubular morphology. With a further increase in W density, the anodized film changes from tubular morphology to a nanoporous like morphology. Also with the increase in W density, the stability of the anodized film decreases, limiting the WO_3 loading capability in the oxide film. With 1.05×10^{19} WO_3 molecules per cm^3 in the anodized film, it is seen that the water splitting photocurrent of PEC increased by 40% in comparison to plain T-NT. It was observed that there is a need for an optimal Ti-W thickness to be present for stable TW-NT to form, which would improve the photocurrent density when compared to TW-NT photoanodes that are completely anodized. Studies with different annealing temperatures showed that when annealed at 250 °C, the nanotubes are amorphous resulting in a low photocurrent. When annealed at temperatures 350 °C and above, the nanotube transforms into the anatase phase, improving the charge transport along with the photocurrent density. When annealed at 550 °C, partial rutile TiO_2 is formed, changing the band gap to 3 eV with an absorption edge at 410 nm and showing the highest photocurrent density of 0.52 mA cm^{-2} at 0.5 V. It was observed that the TiO_2 and WO_3 did not show any alloying even when annealed at 550 °C. Scanning electron microscopy, x-ray diffraction, ICP-MS, x-ray photoelectron spectroscopy and diffuse reflectance UV-Vis spectroscopy were used to study the morphology, crystalline phases,

atomic ratio, oxidation state, and band gap of the nanotubes, respectively, to optimize the performance of the TW-NT-based PEC cell.

6.6 References

- [1] C. Koroneos, A. Dompros, G. Roumbas, and N. Moussiopoulos, "Life cycle assessment of hydrogen fuel production processes," *Int. J. Hydrogen Energy*, vol. 29, pp. 1443–1450, 2004.
- [2] T. Kawai and T. Sakata, "Conversion of carbohydrate into hydrogen fuel by a photocatalytic process," *Nature*, vol. 286, pp. 474–476, 1980.
- [3] N. Kondamudi, S. K. Mohapatra, and M. Misra, "Spent coffee grounds as a versatile source of green energy," *J. Agric. Food Chem.*, vol. 56, 11757–11760, 2008.
- [4] N. Kondamudi, J. Strull, M. Misra, and S. K. Mohapatra, "A green process for producing biodiesel from feather meal," *J. Agric. Food Chem.*, vol. 57, 6163–6166, 2009.
- [5] M. Yu, Y.-Z. Long, B. Sunb, and Z. Fan, "Recent advances in solar cells based on one-dimensional nanostructure arrays," *Nanoscale*, vol. 4, pp. 2783–2796, 2012.
- [6] M. Z. Jacobson, "Control of fossil-fuel particulate black carbon and organic matter, possibly the most effective method of slowing global warming," *J. Geophys. Res.*, vol. 107, pp. 4410–4431, 2002.
- [7] G. Tsatsaronisa, K. Kapankea, and A. M. B. Marigorta, "Exergoeconomic estimates for a novel zero-emission process generating hydrogen and electric power," *Energy*, vol. 33, pp. 321–330, 2008.
- [8] S. Nagano, T. Kitajima, K. Yoshida, Y. Kazao, Y. Kabata, D. Murata, and K. Nagakura, "Development of world's largest hydrogen-cooled turbine generator," *Power Eng. Soc. Summer Meeting*, vol. 2, pp. 657–663, 2002.
- [9] J. M. Modak, "Haber process for ammonia synthesis," *Resonance*, vol. 7, pp. 69–77, 2002.
- [10] C. Godet, N. Layadi, and P. R. I. Cabarrocas, "Role of mobile hydrogen in the amorphous silicon recrystallization," *Appl. Phys. Lett.*, vol. 66, pp. 3146–3148, 1995.

- [11] M. Steinberg and H. C. Cheng, "Modern and prospective technologies for hydrogen production from fossil fuels," *Int. J. Hydrogen Energy*, vol. 14, pp. 797–820, 1989.
- [12] S. U. M. Khan, M. Al-Shahry, and W. B. Ingler Jr., "Efficient photochemical water splitting by a chemically modified n-TiO₂," *Science*, vol. 297, pp. 2243–2244, 2002.
- [13] Y. Negishi, M. Mizuno, M. Hirayama, M. Omatoi, T. Takayama, A. Iwase, and A. Kudo, "Enhanced photocatalytic water splitting by BaLa₄Ti₄O₁₅ loaded with ~1 nm gold nanoclusters using glutathione-protected Au₂₅ clusters," *Nanoscale*, pp. 7188–7192, 2013.
- [14] K. Sun, Y. Jing, C. Li, X. Zhang, R. Aguinaldo, A. Kargar, K. Madsen, K. Banu, Y. Zhou, Y. Bando, Z. Liua, and D. Wang, "3D branched nanowire heterojunction photoelectrodes for high-efficiency solar water splitting and H₂ generation," *Nanoscale*, vol. 4, pp. 1515–1521, 2012.
- [15] E. Greenbaum, "Energetic efficiency of hydrogen photoevolution by algal water splitting," *Biophys. J.*, vol. 54, pp. 365–368, 1988.
- [16] M. Ni, M. K. H. Leung, D. Y. C. Leung, and K. Sumathy, "A review and recent developments in photocatalytic water-splitting using TiO₂ for hydrogen production," *Renew. Sust. Energ. Rev.*, vol. 11, pp. 401–425, 2007.
- [17] C. Das, P. Roy, M. Yang, H. Jha, and P. Schmuki, "Nb doped TiO₂ nanotubes for enhanced photoelectrochemical water-splitting," *Nanoscale*, vol. 3, pp. 3094–3096, 2011.
- [18] I. Cesar, A. Kay, J. A. G. Martinez, and M. Grätze, "Translucent thin film Fe₂O₃ photoanodes for efficient water splitting by sunlight: Nanostructure-directing effect of Si-doping," *J. Am. Chem. Soc.*, vol. 128, pp. 4582–4583, 2006.
- [19] R. Abe, T. Takata, H. Sugihara, and K. Domenb, "Photocatalytic overall water splitting under visible light by TaON and WO₃ with an IO₃^{2/12} shuttle redox mediator," *Chem. Commun.*, vol. 3829–3831, 2005.
- [20] T. G. Deutsch, C. A. Koval, and J. A. Turner, "III-V nitride epilayers for photoelectrochemical water splitting: GaPN and GaAsPN," *J. Phys. Chem. B*, vol. 110, pp. 25297–25307, 2006.
- [21] V. Zwillling, E. Darque-Ceretti, A. Boutry-Forveille, D. David, M. Y. Perrin and M. Aucouturier, "Structure and physicochemistry of anodic oxide films on titanium and TA6V alloy," *Surf. Interface Anal.*, vol. 27, pp. 629–637, 1999.

- [22] V. Zwillling, M. Aucouturier, and E. Darque-Ceretti, "Anodic oxidation of titanium and TA6V alloy in chromic media. An electrochemical approach," *Electrochim. Acta*, vol. 45, pp. 921–929, 1999.
- [23] J. H. Park, S. Kim, and A. J. Bard, "Novel carbon-doped TiO₂ nanotube arrays with high aspect ratios for efficient solar water splitting," *Nano Lett.*, vol. 6, pp. 24–28, 2006.
- [24] O. Diwald, T. L. Thompson, T. Zubkov, E. G. Goralski, S. D. Walck, and J. T. Yates Jr., "Photochemical activity of nitrogen-doped rutile TiO₂(110) in visible light," *J. Phys. Chem. B*, vol. 108, pp. 6004–6008, 2004.
- [25] J. C. Yu, W. Ho, J. Yu, H. Yip, P. K. Wong, and J. Zhao, "Efficient visible-light-induced photocatalytic disinfection on sulfur-doped nanocrystalline titania," *Environ. Sci. Technol.*, vol. 39, pp. 1175–1179, 2005.
- [26] H. Kato and A. Kudo, "Visible-light-response and photocatalytic activities of TiO₂ and SrTiO₃ photocatalysts codoped with antimony and chromium," *J. Phys. Chem. B*, vol. 106, pp. 5029–5034, 2002.
- [27] A. Monnier and J. Augustynski, "Photoelectrolysis of water: Photoresponses of nickel, chromium and zinc-doped polycrystalline TiO₂ electrodes," *J. Electrochem. Soc.*, vol. 127, pp. 1576–1579, 1980.
- [28] Y. R. Smith, B. Sarma, S. K. Mohanty, and M. Misra, "Light-assisted anodized TiO₂ nanotube arrays," *ACS Appl. Mater. Interfaces*, vol. 4, pp. 5883–5890, 2012.
- [29] A. Mazare, I. Paramasivam, K. Lee, and P. Schmuki, "Improved water-splitting behaviour of flame annealed TiO₂ nanotubes," *Electrochem. Commun.*, vol. 13, pp. 1030–1034, 2011.
- [30] Y. Yin, Z. Jin, and F. Hou, "Enhanced solar water-splitting efficiency using core/sheath heterostructure CdS/TiO₂ nanotube arrays," *Nanotechnology*, vol. 18, pp. 495608–495613, 2007.
- [31] W. Smith, A. Wolcott, R. C. Fitzmorris, J. Z. Zhang, and Y. Zhao, "Quasi-core-shell TiO₂/WO₃ and WO₃/TiO₂ nanorod arrays fabricated by glancing angle deposition for solar water splitting," *J. Mater. Chem.*, vol. 21, pp. 10792–10800, 2011.
- [32] J. H. Park, O. O. Park, and S. Kim, "Photoelectrochemical water splitting at titanium dioxide nanotubes coated with tungsten trioxide," *Appl. Phys. Lett.*, vol. 89, pp. 163106 (3), 2006.

- [33] K. Dai, T. Peng, D. Ke, and B. We, "Photocatalytic hydrogen generation using a nanocomposite of multi-walled carbon nanotubes and TiO₂ nanoparticles under visible light irradiation," *Nanotechnology*, vol. 20, pp. 125603–125608, 2009.
- [34] K. N. Chappanda, Y. R. Smith, M. Misra, and S. K. Mohanty, "Site-specific and patterned growth of TiO₂ nanotube arrays from e-beam evaporated thin titanium film on Si wafer," *Nanotechnology*, vol. 23, pp. 385601–385607, 2012.
- [35] K. N. Chappanda, Y. R. Smith, S. K. Mohanty, L. W. Rieth, P. Tathireddy, and M. Misra, "Growth and characterization of TiO₂ nanotubes from sputtered Ti film on Si substrate," *Nanoscale Res. Lett.*, vol. 7, pp. 388–395, 2012.
- [36] Y. R. Smith and V. Subramanain, "Heterostructural composites of TiO₂ mesh–TiO₂ nanoparticles photosensitized with CdS: A new flexible photoanode for solar cells," *J. Phys. Chem. C*, vol. 115, pp. 8376–8385, 2011.
- [37] Y. S. Sohn, Y. R. Smith, M. Misra, and V. R. Subramanian, "Electrochemically assisted photocatalytic degradation of methyl orange using anodized titanium dioxide nanotubes," *Appl. Catal. B*, vol. 84, pp. 372–378, 2008.
- [38] S. M. Eggins, "Laser ablation ICP-MS analysis of geological materials prepared as lithium borate glasses," *Geostandards Newsletter*, vol. 27, pp. 147–162, 2003.
- [39] K. R. Williams and R. S. Muller, "Etch rates for micromachining processing," *J. Microelectromech. S.*, vol. 5, pp. 256–269, 1996.
- [40] K. R. Williams, K. Gupta, and M. Wasilik, "Etch rates for micromachining processing—Part II," *J. Microelectromech. S.*, vol. 12, pp. 761–778, 2003.
- [41] R. Hahn, J.M. Macak, and P. Schmuki, "Rapid anodic growth of TiO₂ and WO₃ nanotubes in fluoride free electrolytes," *Electrochem. Commun.*, vol. 9, pp. 947–952, 2007.
- [42] H. Tsuchiya, J. M. Macak, I. Sieber, L. Taveira, A. Ghicov, K. Sirotna, and P. Schmuki, "Self-organized porous WO₃ formed in NaF electrolytes," *Electrochem. Commun.*, vol. 7, pp. 295–298, 2005.
- [43] N. R. de Tacconi, C. R. Chenthamarakshan, G. Yogeewaran, A. Watcharenwong, R. S. de Zoysa, N. A. Basit, and K. Rajeshwar, "Nanoporous TiO₂ and WO₃ films by anodization of titanium and tungsten substrates: influence of process variables on morphology and photoelectrochemical response," *J. Phys. Chem. B*, vol. 110, pp. 25347–25355, 2006.
- [44] P. Roy, S. Berger, and Patrik Schmuki, "TiO₂ nanotubes: Synthesis and applications," *Angew. Chem. Int. Ed.*, vol. 50, pp. 2904–2939, 2011.

- [45] U. Diebold and T. E. Madey, "TiO₂ by XPS," *Surf. Sci. Spectra*, vol. 4, pp. 227–231, 1998.
- [46] L. Lozzi, L. Ottaviano, M. Passacantando, S. Santucci, and C. Cantalini, "The influence of air and vacuum thermal treatments on the NO₂ gas sensitivity of WO₃ thin films prepared by thermal evaporation," *Thin Solid Films*, vol. 391, pp. 224–228, 2001.
- [47] Y. R. Smith, B. Sarma, S. K. Mohant, and M. Misra, "Formation of TiO₂–WO₃ nanotubular composite via single-step anodization and its application in photoelectrochemical hydrogen generation," *Electrochem. Commun.*, vol. 19, pp. 131–134, 2012.
- [48] J. R. Sohn, H. S. Cho, and H. W. Kim, "Characterization of WO₃ supported on TiO₂–ZrO₂ and catalytic activity for acid catalysis," *J. Ind. Eng. Chem.*, vol. 5, pp. 1–9, 1999.
- [49] X. Yan, X. Zong, G. Q. Lu, and L. Wang, "Ordered mesoporous tungsten oxide and titanium oxide composites and their photocatalytic degradation behavior," *Prog. Nat. Sci.: Mat. International*, vol. 22, pp. 654–660, 2012.
- [50] A. Tighineanu, T. Ruff, S. Albu, R. Hahn, and P. Schmuki, "Conductivity of TiO₂ nanotubes: Influence of annealing time and temperature," *Chem. Phys. Lett.*, vol. 494, pp. 260–263, 2010.
- [51] S. Valencia, J. M. Marín, and G. Restrepo, "Study of the bandgap of synthesized titanium dioxide nanoparticles using the sol-gel method and a hydrothermal treatment," *Open Mater. Sci. J.*, vol. 4, pp. 9–14, 2010.
- [52] C. Das, I. Paramasivam, N. Liu, and P. Schmuki, "Photoelectrochemical and photocatalytic activity of tungsten doped TiO₂ nanotube layers in the near visible region," *Electrochim. Acta*, vol. 56, pp. 10557–10561, 2011.

CHAPTER 7

CONCLUSIONS

The main objectives of this dissertation were to synthesize TiO_2 nanotubes on a stable and planar Si substrate from thin Ti film and demonstrate photocatalytic activity as well as improve the photocatalytic activity of these nanotubes. It was found that TiO_2 nanotubes are a suitable materials for photocatalytic activity such as water splitting due their wide band gap, photocorrosion resistance, and environmentally friendly properties. In this chapter, we summarize the methods used and important results obtained on the electrical properties, structural morphology, and optical properties of TiO_2 nanotubes (T-NT) synthesized on Si substrate. We study the properties of thin films that affect the structural morphology of nanotubes. We draw conclusions about the properties of thin film nanotubes in comparison to foil based nanotubes. We draw some conclusions on the water splitting capabilities of thin film based TiO_2 nanotubes and improve the performance incorporating WO_3 in the nanotubes. Finally, we provide some recommendations for future work.

7.1 Summary

We synthesized TiO_2 nanotubes from thin Ti films deposited on Si substrate using D.C. magnetron sputtering and e-beam evaporation techniques. Films with thickness from 350 nm to 1 000 nm were deposited. The thickness of the film was varied to change the nanotube length with the possibility of having the length of the nanotubes longer, shorter, or the same as the thickness of the deposited film. Thermally grown silicon dioxide was grown on the silicon substrate to electrically isolate the nanotubes from the bulk silicon. The nanotubes were synthesized using the electrochemical anodization technique, which is the most preferred method for most of the practical applications using

a near neutral organic electrolyte. The influence of properties of thin films such as grain size, biaxial stress, and density on the nanotubes was studied. We integrated photolithography with synthesis of TiO₂ nanotubes and studied the properties of the synthesized nanotubes. The TiO₂ nanotubes' photocatalytic activity in splitting water into hydrogen and oxygen was studied. Using the advantages of microfabrication technique, the photocatalytic activity of TiO₂ nanotubes were improved by incorporating WO₃ in the nanotubes.

7.1.1 Thin film deposition

Clean n-type Si was used as substrates with (100) crystal orientation used for depositing the thin Ti films. The RMS roughness of the substrate was less than 1 nm and the resistivity was 1–5 Ωcm. Smooth substrate was used to lower the roughness of the deposited film. About 100 nm SiO₂ was grown on the substrate to electrically isolate the thin film nanotubes from the bulk Si. The thickness of the oxide was chosen such that it was sufficient enough to electrically isolate potentials up to 100 V. Both wet as well as dry thermal oxide was grown on the Si substrate to study the dependence of the substrate on the nanotubes. The oxidation was carried out at 1 000 °C using a canary oxidation furnace. The Ti films were cleaned with acetone, isopropanol, and water before being subjected to anodization. Deposition of thin Ti films by the e-beam evaporation technique was carried out using a Denton SJ20C e-beam evaporator. The deposition was carried out in a clean environment at pressure less than 1 μTorr. Ti pellets (99.995% pure) purchased from Kurt. J. Lesker were used. The crucible for containing the pellets during evaporation was made of carbon. The deposition rate was at about 1–2 Å/s. D.C. magnetron sputtered

films were deposited in Denton Discovery 18 sputter system. Ti target of 99.2% to 99.7% purity purchased from Kurt. J. Lesker was used. The chamber was pumped down to pressure less than 2 μ Torr before carrying out the film deposition.

7.1.2 Electrochemical anodization

A mixture of ethylene glycol (purchased from Fisher), ammonium fluoride ((0.5 wt%) purchased from Fisher), and DI water (10 wt%) was used as the electrolyte to synthesize the nanotubes on the Si substrate. The prepared electrolyte was aged for at least 36 hours before using it for anodization. The anodization was carried in ambient temperature. The gap between the cathode and anode was 2 cm. The Ti film was then connected to the positive terminal of the power supply to form the anode. One cm^2 of platinum was connected to the negative terminal to form the cathode. Agilent E3647A dual output D.C. power supply was used as the power source for anodization. The anodization voltage was ranged from 10 to 60 V to study the change in the morphology of the nanotubes with the change in anodization potential. The expectation was for an increase in tube diameter with an increase in anodization potential. The non-Ti portion of the Ti/SiO₂/Si was covered with Kapton tape to prevent undesired etching of the substrate by the electrolyte. This would also prevent any change in the chemistry of the electrolyte due to anodization effects on the substrate. The anodized e-beam films were annealed at 500 °C to study the stability of the nanotubes when subjected to higher temperatures, which is required for most of the applications demonstrated by the TiO₂ nanotubes. The anodized D.C. magnetron sputtered films were annealed at 350 °C. E-beam evaporated films were used to study integration of photolithography with synthesis of TiO₂

nanotubes. Two photolithography steps were used to achieve site-specific and patterned growth of TiO_2 nanotubes. The first photolithography step was used to pattern the Ti film on the Si substrate. The second photolithography step was used to mask portions of Ti where photoresist was used as the protective layer between the Ti film and the electrolyte to prevent growth of nanotubes. Shipley's S1813 positive photoresist was used for the photolithography. The photoresist was spun at 2000 rpm to achieve about 2 μm thick films. The masks used for photolithography were fabricated using a Heidelberg MicroPG 101 pattern generator. The Suss MA1006 was used for pattern alignment and for exposing the photoresist to UV light. The anodization was carried out at 20 V for site specific and patterned growth of TiO_2 nanotubes studies. The e-beam evaporation technique has little scope in changing the properties of the thin film since the only parameter that could be changed was the deposition rate which had relatively less influence on the film properties. Therefore, D.C. magnetron sputtered films were used to study the influence of the properties of thin films on the synthesized nanotubes. Film deposition parameters such as process gas pressure (argon gas), sputtering power, and substrate temperature were varied to change the properties of the thin film. Film properties such as grain size, biaxial stress, and qualitative density were studied and their influence on the morphology of the anodized films was reported. We hoped for an increase in residual stress to have an effect on the gap between the nanotubes. The grains were expected to define the nanotube diameter since the initial electric field hot spots are defined by these surficial grains. The thickness of the deposited films was between 300 to 400 nm. The thickness was targeted to be 350 nm. However, the thickness varied due to the change in yield with the change in the sputtering parameters. The anodization was

carried out at 30 V. The gap between the cathode and anode was 2.5 cm during this part of the study. The next part of the research was to study the photocatalytic activity of TiO₂ nanotubes in splitting water into hydrogen and oxygen. By incorporating WO₃ in TiO₂ nanotubes, we hoped to enhance the photocatalytic activity, since WO₃ has a lower band gap and also would increase the lifetime of charge carriers. 500 nm thick films were used for studying the water splitting photocurrent. The WO₃ nanoparticles were incorporated in the nanotubes by anodizing Ti–W nanocomposite thin film. The composite films were deposited by simultaneous sputtering of Ti and W. W was deposited using RF magnetron sputtering system, and the Ti was sputtering using a D.C. magnetron sputtering system in the Denton Discovery 18 sputter system. The change in the structural morphology of the anodized film with W in the sputtered film was studied to understand the density incorporating limitation of WO₃ in the nanotubes. The W atomic percentage was changed by changing the sputtering power. The anodization was carried out at 30 V, and the gap between the electrodes was 2.5 cm. For fabricating the photoelectrochemical cell, 100 nm thick ITO was deposited (to form the electrode to monitor the photocurrents) via D.C. magnetron sputtering before depositing the composite film. The films were anodized at 20 V for photoelectrochemical cell water splitting studies. The platinum mesh was used as the cathode and Ag/AgCl was used as the reference electrode. The electrolyte in the photoelectrochemical cell consisted of 0.5M Na₂SO₄, since the electrolyte would not react with the substrate. The photocurrents were monitored for external bias of up to 0.5 V. The photocurrents of plain TiO₂ nanotubes were compared with the photocurrents of composite nanotubes. The performance of the photoelectrochemical cell with annealing temperatures and nanotube length was studied.

7.1.3 Characterization

The nanotubes were characterized for structural morphology, band gap, and crystalline phase. The composite nanotubes, in addition, were characterized for oxidation state and photocatalytic activity. The structural morphology of the nanotubes such as nanotube length and outer diameter were studied using scanning electron microscopy (SEM) micrographs obtained from FEI NanoNova SEM. All the top view micrographs were obtained at magnification of 200 000x, and the side view micrographs were obtained at magnification of 250 000x and 60° tilt. The change in the surface morphology with anodization time was studied using SEM and atomic force microscopy (AFM) micrographs (obtained from Bruker Dimension ICON-PT AFM). The AFM micrographs were obtained using PeakForce QNM (Bruker AXS). The band gap of the nanotubes was studied by diffuse reflectance UV-Vis spectroscopy using a UV-3600 Shimadzu spectrometer. The wavelength was varied from 800 to 250 nm. The band gap was expected to be about 3–3.4 eV. The crystalline phases of the nanotubes were studied by x-ray diffraction (XRD) technique using Philips X'Pert XRD and Rigaku Miniflex XRD systems. The incidence angles were ranged from 20° to 80°. The crystalline phase was expected to be amorphous before annealing and attain anatase and rutile phase when annealed at a temperature above 300 °C. The properties of thin films such as grain size and film thickness before anodization were studied using SEM micrographs. The average grain sizes of Ti films were calculated using stereology technique. The biaxial residual stress of Ti films were measured by laser interferometry technique using Tencor FLX-2320 laser interferometer in which the bow in the Si wafers before and after depositing the films were measured. The oxidation states of composite nanotubes were studied using

x-ray photoelectron spectrometry (XPS) using a Kratos Axis Ultra DLD x-ray photoelectron spectrometer. We expected the alloying of the TiO_2 and WO_3 , reducing the band gap to 2.6 eV. To measure the percentage of W in the Ti–W composite film, an Agilent 7500ce inductively coupled plasma mass spectrometer (ICP-MS) was used. Fluorine-neon laser (193 nm) ablation was used to generate the aerosol of the Ti–W films. The spectrum of the composite sample was compared with the spectrum of the standard sample (NIST 610 glass) with elements of known concentrations. To study the photocatalytic activity of plain and composite nanotubes, the nanotubes were illuminated with a Newport solar simulator with a 1.5 air mass filter. We expected that the optimum WO_3 would have up to a 100% increase in performance. The photocurrents were monitored using PARSTAT 4000 potentiostat. Table 7.1 gives a summary of the tools used and the parameters analysed using the tools.

7.2 Conclusions

We successfully synthesized TiO_2 nanotubes from thin Ti on Si substrate by electrochemical anodization using an organic electrolyte. Nanotubes were synthesized from films deposited by D.C. magnetron sputtering as well as e-beam evaporation technique. The diameter of the nanotubes ranged from 45 to 230 nm linearly when synthesized at potentials from 10 to 60 V (D.C.). The observed trend in the diameter change was as expected. Nanotubes up to 1.4 μm long were successfully synthesized. From SEM micrographs, it was found that the length of the nanotubes were 1.4 times the thickness of the deposited film showing the selectivity electric field assisted etching and low undesired etching of the film by the electrolyte; the T-NT did not have a reduced

Table 7.1: Summary of the tools used and the parameters analysed using the tools

Tool	Analysis
Scanning electron microscope	Structural morphology of nanotubes and thin Ti films
Atomic force microscope	RMS Surface roughness of nanotubes
Diffuse reflectance UV-Vis spectroscopy	Band gap of nanotubes
X-ray diffraction	Crystalline phases of the nanotubes
Laser interferometer	Biaxial residual stress of Ti films
X-ray photoelectron spectrometer	Oxidation states of composite nanotubes
Inductively coupled plasma mass spectrometer	W density in Ti-W thin films
Potentiostat	Monitor photocurrents

or the same length as the thickness of the film. The increase in the length of the nanotubes greater than the Ti film is due to the increase in the volume caused by oxidation of Ti to TiO₂. The nanotubes synthesized from e-beam evaporated films were stable on substrate when annealed at 500 °C and the sputtered films were stable when annealed at 350 °C. All the anodized films had a nanoporous film on the upper portion of the film, which is due to the presence of native oxide and pronounced surficial grains. However, we hoped that the synthesized nanotubes would be without the nanoporous layer. Due to the formation of the nanoporous layer, it was required to cool down the substrates to ambient temperature in a vacuum to reduce the formation of TiO₂ after the film was despoited. The anodization starts at the valleys of the surficial grains where the electric field is the highest. The nanotubes were interconnected via a thin membrane (5–10 nm thick) forming at regular intervals along the length of the nanotubes. The nanotubes synthesized from e-beam evaporation and sputtering were similar to each other in structural morphology with no noticeable differences. From XRD results, the nanotubes were amorphous after anodization as expected. When annealed at temperatures 350 °C and above, they crystallize to form anatase TiO₂ as expected. When annealed at temperatures 550 °C and above, rutile TiO₂ begins to form as expected again. From the diffuse reflectance UV-Vis spectroscopy, the band gap of nanotubes were found to be 3.4 eV with the absorption edge at around 370 nm, which was a little higher than the expected value of 3.2 eV. When annealed at 550 °C, the nanotubes had a band gap of 3 eV with the absorption edge at 410 nm due to formation of rutile TiO₂. Using two photolithography steps, site pecific and patterned growth of TiO₂ nanotubes were successfully achieved. Site specific nanotubes in regions as low as 0.01 mm² with self-

aligned Ti electrodes were fabricated. Patterned growth of nanotubes resembling the logo of the University of Utah with 25 μm size features were fabricated as expected. The structural morphology of nanotubes synthesized in the site specific as well as patterned regions was similar to the nanotubes synthesized on the larger area, however, we anticipated some morphological differences. The photoresist was slightly soluble in the anodization electrolyte, and hence the time for synthesis of nanotubes was limited to about 1 hour. From the study of properties of thin film influencing the morphology of anodized films, it was concluded that the density alone influences the morphology of the anodized film and other properties such as biaxial residual stress and grain size do not affect the morphology. However, we expected the grain size (which defines the initial hot spots) and the biaxial residual stress to have a significant influence on the morphology of the nanotubes. When the Ti was sputtered at constant power (150 W), substrate was at ambient temperatures and argon pressure ranged from 2.5 to 7.5 mTorr, the average grain size increased from 58 to 72 nm, the residual stress decreased from 200 to 140 +MPa, and the density reduced from medium density film to low density film. Upon anodizing these films, the morphology changed from a tubular structure to a semitubular structure. When the Ti was sputtered at constant argon pressure (7 mTorr), substrate was at ambient temperature, and sputtering power ranged from 25 to 500 W, the average grain size increased from 62 to 80 nm, the residual stress increased from 80 to 140 +MPa, and the density increased from very low density to high density film. Upon anodizing these films, the morphology changed from a nanoporous structure to a tubular structure. When the Ti was sputtered at constant power (150 W), there was constant argon pressure (5 mTorr), and substrate temperature ranged from 100 to 300 $^{\circ}\text{C}$, the average grain size increased

from 72 to 95 nm, the residual stress varied 20 to 90 +MPa (with no linear trend), and the density increased from low density film to high density film. Upon anodizing these films, the morphology changed from a semitubular structure to a tubular structure. Therefore, by varying the sputtering parameters, nanoporous to tubular TiO₂ can be fabricated. By comparing the trend of change in grain size, residual stress, and density of the film, it can be concluded that the morphology of the anodized film depends only on the density and not on the grain size or the residual stress.

By anodizing the Ti–W composite film, TiO₂–WO₃ composite nanotubes were synthesized successfully. With W less than 5.25×10^{18} W atoms/cm³ of the composite film, the anodized film has a tubular structure. With a further increase in the W percentage, the morphology gradually changes from tubular to semitubular to a nanoporous structure due to less selective etching of W as well stress induced formation of WO₃. However, we expected to synthesize tubular composite nanotubes even with higher W density. By optimizing the W density, it was found that with 1.05×10^{19} WO₃ molecules/cm³ in the anodized film, the photocurrent is 42% higher than plain TiO₂ nanotubes. For a 500 nm thick composite film, it was found that the nanotubes length should be 200 nm with a portion of unanodized film being present to have good electrical contact to the ITO electrode. We predicted the photocurrents to be the highest when the composite film is completely anodized. From the XRD results the presence of W atoms could not be detected, which is due to low W density. XPS results show that the Ti is at Ti⁴⁺ oxidation state and the W is at W⁶⁺ oxidation state. At 0.5 V the samples annealed at 550 °C showed the highest photocurrent of 0.53 mA cm⁻². Diffuse reflectance UV-Vis spectroscopy showed the band gap was between 3.4 (anatase) to 3 (rutile) eV,

demonstrating that the nanotubes formed were composite, but no alloy, was being formed. The increase in the photocurrent may be due to a reduction in the charge recombination due to the presence of WO_3 ; there was no absorption in the visible spectrum (reducing the band gap to ~ 2.6 eV, which was the expected results), which would ideally occur with the presence of a significant amount of WO_3 . Table 7.2 shows the summary of the experimental parameters varied/studied and the results achieved.

7.3 Future work

In this section, we recommend some of the future work that could improve upon the work demonstrated in this dissertation. In the fourth chapter, we fabricated site specific grown TiO_2 nanotubes with self-aligned Ti electrodes. However, the electrical tests showed no detected conductivity. To solve the issue of low conductivity, some recommended work would be to anneal the nanotubes in a vacuum to crystalize the nanotubes and prevent any oxidation of the Ti electrodes. The next step would be to reduce the site specific nanotubes to regions less than $5 \mu\text{m}^2$, which can be achieved by having sacrificial Ti (for anodizing) when anodizing. This way the electric field would not be concentrated only in regions where the nanotubes are to be synthesized. The unnecessary nanotubes can later be etched using additional photolithography steps. Another approach is to dope the nanotubes with carbon or nitrogen to improve the conductivity. Also, the electrical contacts between nanotubes can be increased by synthesizing nanotubes in electrolyte with 1 wt% water. With low water content, the nanotubes can be synthesized with no interconnecting TiO_2 membrane so the nanotubes would be in direct contact with each other, increasing the contact area. The next part

Table 7.2: Summary of the experimental parameters varied/studied and the results achieved

Experimental parameters studied/ varied	Results
Anodization potential (10–60 V)	Nanotube diameter ~ 40–230 nm
Band gap	3.4 eV when annealed below 500 °C and 3 eV when annealed at above 500 °C
Crystalline morphology	Amorphous (when not annealed), anatase when annealed above 350 °C, and anatase+rutile when annealed above 500 °C
Nanotube length	1.4 times the thickness of thin film
Site specific T-NT synthesis	In regions 0.01 mm ² with 25 μm features
With an increase in argon pressure for Ti sputtering	Density reduces, stress reduces, grain size increases, and tubularity of T-NT decreases
With an increase in sputtering power	Density increases, stress increases, grain size increases, and tubularity of T-NT increases
With an increase in substrate temperature	Density increases, stress does not have a linear relationship with temperature, grain size increases, and tubularity of T-NT increases
With an increase in W density	Tubularity of composite nanotube increases
Before and after anodization	W density increases after anodization
W density vs photocurrent	3.15 x 10 ¹⁸ W atoms/cm ³ showed the optimum photocurrent with a 40% increase compared to plain T-NT
Nanotube length vs photocurrent	200 nm long nanotubes showed highest photocurrent for 500 nm thick Ti-W film
Annealing temperature vs photocurrent	Photocurrents increased with an increase in temperature but were limited to 550 °C due to delamination
Highest photocurrents	0.52 mA/cm ³ with WO ₃ density of 1.05 x 10 ¹⁹ molecules/cm ³ , with 200 nm long composite nanotubes annealed at 550 °C

would be functionalizing the surface of the TiO_2 nanotubes with the material of interest to fabricate the desired sensor and packing the device. In the fifth chapter, we show that the grain size and residual stress do not affect the morphology of the TiO_2 nanotubes. However, the density was qualitative in nature and the exact density, quantitatively, was not presented. Using x-ray reflectivity technique the density of Ti film can be measured, and the dependence on the morphology with quantitative Ti densities can be presented to have a better understanding of the relationship between the density and morphology. In the sixth chapter we present composite nanotubes. The next part of the work would be to form an alloy of nanotubes instead of composites nanotubes by higher temperature annealing. The technique can be used to synthesize and study other composite nanotubes such $\text{TiO}_2\text{-Al}_2\text{O}_3$ and $\text{TiO}_2\text{-Ta}_2\text{O}_5$ composite nanotubes and study their morphology and photocatalytic activity. Also, photolithography can be integrated to achieve site specific synthesis of composite nanotubes.